The cellular response of triple-negative breast cancer to short-term starvation: implications for chemosensitivity

by

Charné Prangley

Thesis presented in fulfilment of the requirements for the degree of Master of Science, in the Faculty of Science at Stellenbosch University.

Supervisor: Prof Anna-Mart Engelbrecht

Co-supervisor: Dr Tanja Davis

The Department of Physiological Sciences

Stellenbosch University

March 2021

Declaration of Originality

Full name of student: Charné Prangley

By submitting this thesis electronically, I declare that the entirety of the work contained herein is my own original work, that I am the sole author thereof (unless to the extent explicitly otherwise stated) and that I have not previously, in its entirety or in part, submitted it for obtaining any qualification.

Signed: Date: March 2021

Abstract

Introduction:

Breast cancer is currently the most common cancer among women globally. Triple-negative breast cancer (TNBC) is an aggressive and often drug-resistant sub-type of breast cancer that is correlated with poor patient outcomes. As a result, adjuvant therapies that may improve drug sensitivity are currently being sought. Due to the unique metabolic hallmarks of cancer, metabolic adjuvant therapies have become an area of increasing interest. We therefore set out to investigate the effect of short-term starvation (STS) on the growth, viability, and metabolism of TNBC cells and a benign breast epithelial cell line. We also investigated the effect of STS on chemotherapy-induced cytotoxicity in these cells to determine whether STS may enhance the effect of doxorubicin in TNBC.

Methods:

Three cell lines were utilised for this study: a benign breast epithelial cell line (MCF-12A), and two triple-negative breast cancer cell lines (BT-549 and MDA-MB-231). Western blotting was employed to determine the effect of starvation over time on growth and proliferation signalling pathways (PI3K/Akt) and markers of autophagy (Atg5, p62 and LC3-II). Immunocytochemistry was utilised to quantify autophagic puncta. Cell cycle progression and viability were assessed using flow cytometry and a WST1 assay, respectively. The effect of STS on chemosensitivity was then established by incubating cells in standard or starvation-mimicking media for 24 hours, whereafter they received doxorubicin at a concentration of 2.5 µM. Chemosensitivity was then established in terms of live cell number, cell death and viability, and cell cycle progression.

Results and Discussion:

In response to STS, the MCF-12A cells downregulated pro-growth signalling pathways, while the MDA-MB-231 cells showed significant upregulation. A 24-hour starvation period had no significant effects on these pathways or on autophagic flux in the BT-549 cells. Both the MCF-12A and MDA-MB-231 cell lines significantly upregulated autophagic flux in response to STS, with the latter achieving the most significant effect at 24-hours. This may have offered protection to these cells, as a period of starvation prior to drug administration reduced doxorubicin-induced G_2/M arrest. Additionally, STS had no other significant effects on chemosensitivity in these cells. In the BT-549 cells, however, starvation was able to significantly increase the percentage of dead cells in the group that received STS prior to doxorubicin treatment. As autophagy was not significantly increased in this cell line during starvation, this suggests that autophagy may indeed play a role in drug resistance.

Conclusion:

In summary, the cell lines which displayed an upregulation of autophagy at 24 hours of starvation were not sensitised to doxorubicin in terms of cell death, and also experienced amelioration of doxorubicin-induced G_2/M arrest. This supports the notion that autophagic upregulation may protect cancer cells from doxorubicin-induced cytotoxicity and contribute to drug resistance. However, to gain a more thorough understanding of this phenomenon, future studies investigating the mechanisms by which autophagy promotes chemoprotection are recommended.

Opsomming

Inleiding:

Borskanker is die mees algemene kanker in vroue wêreldwyd. Trippel negatiewe borskanker (TNBK) is ‘n aggressiewe en menigmaal ‘n middel-weerstandige subtipe borskanker wat met ‘n swak prognose geassosieer word. As gevolg hiervan, word adjuvante terapeutiese opsies ondersoek om middel sensitiwiteit te verbeter. Metaboliese adjuvante terapeutitese opsies word toenemend ondersoek as gevolg van die unieke metaboliese kenmerke van kanker. Die doel van hierdie studie was om die effek van kort termyn uithongering (KTU) op selgroei, sel lewensvatbaarheid en metabolisme in TNBK selle en benigne bors epiteelselle te ondersoek. Die effek van KTU op chemosensitiwiteit in hierdie selle is ook ondersoek om te bepaal of dit as ‘n moontlike behandelingsopsie kan dien.

Metodes:

Drie sellyne is in hierdie studie gebruik: ‘n benigne borsepiteel sellyn (MCF-12A), en twee TNBK sellyne (BT-549 en MDA-MB-231). Westelike kladtegniek is gebruik om die effek van uithongering oor tyd op selgroei seinoordragpaaie (PI3K/Akt) en merkers van autofagie te bepaal (Atg5, p62 en LC3-II). Immunositochemie is gebruik om autofagie punktae te kwantifiseer. Selsiklus progressie en sel lewensvatbaarheid is deur middel van vloeisitometrie en ‘n WST-1 toets onderskeidelik bepaal. Die effek van KTU op chemosensitiwiteit is bepaal deur selle in standaard- en uithongering nabootsende media vir 24 uur te inkubeer waarna dit doxorubicin teen ‘n konsentrasie van 2.5 μM ontvang het. Chemosensitiwiteit is daarna vasgestel deur middel van die bepaling van die aantal lewende selle, seldood en sel lewensvatbaarheid, asook selsiklus progressie.

Resultate en Bespreking:

Die MCF-12A selle het groei seinoordragpaaie afgereguleer in reaksie op KTU, terwyl die MDA-MB-231 selle weer ‘n insiggewende opregulering van hierdie paaie getoon het. ‘n Vier-en-twintig uur uithongeringsperiode het geen insiggewende effek of hierdie paaie of autofagie vloei in die BT-549 selle gehad nie. Beide die MCF-12A en die MDA-MB-231 sellyne het autofagie vloei insiggewend opgereguleer in reaksie op KTU, met die MDA-MB-231 selle wat die mees insiggewende effek na 24 uur getoon het. Dit kon beskerming aan hierdie selle gebied het, aangesien die uithongeringstydperk voor die toediening van doxorubicin, die doxorubicin-geinduseerde G2/M inperking verminder het. KTU het geen verdere effek ten opsigte van chemosensitiwiteit in hierdie sellyne gehad nie. In die BT-549 selle, het uithongering die persentasie dooie selle insiggewend verhoog in die groep wat KTU ondergaan het voor doxorubicin behandeling. Autofagie vloei was nie insiggewend verhoog tydens uithangering in hierdie groep nie wat moontlik kan beteken dat autofagie inderdaad ‘n rol in middelweerstandigheid in hierdie sellyne speel.

Gevolgtrekking:

Ter opsomming, die sellyne wat ‘n opregulering in autofagie vloei getoon het na 24 uur uithongering, is nie gesentitiseer vir doxorubicin in terme van seldood nie en het verder ook vermindering in doxorubicin-geinduseerde G2/M inperking getoon. Dit ondersteun die begrip dat autofagie opregulering kankerselle teen doxorubicin-geinduseerde sitotoksisiteit beskerm en middelweerstandigheid kan bewerkstellig. Om ‘n meer breedvoerige verstaan van hierdie fenomeen te verkry, word verdere studies aanbeveel wat die meganismes ondersoek waardeur autofagie beskerming van kankerselle teen chemoterapie verleen.

Soli Deo Gloria

Acknowledgements

To the Father Who created that which we seek to understand – I remain indefinitely in awe of You.

To my husband, Johan – your immense love and patience has carried me through this. I am profoundly grateful for you.

To my mom, Chelayne, dad, Neal, and sister, TeNeale – thank you for all your support and love. It has meant the world to me.

To my grandparents, Peter and Maureen, for all their prayer, love and care.

To Prof Engelbrecht, for your unwavering kindness, patience, faith and support. I am so grateful to you for everything.

To Dr André du Toit for all his effort, time and patience. To Mrs Lize Engelbrecht for all her kindness and assistance in CAF. To Dr Tanja Davis, for all her help.

To the Cancer Research Group, for all their help and advice.

To Prof Resia Pretorius and Prof Louise Warnich for their generosity and kindness in providing me with postgraduate funding.

Table of Contents

List of Figures

List of Tables

Abbreviations

A:

ADA	American Diabetes Association
ADP	adenosine diphosphate
AMP	adenosine monophosphate
AMPK	5'-AMP-activated protein kinase
APAF-1	apoptotic protease activating factor 1
APS	ammonium persulfate
AS160	Akt substrate of 160 kilodaltons
ATCC	American Type Culture Collection
Atg	autophagy related protein
ATGL	adipose triglyceride lipase
ATP	adenosine triphosphate

B:

BAX	Bcl-2-associated X protein
BAK	Bcl-2 homologous antagonist killer
BCL-2	B-cell lymphoma 2 protein
BCL-xL	B-cell lymphoma-extra large
BCAA	branched-chain amino acids
BRCA1	breast cancer type 1 susceptibility gene
BRCA2	breast cancer type 2 susceptibility gene
BSA	bovine serum albumin

C:

CANSA	Cancer Association of South Africa
CD4+	cluster of differentiation 4 protein positive
CDK	cyclin-dependent kinase
cm	centimeters
CoA	coenzyme A
CPT-1	carnitine palmitoyltransferase 1
CR	caloric restriction

D:

dH$_2$O	distilled H_2O
DMEM	Dulbecco's modified Eagle's medium
DNA	deoxyribonucleic acid
DSR	differential stress resistance
DSS	differential stress sensitisation
DTT	dithiothreitol

E:

E2F	E2 transcription factor
ECL	enhanced chemiluminescence
EDTA	ethylenediaminetetra-acetic acid
EGF	human epidermal growth factor
EGTA	ethylene glycol tetra-acetic acid

F:

F12	Ham's F12 nutrient mixture
FADD	Fas-associated death domain
FBS	foetal bovine serum
Fip200	FAK family-interacting protein of 200 kilodaltons

G:

g	grams
G_0	gap zero phase
G_1	gap one phase
G_2	gap two phase
G418	geneticin
GFP	green fluorescent protein
GLUT	glucose transporter

H:

HBSS	Hank's Balanced Salt Solution
HER2	human epidermal growth factor receptor 2

I:

IF	intermittent fasting
IGF-1	insulin-like growth factor 1
IR	insulin receptor
IRS1/2	insulin receptor substrate 1/2

K:

kDa	kilodalton
kg	kilogram

L:

l	liter
LC3	microtubule-associated protein 1A/1B light chain 3B
LKB1	liver kinase B1

M:

M	mitotic phase
MCT	monocarboxylate transporter
mg	milligram
ml	milliliter
mM	millimolar
µg	microgram
µL	microliter
µM	micromolar
mTOR	mammalian target of rapamycin

N:

Na_3VO_4	sodium orthovanadate
NAD(P)H	nicotinamide adenine dinucleotide phosphate
NaF	sodium fluoride

nm	nanometer
nM	nanomolar
NP-40	nonyl phenoxypolyethanol 40

P:

p53	tumour suppressor protein 53
p62	ubiquitin-binding protein p62
PARP	poly (ADP ribose) polymerase
PBS	phosphate buffered saline
PDK1	3-phosphoinositide-dependent protein kinase-1
PenStrep	penicillin/streptomycin
PI	propidium iodide
PI3K	phosphatidyl-inositol 3-kinase
PIP_2	phosphatidyl-inositol 4,5-bisphosphate
PIP_3	phosphatidyl-inositol 3,4,5-trisphosphate
PKB	protein kinase B
pM	picomolar
PMSF	phenylmethylsulfonyl fluoride
PTEN	phosphatase and tensin homologue
PVDF	polyvinylidene difluoride

R:

Rb	retinoblastoma protein
RIPA	radio-immunoprecipitation

RNase	ribonuclease
rpm	revolutions per minute
RPMI	Roswell Park Memorial Institute

S:

S	synthesis phase
SASP	senescence-associated secretory phenotype
SDS	sodium dodecyl sulphate
SDS-PAGE	sodium dodecyl sulphate and polyacrylamide gel electrophoresis
SEM	standard error of the mean
SQSTM1	sequestosome 1
STS	short-term starvation

T:

T2DM	type 2 diabetes mellitus
TCA	tri-carboxylic acid
TEMED	tetramethylethylenediamine
TBS-T	tris-buffered saline Tween
TGX	tris-glycine eXtended
TNBC	triple negative breast cancer
TNFα	tumour necrosis factor alpha

U:

ULK1	unc-51 like autophagy activating kinase 1

V:

V	volts

W:

WHO	World Health Organisation
WST1	water-soluble tetrazolium salt 1

Chapter 1: Literature Review

1.1 Cancer in context

1.1.1 Definition, global and local incidence, and risk factors

Cancer may be defined as the uncontrolled division of cells, leading to abnormal growth and differentiation, the invasion of surrounding tissues, and spread to distal parts of the body (WHO, 2018).

In 2018, a diagnosis of cancer was given to approximately 18 million people worldwide, with a further 9.6 million deaths having been caused by the disease (WHO, 2018). Globally, one in six people are predicted to develop cancer throughout their lifetime, with alarming increases in incidence over the past several decades (WHO, 2018).

With approximately 70% of cancer-related deaths occurring in low- to middle-income countries (WHO, 2018), South Africa is no exception to these high prevalence rates. In the South African context, one in seven men and one in eight women will be diagnosed with cancer during their lifetime (CANSA, 2019). The most common types of cancer, by sex, are as follows:

Males	**Females**
Prostate cancer (19,18%)	Breast cancer (21,78%)
Colorectal cancer (5,28%)	Cervical cancer (15,17%)
Lung cancer (4,87%)	Cancer of unknown primary origin (4,47%)
Cancer of unknown primary origin (4,73%)	Colorectal cancer (4,29%)
Kaposi sarcoma (2,66%)	Cancer of the uterus (3,32%)

Table 1.1: The most commonly diagnosed types of cancer in the South African population, by gender, as a percentage of all cancer diagnoses (CANSA, 2019).

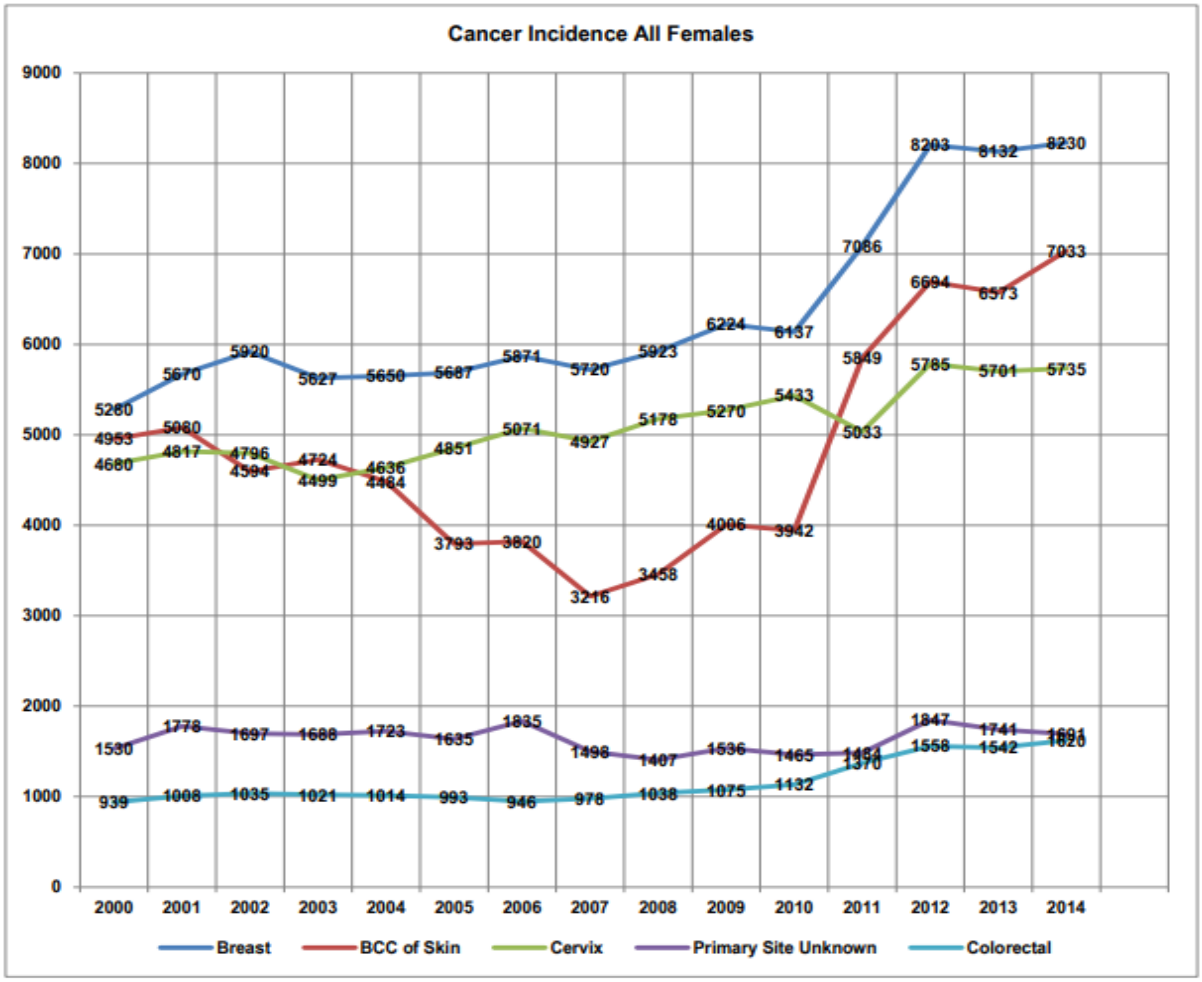

Figure 1.1: Increases in incidence of the top five cancers affecting women in South Africa (CANSA, 2014).

With breast cancer being the most commonly diagnosed cancer in South Africa (CANSA, 2014), and the fifth leading cause of cancer-related deaths worldwide (WHO, 2018), increasingly more research is being conducted in order to better understand the causes, risk factors, mechanisms and potential treatments for breast cancer. Currently, the disease is understood to be the result of complex interactions between a wide variety of known and unknown factors (Blackadar, 2016). The discovery of the *BRCA1* and *BRCA2* genes led to the understanding of a strong genetic component in certain breast cancers (Dumalaon-Canaria, *et al., 2*014). This was further elucidated by the identification of the *TP53* gene (Elmore, 2007). Besides heredity, diet, lifestyle and environmental factors also play an additional role in the development of breast cancer (Gonzalez & Riboli, 2010; CANSA, 2019). Protective factors include physical activity, maintaining a healthy body weight, and breast-feeding, while risk factors include overweight and obesity, sedentary behaviour, unhealthy dietary patterns, the

use of tobacco, and alcohol consumption (Gonzalez & Riboli, 2010; CANSA, 2019). Prolonged exposure to endogenous oestrogens, such as early menarche, or the late onset of menopause, represent non-modifiable risk factors, while the use of exogenous oestrogens (in the form of combined oral contraceptives and hormone replacement therapy) are considered modifiable risk factors with the same underlying mechanism (Kulkoyluoglu-Cotul, *et al.,* 2019).

1.1.2 Types of breast cancer and current treatment regimes

Breast cancer, in pathology, is quite diverse. Breast cancer may originate at different sites within the breast and is usually named accordingly. The most common types of breast cancer include those in the milk-producing lobules (lobular carcinoma *in situ* and invasive lobular carcinoma) as well as those in the milk-storing ducts (ductal carcinoma *in* situ and invasive ductal carcinoma) (Kulkoyluoglu-Cotul, *et al.,* 2019). Rare types of breast cancer include inflammatory breast cancer, Phyllode's tumours of the breast, Paget's disease of the nipple, and male breast cancer (Waks & Winer, 2019). Beyond classification according to the tumour site, breast cancer may be subtyped according to its molecular profile, that is, whether it expresses receptors on the cell surface for oestrogen, progesterone, or human epidermal growth factor receptor 2 (HER2) (Kulkoyluoglu-Cotul, *et al.,* 2019). Luminal A, luminal B, normal-like and HER2-enriched breast cancers all express one or more of the aforementioned receptors, and are thus candidates for targeted therapies (Foulkes, *et al.,* 2010). However, triple-negative breast cancer (TNBC) represents a class of cancers which does not express any of the three receptors listed. TNBC represents 10-20% of all breast cancer cases and is often more difficult to treat as targeted therapies are not indicated (Foulkes, *et al.,* 2010). TNBC is also more aggressive, shows resistance to treatment, and has the poorest prognosis of all the molecular subtypes of breast cancer (Foulkes, *et al.,* 2010).

In non-TNBC, targeted and hormonal therapies represent an efficacious method to attack cancer cells specifically, as they express the receptors to which the drugs can bind. However, when targeted treatments are not indicated, as in the case of TNBC, the three main therapeutic avenues include surgery, radiation therapy, and chemotherapy (Waks & Winer, 2019). The goal of surgery is to excise the tumour or

cancerous tissue, as well as some adjacent tissue, to prevent recurrence (Waks & Winer, 2019). Surgical procedures may involve removing the affected region (lumpectomy), or the entire breast (mastectomy) in more severe cases (Waks & Winer, 2019).

Radiation treatment involves the delivery of ionising beams to the tumour and surrounding tissues in order to kill malignant cells. Acute side effects include fatigue, nausea, vomiting and mucositis (Mahan, *et al*., 2012). Additionally, there has been significant controversy over whether radiation therapy may increase the relative risk of developing cancer in the future, due to the mutagenic effect of ionising radiation (Waks & Winer, 2019).

Chemotherapy, on the other hand, involves the use of cytotoxic drugs administered orally or intravenously. One of the most common chemotherapeutic agents indicated for the treatment of breast cancer includes doxorubicin, an anthracycline (Waks & Winer, 2019). Doxorubicin has two predominant mechanisms of actions whereby it eliminates cancer cells. The first involves the production of free radicals, which damage multiple cellular components: lipids in organelle and cell membranes, intracellular proteins, and DNA (McClendon & Osheroff, 2007). The second is through more targeted damage that is specific to DNA. Doxorubicin renders DNA dysfunctional by intercalating into the strands and prevents both DNA repair and replication by inhibiting the enzyme topoisomerase II (McClendon & Osheroff, 2007). When DNA unwinds for transcription, supercoils form in the strands that could lead to tangles, or superhelical twists. In order to relieve this torsional stress, topoisomerase II creates a transient double-stranded break in the DNA, and then passages the double-stranded DNA once the supercoil is relaxed (McClendon & Osheroff, 2007). Inhibition of this process prevents DNA replication and may lead to mitotic cell death. Ultimately, the drug targets rapidly dividing cells and promotes apoptosis with the goal of eliminating the cancer cells (Waks & Winer, 2019). Chemotherapy, however, has several disadvantages, as there may be acute or chronic side effects of varying severity. Typical side effects include nausea, vomiting, diarrhoea, mucositis, hair loss, fatigue and headaches (Mahan, *et al*., 2012). More severe side effects include a drastic loss of lean body mass which can increase morbidity and result in poorer clinical outcomes; neutropenia which can impair immune function; thrombocytopenia, which can facilitate excessive bleeding and bruising; and arrhythmias (Mahan, *et al*., 2012). The chronic

side effects of chemotherapy include osteoporosis, cardiac hypertrophy, cachexia and cardiac failure (Safdie, *et al*., 2009).

1.1.3 Rationale and potential for adjuvant therapies

In summary, therapies are generally only indicated if the oncologist or clinician considers the risks as outweighed by the potential benefit, as all modes of treatment present with both advantages and disadvantages. For this reason, adjuvant therapies have become an increasingly popular area of research over the past two decades (Chew, 2001). Adjuvant therapies are therapies which are used prior to or alongside surgery or other cancer treatments in order to: a) reduce the acute side effects of the main treatment, b) to protect the patient from severe and chronic complications, or c) to heighten the sensitivity of malignant cells to treatment, thereby increasing treatment efficacy (Chew, 2001). Adjuvant therapy has been described as a “helping hand”, not to replace existing therapies, but rather to render them more effective (Chew, 2001).

As of late, there has been a surge in the branch of research concerned with dietary adjuvant therapies. Considering the role played by obesity, dietary factors and metabolic alterations in the pathogenesis and propagation of cancer (Berger, 2014; Gonzalez & Riboli, 2010), metabolic interventions may thus hold the potential to serve as an adjuvant therapy alongside the treatment of cancer. Additionally, as the body of literature surrounding cancer metabolism has expanded, so too has the potential for targeting these metabolic vulnerabilities of cancer cells. However, in order to fully appreciate the potential for a dietary adjuvant therapy, the metabolism of normal tissue must be explored for the purpose of highlighting the distinguishing features of cancer metabolism.

1.2 Metabolism and molecular pathways during the fed state

1.2.1 The digestion and metabolic fate of lipids

Typically, the majority of systemic daily energy requirements are met by exogenous fuels. A typical meal contains different forms of carbohydrates, protein and lipids, all of which are macromolecules with large molecular weights (Berg, *et al.*, 2002).

Lipids are physically and chemically digested to yield monoacylglycerides and free fatty acids. These molecules are absorbed in the intestine in the form of micelles, and transported in chylomicrons through circulation to the liver, skeletal muscle and adipose tissue for either catabolism or storage (Sherwood, 2010). While lipids may be used for functional roles, such as to be incorporated into the lipid bilayer of organelles and cell membranes, as signalling molecules or to partake in myelination of nervous tissue, the majority of ingested lipids are stored in adipocytes or used immediately as a source of fuel (Stipanuk & Caudill, 2013).

1.2.2 Protein and carbohydrate metabolism, and consequent effects on pro-growth pathways

In terms of protein metabolism, small peptides and single amino acids are yielded from mechanical and chemical digestion, and are absorbed through the intestinal border (Berg, *et al.*, 2002). Once in the blood stream, amino acids are either used for protein synthesis, or for energy production by tissues that can utilise amino acids, such as the kidneys and intestines. The remainder are converted to glucose through the process of gluconeogenesis in the liver (Stipanuk & Caudill, 2013).

Dietary carbohydrates are typically consumed in the form of starches and sugars, that is, polysaccharides and disaccharides. In the stomach and duodenum, mechanical and enzymatic breakdown occurs until monomers are yielded (Sherwood, 2010). Here, they can be absorbed across the intestinal border into circulation, where they bring about their glycaemic effect. While serum glucose is maintained homeostatically during the post-absorptive, or fasting, state at 4-5 mM, postprandial glucose levels usually peak at approximately 8 mM (American Diabetes Association, 2001). This rise in glucose above homeostatic levels triggers the release of insulin by the β-cells of the pancreas, so that the baseline insulin level of <174 pmol/L may rise to between 208 and 1900 pmol/L during the postprandial period (Melmed, *et al*., 2016). It should be noted that amino acids from protein digestion may also elevate insulin levels, but that this effect is more modest than that of carbohydrates. Notably, the rise in serum insulin stimulates the production of insulin-like growth factor 1 (IGF-1) in the liver (Cangemi, *et al.,* 2016). This rise in insulin and IGF-1 favours anabolic pathways and facilitates protein synthesis, cell growth and proliferation (Cangemi, *et al.,* 2016). Furthermore, insulin also inhibits lipolytic pathways by suppressing hormone-sensitive lipase. This

prevents the release of free fatty acids and monoacylglycerides from adipocytes into circulation, making them less available for metabolic processes (Sherwood, 2010).

On a cellular level, phosphatase-and-tensin homologue (PTEN) keeps insulin receptor substrates 1 and 2 (IRS1/2) inactive through inhibition in the absence of insulin binding. However, during postprandial conditions, insulin binds to its receptor, resulting in the phosphorylation and activation of IRS1/2 (Cantley, 2002; Hemmings & Restuccia, 2012). This allows binding from phosphatidyl-inositol 3-kinase (PI3K), a central and fundamental regulator of cellular survival, growth and proliferation (Cantley, 2002). The result of PI3K's activity is the recruitment and activation of pyruvate dehydrogenase kinase 1 (PDK1) and protein kinase B (PKB), also known as Akt. This consequently inhibits AS160, thereby lifting the inhibition of glucose transporter 4 (GLUT4) translocation. These transporters are then able to embed themselves in the cell membrane and facilitate glucose entry (Cantley, 2002). Insulin also activates hexokinase, the first enzyme in the glycolytic pathway. Hexokinase is responsible for the conversion of glucose to glucose-6-phosphate. This reduces the intracellular glucose concentration thereby promoting additional glucose uptake (Stipanuk & Caudill, 2013).

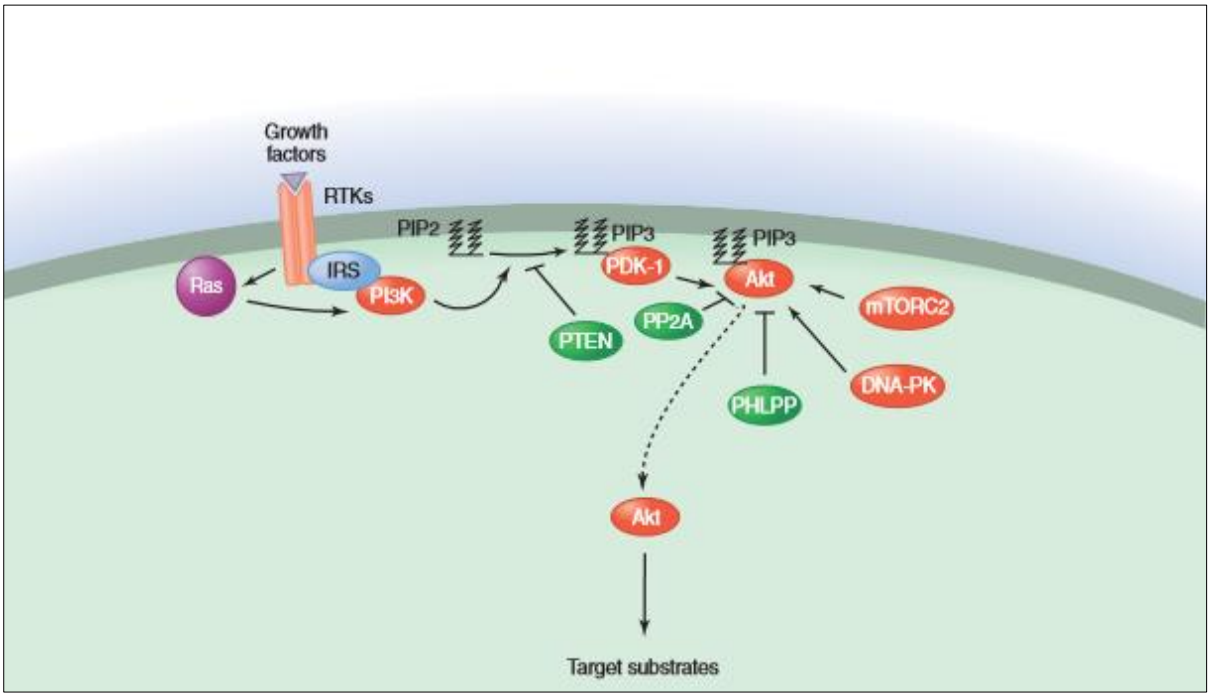

Figure 1.2: The insulin receptor pathway (Hemmings & Restuccia, 2012).

Ultimately, the systemic and intracellular responses during the postprandial period result in the reduction of serum glucose through the uptake of glucose into cells for utilisation or storage (Cantley, 2002).

1.2.3 Metabolic flexibility and the production of ATP

Considering the competitive effect between metabolites, it should be noted that most physiological tissues can use either glucose or lipids in some form or another. With the exception of the retina, renal medulla and erythrocytes, which are all obligatory glycolytic cells, all other tissues can utilise fuel sources other than glucose. The brain, skeletal muscle, adipose tissue, intestine and kidneys all show a strong preference for glucose but can rely on alternate fuels when glucose availability is insufficient (Berg, *et al.*, 2002). The brain can utilise ketone bodies produced by the liver during starvation and, to a much lesser extent, lactate. Skeletal muscle is able to consume free fatty acids, triacylglycerols, branched-chain amino acids (BCAA) and lactate. Adipose tissue can catabolise triacylglycerols for energy, the intestine can use glutamine, and the kidney free fatty acids, ketone bodies, lactate and glutamine. Thus, the majority of tissues are able to switch between lipolytic and glycolytic pathways (Mahan, *et al*., 2012).

Regardless of the preferred metabolite, the ultimate goal of catabolism is the production of adenosine triphosphate (ATP) to power cellular processes. When glucose is the preferred metabolite, degradation occurs through one of two pathways – aerobic or anaerobic (Sherwood, 2010). Both pathways share a common entry point, namely glycolysis, whereby glucose is converted through a series of enzymatic reactions in the cytoplasm to form pyruvate (Sherwood, 2010). After glycolysis, the anaerobic and aerobic pathways diverge. During anaerobic respiration, which is usually only favoured in the absence of oxygen, pyruvate is converted to lactate. This process is considerably less efficient than the aerobic pathway as it produces only two ATPs per molecule of glucose, while the latter produces approximately 38 (Sherwood, 2010). Additionally, the lactate yielded by the anaerobic pathway would need to be removed from the cell and transported to the liver before any further metabolic advantage is reached (Berg, *et al.*, 2002).

Notably, ATP can also be produced from fatty acids. When the need arises, fatty acids are taken up into the cell, modified and transported via carnitine palmitoyltransferase

1 (CPT-1) into the mitochondria. Once inside, the fatty acid undergoes beta-oxidation, a process whereby pairs of carbon atoms are cleaved to produce acetyl-CoA. These acetyl-CoA molecules are then shuttled into the tricarboxylic acid (TCA) cycle as the pathway converges with that of glucose oxidation, resulting in the production of ATP (Stipanuk & Caudill, 2013).

1.3 Metabolism and molecular pathways during starvation

1.3.1 Acute starvation and endogenous energy sources

After the postprandial period, which lasts approximately two hours in duration, serum glucose begins to fall as exogenous sources have been fully utilised. However, it is essential that serum glucose be maintained at homeostatic levels, especially for the survival and functioning of obligatory glycolytic cells. Thus, as serum glucose begins to fall, so too does the production and secretion of insulin by the pancreatic β-cells, as mediated by negative feedback (Berg, *et al.*, 2002). With serum insulin now at modest levels, the inhibition of glycogenolysis is reversed. Glucagon is produced and released by pancreatic α-cells, which allows glycogen to be catabolised to provide the body with glucose. While there can be substantial amounts of glycogen stored in the liver and muscle tissues, these stores are not interminable and are often depleted within 18-24 hours of starvation. The body is thus tasked with finding an alternative source of glucose, and its next resort is to initiate muscle catabolism and gluconeogenesis (Mahan, *et al.*, 2012). During this stage of starvation, the upregulation of catabolic hormones involved in glycogenolysis becomes even more evident, and the breakdown of skeletal muscle commences. Cortisol and catecholamines, like epinephrine and norepinephrine, instigate skeletal muscle catabolism in order to release amino acids into the blood stream. These metabolites are transported to the liver and kidneys where they are deaminated and converted to α-ketoglutarate and pyruvate, then to oxaloacetate, and, eventually, to glucose (Mahan, *et al.*, 2012). This process, however, is metabolically demanding and unsustainable, as muscle tissue is necessary to sustain basic functions, such as breathing, digestion and cardiac output. Thus, the continuation of muscle catabolism for the purposes of energy production

would prove detrimental, and after 24-48 hours, adaptive metabolic shifts occur to enable lipid stores to be utilised (Stipanuk & Caudill, 2013).

1.3.2 Adaptations to long-term starvation

Due to the lower levels of serum insulin, hormone-sensitive lipase is relieved from its inhibition. Fatty acids are cleaved from triglycerides within adipocytes and are released into the blood stream to act as the predominant source of energy. Skeletal and cardiac muscle cells, liver tissue and adipocytes all switch to lipolytic pathways, rather than glycolytic ones, and beta-oxidation becomes the main source of acetyl-CoA for ATP production within those cells (Stipanuk & Caudill, 2013).

Although the shift to lipids as a fuel source for metabolically flexible tissues reduces the need for glucose, it is not sufficient to prevent significant muscle loss. The brain and nervous system still require 110-120 g of glucose per day for adequate functioning, which equates to 160-200 g of protein, or approximately 1 kg of muscle tissue (Mahan, *et al.*, 2012). If this were to continue, the effects would be devastating as not only skeletal muscle, but cardiac and smooth muscle would begin to waste. As a last resort, and in accordance with the pro-lipolytic metabolic profile, ketogenesis commences to provide the brain with an alternate fuel source (Berg, *et al.*, 2002).

Through this, the consumption of glucose is reduced, and ketones provide a suitable substitute for 80% of the glucose previously required by the brain and nervous system. The remaining 20%, along with the glucose needed to sustain obligatory glycolytic cells, represent the only portion of glucose consumption for which there can be no substitute. Notably, much of this is synthesised from the glycerol backbone of triglycerides released during lipolysis, and amino acids, in almost equal proportions (Berg, *et al.*, 2002).

By this stage, the body has made its final metabolic adaptation, and, provided fluid intake is sufficient, this may endure for several days. However, although this is much more sustainable than previous stages of starvation, is still only expected to be possible for a maximum of 40 days before death becomes inevitable (Mahan, *et al.,* 2012).

1.4 Intracellular adaptations to starvation

1.4.1 Intracellular metabolic signalling pathways

As macronutrients become scarce, systemic changes, such as those listed above, enable survival through both acute and chronic starvation. However, there are also several intracellular mechanisms which enable this adaptation to take place, enabling cellular energetics to compensate for metabolic stress.

Firstly, nutrient deprivation, in the form of a high AMP/ATP ratio is sensed by a protein known as liver kinase B1 (LKB1). As the name suggests, this protein is abundant in liver hepatocytes, but is found in cells throughout the body. LKB1 activates 5'-AMP-activated protein kinase (AMPK), which is known as the "nutrient sensor" of the cell and the master regulator of energy metabolism (Kuhajda, 2008). AMPK activates unc-51-like kinase 1 (ULK1), a protein required for the formation of pre-autophagosomes, which is discussed in more detail below. Additionally, AMPK phosphorylates and inactivates the mammalian target of rapamycin (mTOR), consequently lifting the inhibition on autophagy and preventing protein synthesis (Mizushima & Komatsu, 2011). Furthermore, AMPK also stimulates adipose triglyceride lipase (ATGL), which enables the cleavage of fatty acids from triglycerides within adipocytes and prevents fatty acid synthesis. Overall, AMPK mobilises existing cellular stores to release metabolites to correct the AMP/ATP ratio, thereby restoring homeostasis to intracellular energetics (Kuhajda, 2008).

Another pathway implicated in the cellular response to starvation is that of PI3K and Akt. During the fed state, extracellular insulin signalling leads to the activation of IRS1/2, and consequently, PI3K and Akt (Hemmings & Restuccia, 2012) This favours anabolic pathways, such as glycogen synthesis, fatty acid synthesis and protein synthesis. In the absence of insulin signalling, PI3K and Akt are downregulated, along with their downstream targets, such as mTOR (Hemmings & Restuccia, 2012). Thus, during starvation, mTOR activity is dampened, both by the activation of AMPK and the inactivation of Akt. The result is the inhibition of protein synthesis and the upregulation of autophagy (Kuhajda, 2008).

1.4.2 Types of autophagy, autophagic pathways and functions

Three different types of autophagy exist, all of which employ lysosomal activity to degrade intracellular proteins (Glick, *et al.*, 2010). Chaperone-mediated autophagy involves the escorting of target proteins by chaperone proteins to the lysosome for degradation (Mizushima & Komatsu, 2011). In micro-autophagy, the lysosomal membrane forms an invagination to take up proteins from the cytosol directly. However, the majority of protein degradation and recycling is owed to macro-autophagy – a sort of "bulk" degradative system (Singh & Cuervo, 2012).

Macro-autophagy (hereafter referred to as "autophagy") refers to the intracellular degradation of proteins and organelles through a highly organised and conserved pathway involving autophagosomes (Mizushima & Komatsu, 2011). Autophagy is induced by a variety of stressors, such as cellular and endoplasmic reticulum stress, hypoxia, radiation, high temperatures, toxic compounds, and most notably, nutrient deprivation. Under these conditions, and in response to a high AMP/ATP ratio and consequent AMPK signalling, the stimulus for autophagy is received (Mizushima & Komatsu, 2011).

Despite being a process employed to degrade existing proteins, the process of autophagy begins in the endoplasmic reticulum with the synthesis of proteins necessary for the formation of pre-autophagosomes (Glick, *et al.*, 2010). These include ULK1, autophagy related protein 13 (Atg13), Atg101 and Fip200. These proteins, along with a cup-shaped section of membrane, bud off the endoplasmic reticulum to form the pre-autophagosome. As this grows and matures, Beclin 1 is added and activated through phosphorylation by ULK1. In this state, Beclin 1 is able to phosphorylate phosphatidylinositol 4,5-bisphosphate (PIP_2) to phosphatidylinositol 3,4,5-trisphosphate (PIP_3), similar to the actions of PI3K (Mizushima & Komatsu, 2011). The increased ratio of PIP_3 to PIP_2 results in the downstream recruitment of the ubiquitin-binding protein p62 and microtubule-associated protein 1A/1B light chain 3B-I (LC3-I). Another protein complex, consisting of Atg5, Atg16 and Atg12, is added to the membrane of the pre-autophagosome. LC3-I is converted to LC3-II through the addition of phosphatidylethanolamine during the extension of the phagophore, and this indicates autophagosomal maturation. By the time the autophagosome has fully matured, it is ready to fuse with the lysosome to form an autophagolysosome, or

autolysosome (Glick, *et al.*, 2010). Along with other proteins, Rab7 facilitates the binding of the membranes and the fusing of these two organelles – the end goal being intracellular digestion. Once inside the autolysosome, proteins undergo acidic and enzymatic degradation (Singh & Cuervo, 2012).

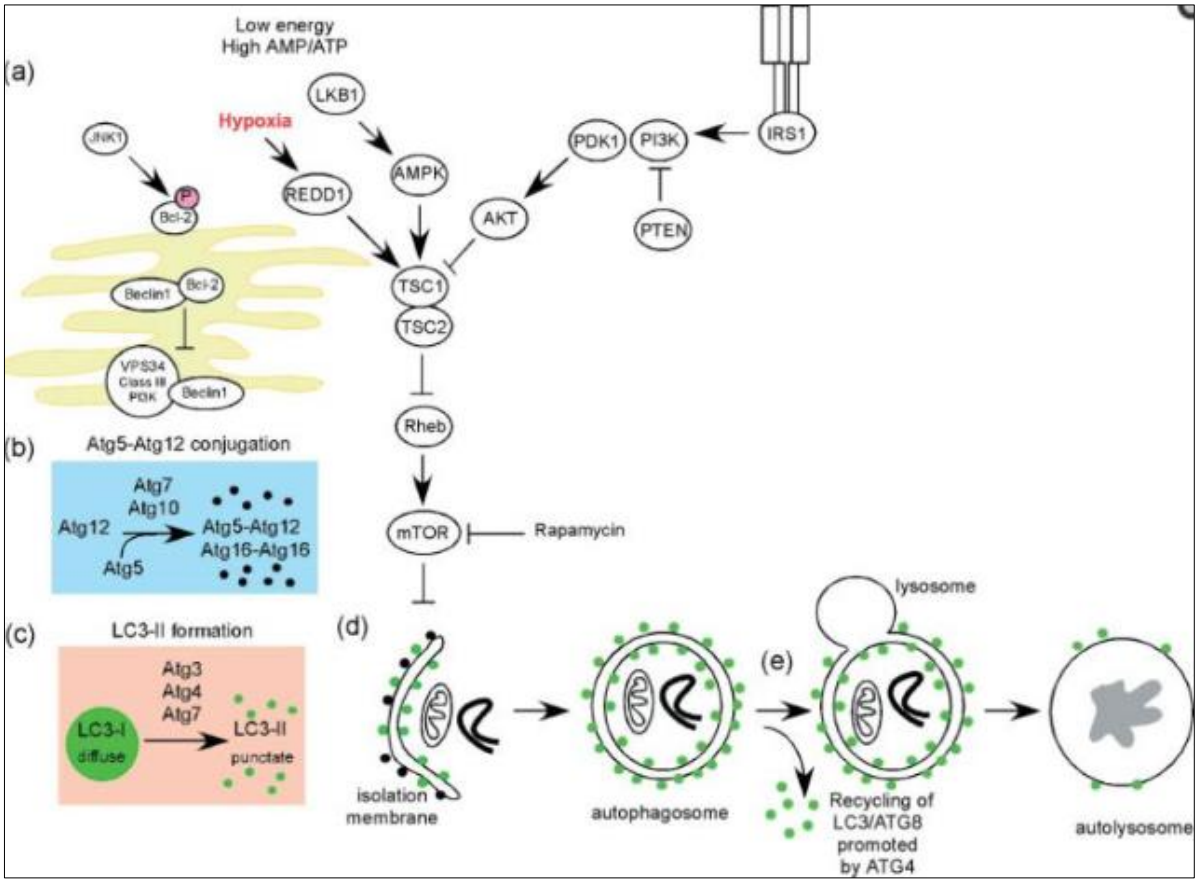

Figure 1.3: The formation of the autophagosome and fusion with the lysosome (Mizushima & Komatsu, 2011).

The ultimate purpose of autophagy is to make provision during nutrient stress and to remove unwanted proteins and/or organelles (Singh & Cuervo, 2012). However, in the event that metabolic homeostasis cannot be reached, and the cell experiences more significant nutrient stress, the cell is forced to resort to more extreme measures, such as cell cycle arrest.

1.4.3 The cell cycle and growth arrest

Many cell types, such as neurons, adipocytes and myocytes, do not undergo mitosis after fully differentiating, and exist in the growth zero or gap zero phase (G_0) (Terzi, *et al.*, 2016). This refers to a state wherein the cells remain viable and metabolically active but are found outside of the cell cycle and do not actively divide (Schaefer,

1998). The G_0 phase also includes cells that are in a quiescent state, which may be described as a “reversible, non-proliferating state” (Yao, 2014). Tissues that require mitotic cell division for regenerative purposes only may contain many cells in G_0, which may re-enter the cell cycle to produce additional daughter cells when needed (Yao, 2014).

However, apart from quiescent or terminally differentiated cells, most other cells in the body pass through the cell cycle and undergo mitotic cell division (Blagosklonny, 2011). The cell cycle consists of several, distinct phases: During the first gap phase (G_1), which follows immediately after mitotic cell division, the cell produces proteins and organelles that are required for DNA synthesis. The G_1 phase is followed by the synthesis phase (S), during which a complete copy of cellular DNA is produced (Cooper, 2000). The second gap phase (G_2) is marked by additional growth and the reorganisation of intracellular structures as the cell begins to prepare for mitotic cell division (Cooper, 2000). The first gap phase, synthesis phase, and second gap phase are collectively known as “interphase” – the first, and longest, stage of mitotic cell division. The end of the second gap phase signals the cessation of interphase, and mitosis (M) begins (Schafer, 1998).

Several regulatory mechanisms exist to ensure controlled and appropriate cell division. These include negative and positive regulators of the cell cycle which allow progression through the checkpoints and facilitate transition between stages (Barnum & O’Connell, 2014). The former includes tumour suppressor proteins such as retinoblastoma protein (Rb), p53 and p21 (Terzi, *et al.*, 2016). These can induce cell cycle arrest, often by inhibiting the positive regulators to prevent passage between stages (Blagosklonny, 2011). On the other hand, the cell cycle is positively regulated by the expression and degradation of four main cyclins which bind to the relevant CDKs forming cyclin-CDK complexes (Bar-On, *et al.*, 2007).

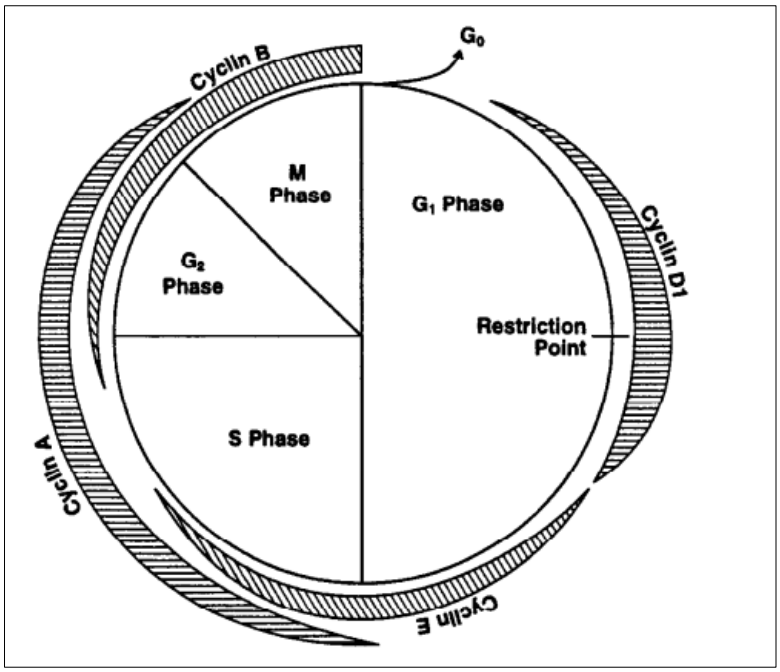

Figure 1.4: The relative intracellular expression of cyclins in each stage of the cell cycle (Schafer, 1998).

For a cell to progress through a checkpoint, the negative regulators of the cell cycle must be absent or inactive while the positive must be present and active (Barnum & O'Connell, 2014). Rb, for example, is typically bound to E2 transcription factor (E2F), which, when unbound, promotes the transcription of proteins that facilitate the G_1/S transition (Yao, 2014). In order for the cell to progress to the S phase, Rb must be inhibited to reverse its suppression of E2F (Yao, 2014). This is accomplished by the complexes formed between cyclin D and both CDK4 and CDK6, as well as cyclin E and CDK2. E2F then promotes the upregulation of cyclin A, allowing the cell to pass through the G_1/S checkpoint and enter into the S phase. This will only occur if the cell meets the criteria for this checkpoint, as it is assessed for adequate size, nutrient availability and DNA integrity (Terzi, *et al.*, 2016).

In the nucleus, cyclin A-CDK2 complexes initiate DNA replication, and the cell enters the G_2 phase upon completion. At the end of the G_2 phase, this DNA is examined, and the cell passes through the G_2 checkpoint (Barnum & O'Connell, 2014). However, if the DNA is damaged or incomplete, the cell may undergo temporary cell cycle arrest to repair or complete its DNA (Bar-On, *et al.*, 2007).

During the third checkpoint, which occurs during the metaphase of mitosis, the cell is checked for the appropriate attachment of the sister chromatids to spindle microtubules. If this is sufficient, the cell will complete mitotic cell division (Caccuri, *et*

al., 2019). Dysregulation of the cell cycle is commonly observed in cancer cells, resulting in uncontrolled mitotic cell division (Sun, *et al.*, 2014). Not only do cancer cells have an infamously high rate of cell division, but poor control over the progression between stages resulting in the resistance of both cell cycle arrest and senescence (Sun, *et al.*, 2014). While benign cultured cells have been reported to enter growth arrest in response to starvation (Schafer, 1998), the effect of starvation on cancer cells is much less clear.

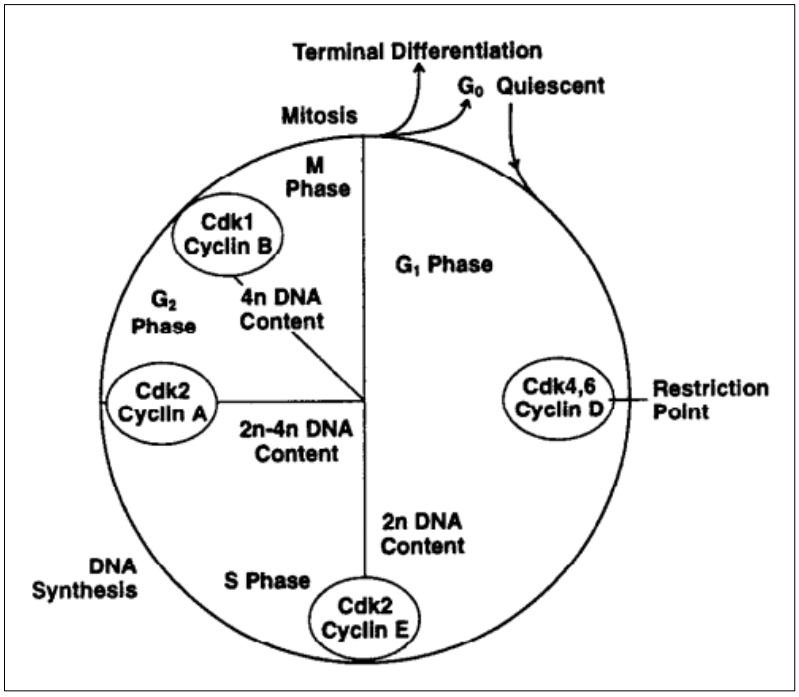

Figure 1.5: Phases of the cell cycle, and associated cyclins and CDKs (Schafer, 1998).

Besides growth arrest as a consequence of starvation, DNA damage or mutation may also cause cells to arrest the cell cycle for the purpose of repair. However, if the DNA damage is severe, or cells cannot progress through the cell cycle, they become stressed and may induce apoptosis (Caccuri, *et al.,* 2019).

1.4.4 Apoptotic triggers, pathways, and mechanisms

Apoptosis may be described as an organised and highly conserved process of programmed cell death (Savitskaya & Onishchenko, 2015). This occurs in a wide array of circumstances and is essential to maintain normal physiological functioning and ensure survival. For instance, apoptosis ensures survival by eradicating old and dysfunctional cells in almost all physiological tissues, as well as cells hosting infectious

pathogens and those showing cancerous activity (Elmore, 2007). This helps the body to regulate immune functioning, to prevent the spread of infection, to eradicate malignancies and to function optimally as the quality of cells are maintained. Apoptosis may be divided into three continuous steps, with the start of the process depending entirely on the cause of initiation (Elmore, 2007).

1. Initiation: this is the first step of apoptosis, and may be initiated through one of two pathways:
    a. Extrinsic pathway: As the name suggests, the extrinsic pathway is activated by the binding of extracellular tumour necrosis factor α (TNFα) and Fas-ligands to receptors on the cell surface. TNFα is a cytokine produced by activated macrophages, natural killer cells and CD4+ cells, while Fas-ligands are found on the surfaces of T-lymphocytes (Savitskaya & Onishchenko, 2015). Upon binding, the stimulated receptor in the cell membrane activates an intracellular death domain. The consequent recruitment and activation of Fas-associated death domain (FADD) leads to the cleavage and activation of pro-caspase 8, which, in turn, leads to the activations of caspase 3 and the self-amplifying caspase cascade (Elmore, 2007).
    b. Intrinsic pathway: When homeostasis within the cell is severely disrupted and recovery is unlikely, as in the case of severe nutrient stress or hypoxia, the mitochondria sense this disruption, and the mitochondrial membrane becomes permeabilised. Similarly, if the cell experiences DNA damage beyond repair, p53, a potent tumour suppressor, is activated, resulting in the mobilisation of Bcl-2-associated X protein (BAX) in the cytosol. BAX and Bcl-2 homologous antagonist killer (BAK) are pro-apoptotic proteins that are bound to anti-apoptotic proteins, such as B-cell lymphoma 2 protein (BCL-2) and B-cell lymphoma-extra large (BCL-xL), under normal circumstances (Savitskaya & Onishchenko, 2015). Should p53 induce the intrinsic pathway, and pro-apoptotic signals exceed that of anti-apoptotic signals, these proteins are released and form channels in the mitochondrial membrane. Following permeabilisation of the mitochondrial membrane, cytochrome C leaches out of the mitochondria and is free to bind to apoptotic protease activating factor 1 (APAF1) and pro-caspase 9 to form the apoptosome in the cytosol. This activates the caspase cascade, starting with the activation of caspase 9

(initiator caspase) and converging with the extrinsic pathway through cleavage of the effector caspases (Elmore, 2007).

2. Execution: After initiation by the extrinsic or intrinsic pathways, caspase 3 is cleaved, which, in turn, cleaves poly (ADP-ribose) polymerase, or PARP. This is a DNA repair enzyme that, when cleaved, can no longer carry out its function (Savitskaya & Onishchenko, 2015). The immobilisation of PARP allows DNA fragmentation to occur, while endonucleases and proteases degrade cytoskeletal proteins, resulting in cellular degradation. By this stage, the cellular morphology typically represents apoptosis as shrinkage, pyknosis, karyorrhexis and the formation of apoptotic bodies is observed (Elmore, 2007).
3. Phagocytosis: The final step in apoptosis involves only the removal of apoptotic bodies by phagocytic cells. This is stimulated by the presentation of ligands on the cell membrane for phagocytic binding (Savitskaya & Onishchenko, 2015).

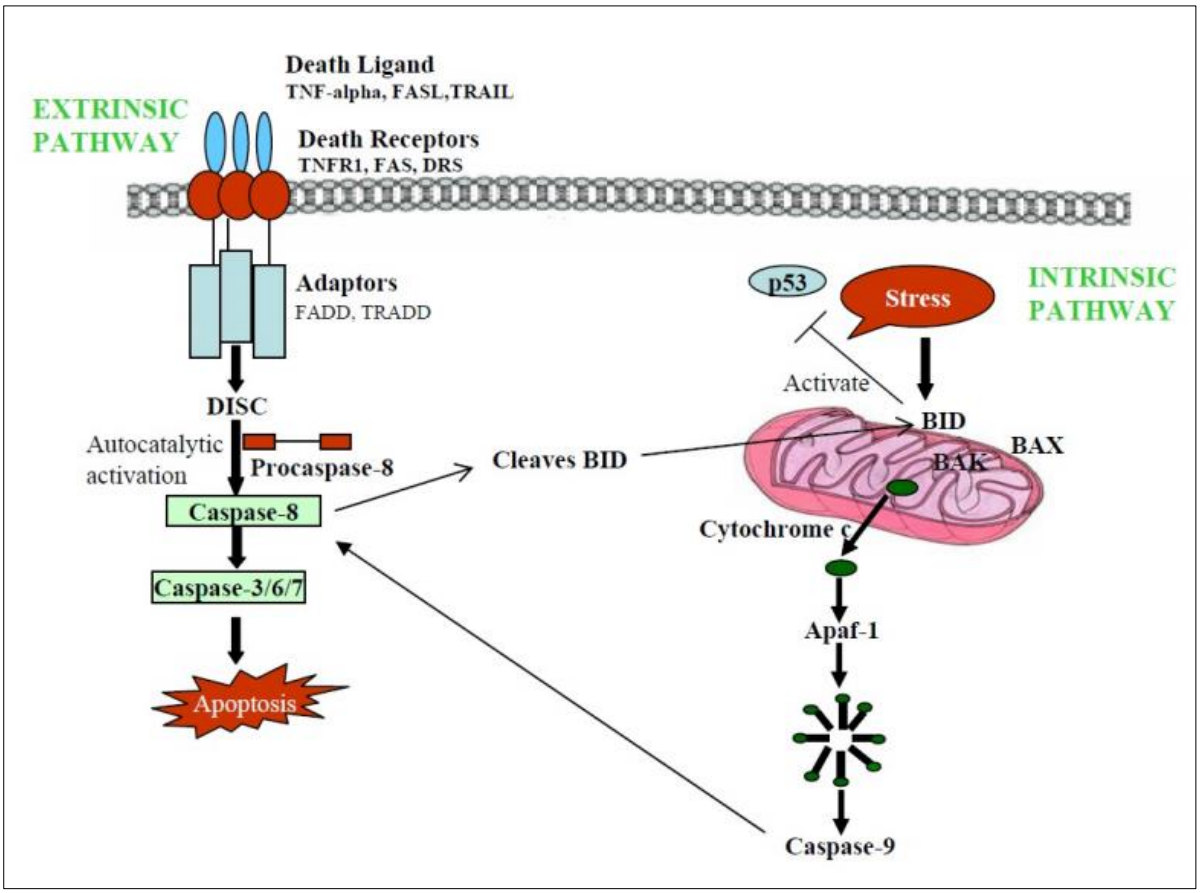

Figure 1.6: The convergence of apoptotic pathways (Rampal, et al.*, 2012)*

Despite the negative connotations carried by the concept of cell death, apoptosis is adaptive in nature, and intercepts the potential crisis that would result if defective cells

were permitted to survive (Savitskaya & Onishchenko, 2015). However, cancer cells are able to evade this programmed cell death through multiple adaptive mechanisms. These may include the downregulation and upregulation of pro-apoptotic and anti-apoptotic genes, respectively; through the production of growth factors; and by ensuring a consistent and adequate nutrient supply (Rampal, et al., 2012).

1.5 Cancer metabolism and hallmarks of cancer

1.5.1 Procurement of glucose and growth signals

To avoid metabolic stress and unnecessary cell death, the majority of tissues regulate glucose homeostasis through the intelligent co-ordination of several mechanisms. Cancer cells, on the other hand, surpass this, in their nearly aggressive procurement of glucose. Firstly, benign cells express appropriate quantities of the relevant insulin receptors (IRs) on their cell membrane, which mediate the controlled influx of glucose into insulin-dependent tissues. However, several studies demonstrate an overexpression of IRs on malignant cell surfaces (Frasca, *et al.,* 2008). Up to 80% of breast cancers express above-average levels of IRs. Furthermore, up to 20% show as much as a ten-fold increase in IR expression (Frasca, *et al.,* 2008).

Secondly, GLUTs in benign cells are specifically expressed to sustain the needs of the cell. However, in cancer cells, overexpression of several types of GLUTs have been reported in various malignancies (Adekola, *et al.*, 2012). In addition to GLUT4, an insulin-dependent GLUT, the insulin-independent GLUT1-3 are expressed and ensure unlimited and unconditional uptake of glucose (Adekola, *et al.*, 2012). These adaptations in receptors and glucose transporters represent only two mechanisms whereby malignant tissues ensure a constant supply of glucose, with additional adaptations existing within the cell.

1.5.2 Hypermetabolism and *de novo* synthesis of biomolecules

On an intracellular level, cancer is unusually metabolically active, and has an exceptionally high consumption rate of nutrients for its relative tissue size (Cathcart, *et al.,* 2017). Due to the aforementioned adaptations in GLUTs, cancer cells have

exceptionally high rates of glucose uptake, which in turn, accounts for its high levels of utilisation (Cathcart, *et al.,* 2017).

Once inside, there are two potential metabolic fates for the plethora of glucose molecules flooding into the cell: *de novo* synthesis of other metabolites, or utilisation for energy (Cathcart, *et al.,* 2017). For cancer cells to sustain their dynamic level of functioning, growth and replication, all sorts of macromolecules are needed: glucose, lipids, nucleic acids and amino acids. These molecules are used, not only for energy, but to provide structural components for malignant cell division (Longo & Fontana, 2009). New nucleic acids and amino acids may be synthesised from the abundance of glucose within the cell and organised into new strands of DNA and proteins, respectively; synthesised lipids may be used to form new cell membranes and organelles. Ultimately, the *modus operandi* of cancer cells is to divide and conquer the surrounding microenvironment, while intracellular metabolic pathways must make provision for this (Longo & Fontana, 2009).

1.5.3 The Warburg Effect in cancer

Besides the shuttling of glucose molecules into pathways for the *de novo* synthesis of macromolecules, glucose metabolism in cancer is notoriously counterintuitive. In hypermetabolic cells, optimal use of glucose to obtain the maximum number of ATP per molecule would be expected. This is, however, not always the case in cancer cells. The infamous Warburg Effect was described as early as the 1920's, wherein cancer cells utilise glucose, not through oxidative pathways, but through what is described as "anaerobic glycolysis" – glycolysis and the conversion of pyruvate to lactate, even in the presence of oxygen (Bonucelli, *et al.,* 2010). This favouring of anaerobic respiration is metabolically inefficient because, as previously described, the process yields only two molecules of ATP per glucose, while aerobic respiration holds the potential for approximately 38 (Stipanuk & Caudill, 2013).

However, despite the metabolic inefficiency of this pathway, it is postulated to offer a survival advantage to the tumour cells beyond that of ATP production. Interestingly, some research indicates that lactate may support tumour growth and metastasis (Bonucelli, *et al.,* 2010). Additionally, the production of lactate yields hydrogen ions, and when this is expelled from the cell, it can be used to acidify the extracellular matrix. An acidic microenvironment weakens intercellular adhesion in the surrounding tissues

and enables invasion for further growth of the solid tumour (Kato, *et al.,* 2013). In addition, degradation of the surrounding structure aids in the development of additional vasculature – a process known as angiogenesis (Kato, *et al.,* 2013). This is essential to maintain continual tumour growth, as parts of the tumour are far from an adequate blood supply. The proximity of the tumour to vasculature also enables metastasis, or, the spreading of malignant cells from its original site to distal sites around the body (Kato, *et al., 2*013). Ultimately, this abnormal and counterintuitive selection for anaerobic glycolysis, and the consequent yielding of lactate, may convey several advantages to the tumour itself. Indeed, high lactate levels have been correlated with increased tumour aggression, metastasis, tumour recurrence and a poorer prognosis in patients (Kato, *et al., 2*013).

1.5.4 Altered metabolic signalling and levels of autophagy in cancer cells

In terms of signalling pathways, several studies have reported mutations in pro-survival genes in a wide array of human cancers (Kuhajda, 2008; Yuan & Cantley, 2008; Courtney, *et al., 2*010). This can result in significant over- or under-expression of specific functional proteins, enabling increased cell survival, growth and proliferation. Besides adaptations in insulin and IGF-1 receptors, many tumours show independent adaptations in the PI3K/Akt pathway, with both the former and the latter being overexpressed in several cancer cell lines (Yuan & Cantley, 2008; Courtney, *et al., 2*010). Additionally, PTEN, a potent tumour suppressor gene, is often mutated in tumours, rendering it partially or completely dysfunctional (Yuan & Cantley, 2008). Similarly, AMPK, along with LKB1, is often downregulated too, preventing adequate regulation of cellular metabolism, and apoptotic cell death (Kuhajda, 2008). Ultimately, these mutations are advantageous to the cancer cell as it allows the evasion of cell death and assists in cell growth and replication.

Autophagy, which lies downstream of the PI3K/Akt pathway, is strongly suggested to play a protective role against tumourigenesis (Glick, *et al.,* 2010; Mizushima & Komatsu, 2011). Additionally, defective autophagic genes may promote the development of malignant tumours (Qu, *et al.*, 2003). However, once a tumour is established, autophagy seems to play a protective role against cancer cell death, buffering the cells from various stressors. While there has been controversy surrounding the role of autophagy in cancer, the majority of studies illustrate an

upregulation of autophagy in malignant cells to aid in the provision of intracellular substrates, and that the inhibition of autophagy promotes cell death (Mizushima & Komatsu, 2011; Leisching, *et al.*, 2014; Jung, *et al.*, 2017; Jiang, *et al.*, 2018; Rupniewska, *et al.*, 2018). Furthermore, high levels of autophagy have been correlated with tumour aggressiveness and metastasis (Lazova, *et al.*, 2011; Yao, *et al.*, 2016; Zhu, *et al.*, 2019). However, this may vary between cancer types and stages, especially in a clinical setting (Glick, *et al.,* 2010).

Considering that cancer cells display unique metabolic hallmarks, it would suffice to assume that it may also harbour unique metabolic vulnerabilities. Cancer is significantly more metabolically active, and therefore has greater nutrient requirements. Cancer cells also display a greater dependence on glucose, not only for survival and proliferation, but for the degradation of surrounding tissues for invasion as well. Thus, investigation into the behaviour of cancer in the absence of sufficient nutrients is warranted.

1.6 Caloric restriction, intermittent fasting and cancer

1.6.1 Caloric restriction for the prevention of chronic diseases

Over the past few decades, there has been increasing interest in the field of caloric restriction (CR). This may be defined as a reduction in dietary intake without causing malnutrition (O'Flanagan, *et al.,* 2017). In essence, this ensures that the body does not meet its caloric requirements, but without causing a significant loss of lean body mass. This can be achieved through a number of means: through consistent caloric restriction, where an individual is not restricted in terms of when they may eat, but rather, by food quantity; intermittent fasting (IF), also known as short-term starvation (STS), where the quantity of food is not restricted, but rather when food may be consumed; or a combination of both. In other words, consistent CR represents a reduction in daily caloric intake over extended periods of time, where STS is the complete elimination of caloric intake over shorter periods of time (Longo & Fontana, 2009).

CR has long been established as a powerful strategy for the prevention of chronic diseases, including cardiovascular disease, type two diabetes mellitus (T2DM), and

neurodegenerative diseases (O'Flanagan, *et al.,* 2017). This has been well-documented in both pre-clinical and observational human studies (Longo & Fontana, 2009; Cangemi, *et al.*, 2016; Hanjani & Vafa, 2018). CR also offers the potential to extend lifespan, delay premature aging and to improve immunity and overall physiological functioning (O'Flanagan, *et al.,* 2017).

While the effect of CR on cancer prevention has been well-documented in animal models (James, 1994; Stewart, 2005; Carver, 2011; Moore, 2012; Lanza-Jacoby, 2013), more research is needed to validate this effect in humans. Furthermore, chronic CR is deemed inappropriate as a clinical intervention. During critical illness, the body enters a catabolic and cachexic state, and chronic CR may exacerbate this. Additionally, chronic CR requires an extended period of time for results to be achieved, making it unsuitable to an acute, clinical setting.

1.6.2 Short-term starvation in the context of cancer

Consequently, as of late, there has been deepening interest in the potential for STS to impair cancer cell growth. Cancer, as a metabolically hyperactive tissue with high energy requirements may prove especially vulnerable when deprived of these nutrients – more so than non-malignant tissues. Furthermore, during STS, serum glucose remains at homeostatic levels and does not peak as it would during the postprandial period (Cangemi, *et al.*, 2016). Consequently, insulin and accompanying growth factors, such as IGF-1, also remain low. This could render malignant tissues not only undernourished, but under-stimulated as well. This reduction in insulin-derived stimulation could further result in core proliferation pathways, such as PI3K, being somewhat dampened (Raffaghello, *et al.*, 2008). Further downstream, this reduction in dietary and caloric intake would likely result in the upregulation of autophagy. As previously mentioned, autophagy seems to have a dual role in cancer cells, with various studies implicating increased autophagic flux with both decreased and increased cell viability, depending on the cancer type (Kounakis, *et al.*, 2019).

In terms of substrates available during the fasting state, glucose availability declines between 24 and 48 hours into fasting and lipids become increasingly abundant. While many cancers can utilise fatty acids, they are less metabolically efficient in a hypoxic setting and are converted to other macromolecules with greater difficulty. Additionally, ketogenesis commences, resulting in increased serum ketone levels while serum

glucose is slightly diminished. Ketones are thought to inhibit cancer cell growth for the following reasons: Firstly, many, if not most cancer tissues rely largely on glucose for energy and macromolecule biosynthesis and cannot use ketones for the same ends (Poff, *et al.*, 2014). Secondly, ketones cannot be converted to lactate, and may thus compromise local invasion and metastasis by preventing the acidification of the extracellular matrix (Poff, *et al.*, 2014). Thirdly, if some degree of glycolysis were to continue, even in a ketotic state, the presence of ketones may cause lactate accumulation within the cell and hamper cellular functioning in tumour tissue. Ketones enter the cell through the same transporter that is used to export lactate from the cell – the monocarboxylate transporter (MCT). Therefore, the uptake of ketones may compromise the export of lactate out of the cell (Poff, *et al.*, 2014).

As previously described, circulating growth signals are reduced during STS, and while most cancers do not rely on external cues alone to grow and replicate, many normal tissues consider this a cue to reduce their metabolic activity (Raffaghello, *et al.*, 2008). In this case, non-malignant tissues may attempt to conserve resources, and diminish the proportion of energy dedicated to growth and replication. Rather, pathways aimed at survival and repair would be favoured in normal cells, while malignant cells continue to proliferate. This difference in response to starvation forms the basis of two treatment-related phenomena, known as Differential Stress Resistance (DSR) and Differential Stress Sensitisation (DSS) (Buono & Longo, 2018). DSR describes the enhanced protection that normal cells experience from chemotherapy-induced cytotoxicity because of the starvation-induced reduction in metabolic activity (Buono & Longo, 2018; De Groot, *et* al., 2019). DSS, on the other hand, refers to the enhanced efficacy of chemotherapy in killing malignant cells. This is owed to the cumulative stress placed on them by nutrient deprivation in conjunction with chemotherapeutic insult (Buono & Longo, 2018; De Groot, *et* al., 2019). Current *in vitro* and *in vivo* research is limited but has confirmed these phenomena in several cancer cell lines.

1.6.3 Previous studies investigating the effect of starvation on chemosensitivity

D'Aronzo, *et al.* (2015) demonstrated the effect of fasting cycles on the efficacy of gemcitabine, a chemotherapeutic agent used to treat malignant tumours of the pancreas, as well as those of the breast, ovaries and bladder. Using media with

reduced glucose (0.5 g/L rather than 1.0 g/L) and foetal bovine serum (FBS) (1% rather than 10%) to mimic starvation conditions, the authors investigated various outcomes on three pancreatic cancer cell lines. While gemcitabine alone had no significant effect on the cell cycle, a 24-hour starvation period prior to gemcitabine treatment significantly increased the proportion of cells in the G_0/G_1 phase and reduced the percentage of cells in the S and G_2/M phase (D'Aronzo, *et al.*, 2015). Cell death was also highest in the combination group, successfully sensitising all three cell lines to the drug. These findings were further confirmed by an *in vivo* study, where mice that received pancreatic cancer xenografts displayed a 40% reduction in tumour growth when they received gemcitabine injections after 24 hours of fasting compared to that of the drug alone (D'Aronzo, *et al.*, 2015).

A similar increase in chemosensitivity was observed in mouse, rat and human glioma cell lines, but not in primary mouse glial cells, when cells were cultured in starvation-mimicking media for 24 hours prior to treatment with temozolamide (Safdie, *et al.*, 2012). Using both a subcutaneous and intracranial mouse model, Safdie, *et al.* (2012) investigated the effect of a 48-hour fasting period on the efficacy of temozolamide. While the drug alone was able to significantly slow tumour progression when compared to the control mice, the combination group (fasting + temozolamide) had significantly reduced tumour volumes at the 28-day endpoint, even when compared to the treatment group. The authors attributed this largely to the reduction in serum glucose and IGF-1 following the induction of a starvation period (Safdie, *et al.*, 2012).

Raffaghello, *et al.* (2008) examined the effects of starvation prior to cyclophosphamide treatment on primary rat glial cells, as well as on one human and four rat glioma cell lines, and one human neuroblastoma cell line. While only 20% of glial cells in the control group survived the cyclophosphamide treatment, 80% of pre-starved glial cells showed resistance (Raffaghello, *et al.,* 2008). Conversely, starvation did not offer protection in the cancer cell lines but reduced the resistance of the RG2 glioma cells to treatment. An *in vivo* study corroborated these findings with only 57% of control mice surviving a high-dose administration of etoposide, while the mice starved for 48 hours prior to treatment attained a significantly greater viability of 94% (Raffaghello, *et al.,* 2008). Interestingly, although starvation caused the mice an approximate 20% loss in body mass, the majority of the weight was regained within four days of receiving high-dose chemotherapy treatment, indicating reduced chemotherapy-associated

toxicity. Non-starved mice, in turn, lost 20% of their body mass in response to the chemotherapy while the starved mice were recovering theirs. This suggests the partial protection of non-malignant tissues from chemotoxicity (Raffaghello, *et al.,* 2008).

Nearly identical findings were reported by Bianchi, *et al.* (2015) illustrating the increased sensitivity of colon cancer cell lines to oxaliplatin, both *in vivo* and *in vitro* when preceded by at least 24 hours of starvation (Bianchi, *et al.,* 2015).

More specific to breast cancer, a study by Lee, *et al.* (2012) involved the culturing of a murine breast cancer cell line in medium supplemented with serum from mice that were either fed or fasted for 48 hours. Consequently, cancer cells were significantly more susceptible to chemotherapy-induced cell death when treated with serum from fasted mice than those from fed mice (Lee, *et al.*, 2012). Additionally, when 17 mammalian cancer cell lines were treated with either normal or starvation-mimicking media, 15 showed increased sensitivity to chemotherapeutic agents. These results were confirmed *in vivo* as subcutaneous allografts with four of the eight cancer cell lines also showed significantly greater chemosensitivity when mice were starved prior to treatment (Lee, *et al.*, 2012).

In a similar study by Brandhorst, *et al.* (2013), mice were injected with either breast cancer or glioma cells from murine cell lines. Treatment involved either a fasting period of up to 60 hours (STS) or a 50% reduction in caloric intake for three consecutive days (CR), followed by high-dose intravenous injections of doxorubicin. When compared to the mice fed a standard chow, mice in the STS group had significantly greater survival rates 25 days post-injection (16% vs 89%). Those in the CR group had an approximately 50% survival rate by comparison (Brandhorst, *et al.,* 2013). This supports the notion that CR, especially through STS, increases the resilience of peripheral tissues to chemotherapy. However, in this study, breast cancer tumours did not show increased chemosensitivity when combined with CR, and the effect of STS on chemosensitivity was not investigated (Brandhorst, *et al.,* 2013). In contrast, Yakisich, *et al.* (2016) reported potentially opposing outcomes. Following prolonged serum starvation for periods of 7-12 days, breast and lung cancer cells became resistant to previously efficacious drugs, such as paclitaxel and colchicine (Yakisich, *et al.*, 2016). However, this is not currently supported by additional *in vitro* or *in vivo* studies and represents greater periods of starvation than proposed with STS.

Currently, clinical studies investigating DSR and DSS are extremely limited. However, a case series report released in 2009 describes the experiences of ten patients who fasted voluntarily for periods of 48-140 hours prior to chemotherapy, and between five and 56 hours afterwards (Safdie, *et al.*, 2009). None reported significant side effects from fasting besides hunger and light-headedness, while six patients reported reduced side-effects from chemotherapy, such as fatigue and gastrointestinal intolerance. Furthermore, tumour growth was monitored in six patients, and demonstrated that fasting did not compromise the efficacy of chemotherapy (Safdie, *et al.*, 2009). While this study comprised of a small sample size, it may serve as a pioneering study to elicit future trials in this regard.

1.6.4 Potential advantages and disadvantages of short-term starvation as an adjuvant therapy in cancer treatment

In summary, based on *in vitro* and *in vivo* models, short-term starvation seems to not only slow tumour growth and progression, but also to enhance chemosensitivity in malignant cells, as well as to protect normal cells from chemotherapy-induced cytotoxicity. Small-scale observational studies have supported these claims but warrant further investigation. If future studies do, however, support and verify these preliminary findings, fasting, as an adjuvant therapy may hold several advantages. Firstly, it may protect patients from the harmful side effects of chemotherapy, improving quality of life during treatment and mitigating morbidity. Furthermore, it may also have the potential to protect patients from chronic side effects and complications, thereby diminishing long-term morbidity and mortality. If fasting proves to sensitise cancer cells to chemotherapy or radiation, this may impact the clinical outcome in several ways, depending on the stage of disease. For patients whose tumours are in early stages and whose prognoses are good, it may shorten the time to remission, or minimise the need for chemotherapy, whether in intensity or duration. Alternatively, for those with potentially poor prognoses and middle to late-stage disease, it may potentially increase progression-free survival.

Finally, in terms of practicality as an adjuvant therapy, fasting is an affordable and accessible intervention that could be implemented globally. As it is something that the patient can implement with the necessary education and guidance, it places little to no additional burden on the healthcare system. It circumvents the need for equipment,

staffing, resources, or funding, and would be accessible to patients attending any type of healthcare facility. Additionally, such an intervention requires little skill to implement, is reported to have minimal side effects, and can be terminated at any time with little to no risk to the patient.

However, no intervention can be represented without highlighting the potential risks and concerns. Firstly, fasting for long intervals, such as 48-72 hours, may induce mild side effects, such as fatigue, inability to concentrate, and hunger pains (Safdie, *et al., 2*009). The potential chronic side effects are however of greater concern, and may include weight loss, especially the loss of lean body mass as the body enters a catabolic and cachexic state. This has the potential to impair clinical outcomes, as cancer and the treatment thereof is already associated with malnutrition. However, the long-term consequences of fasting in combination with chemotherapy has not been established (Safdie, *et al., 2*009). Conversely, the potential exists for the reduction of gastrointestinal side effects post-treatment to allow for greater caloric intake afterwards, where the patient may compensate for the fasting period.

Besides concerns regarding the side effects of fasting, patients may be reluctant to consider or initiate fasting, and may also find adherence problematic. Thus, sustainability in the long-term, especially for patients receiving frequent or long-term treatment, is questionable, and may not be acceptable in patients who are critically ill. Other patients for whom this intervention would not be suited may include children, the elderly, pregnant or breastfeeding women, patients who are already at-risk of malnutrition, and patients with existing metabolic conditions, such as T2DM. However, many of these challenges and concerns are not insurmountable, and may be outweighed by the potential benefits and promise that this regime holds. Patients could be screened to identify ideal candidates for fasting who are less at-risk for complications, thereby reducing the risk of malnutrition. Comprehensive information sessions could be offered to patients considering this therapy, outlining the potential beneficial effects or outcomes over the expected difficulties. This may facilitate improved adherence, should the intervention prove worthwhile.

1.7 Hypothesis, Aims and Objectives

Cancer is currently responsible for one in six deaths worldwide, making it the second leading cause of death after cardiovascular disease (WHO, 2018). In the light of the potential benefit that short-term starvation may pose, and the need for investigation into whether all types of cancer would show this same benefit, we thought it fit to investigate the effect of STS on the growth, viability, and metabolism of cancer cells, as well as whether it offers any potential in the face of current treatment regimes.

1.7.1 Hypothesis

We hypothesise that a period of starvation prior to doxorubicin treatment will selectively enhance treatment efficacy in cancer cells, while offering protection to non-malignant cells

1.7.2 Aims

In order to test the hypothesis, the study comprised of three main aims:

- To explore the effect of starvation over time on intracellular signalling pathways, autophagic flux, cell cycle progression and cell viability.
- To establish the effects of starvation, doxorubicin treatment, and the combination thereof on live cell number, cell viability and cell cycle progression.
- To determine the effect of starvation on chemosensitivity in MCF-12A breast epithelial cells, as well as in BT-549 and MDA-MB-231 breast cancer cells.

1.7.3 Objectives

To achieve the aforementioned aims, our objectives included the following:

- To utilise western blotting to quantify the relative protein expression of PI3K, total Akt and phosphorylated Akt.
- To detect changes in autophagic flux through the use of western blotting (Atg5, p62 and LC3-II) and immunocytochemistry (quantification of the number of autophagosomes).
- To conduct cell cycle analyses to establish the effects of the treatments on cell cycle progression.

- To perform WST1 viability assays to determine the effects of the treatments on cell viability.
- To utilise flow cytometry with propidium iodide staining to establish the percentage of dead cells within each group, thereby confirming cell viability.
- To perform a live cell count with trypan blue in order to determine the total number of live cells within each group.

Chapter 2: Methods and Materials

2.1 Study design

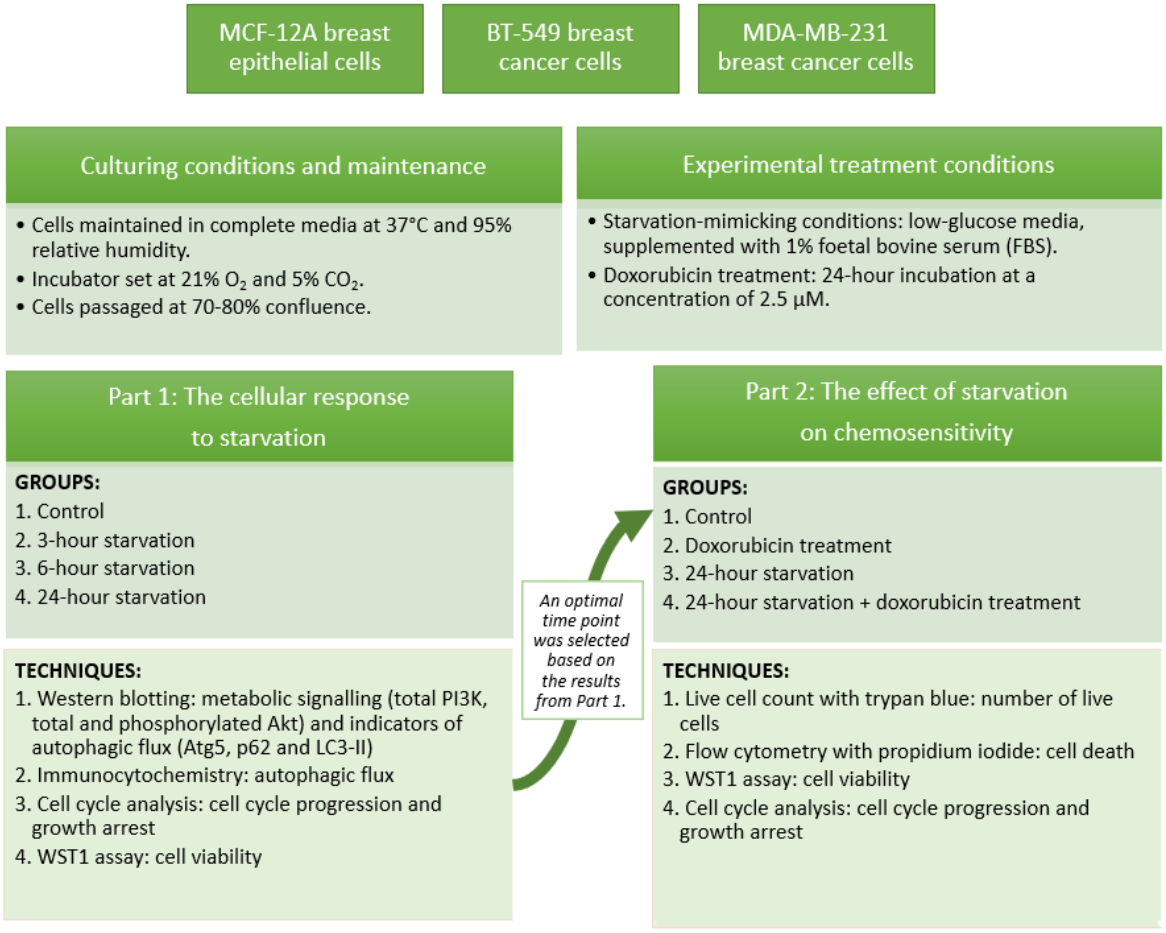

Figure 2.1: In vitro *study design.*

A non-malignant breast epithelial cell line (MCF-12A) and two triple-negative breast cancer cell lines (BT-549 and MDA-MB-231) were starved for three different time periods, while the control cells were maintained under standard conditions. Metabolic signalling pathways (PI3K, Akt), markers of autophagy (Atg5, p62, LC3-II) and autophagic flux, cell cycle progression and growth arrest, and cell viability were assessed. Based on this data, an optimal time point was selected and served as the starvation period for the remainder of the study. Cells were then treated with doxorubicin, with or without a preceding starvation period, to establish the effect of starvation on chemosensitivity. This was determined by quantifying live cell number, cell death, viability and cell cycle progression.

2.2 Cell lines and conditions

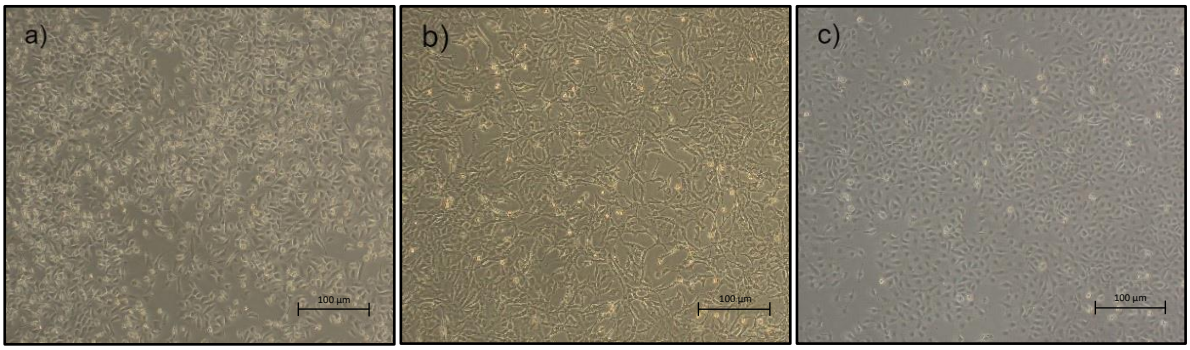

Figure 2.2: Typical morphology of a) MCF-12A, b) BT-549 and c) MDA-MB-231 cells under 10x objective, under normal conditions, and at approximately 80% confluence.

2.2.1 Cell lines

Three cell lines were utilised for the purpose of this study. MCF-12A breast epithelial cells, originally isolated from the mammary gland of a patient with no history of cancer, were used as the control cell line, demonstrating the effects of the treatments on non-malignant cells. BT-549 cells, a triple-negative breast cancer (TNBC) cell line, were originally excised from the mammary gland of a patient with an invasive ductal carcinoma. A second TNBC cell line was employed, but with the distinguishing feature of mesenchymal-like (as opposed to epithelial) characteristics. The MDA-MB-231 cell line originates from a patient with a metastatic adenocarcinoma of the breast; the cell sample was sourced from a pleural effusion. The MCF-12A and MDA-MB-231 cell lines were generously gifted to our department by Professor Sharon Prince at the University of Cape Town, while the BT-549 cell line was kindly donated by Professor Adrienne Edkins from Rhodes University.

2.2.2 Maintenance conditions

The MCF-12A cells were cultured in a 1:1 ratio of Dulbecco's Modified Eagle's Medium (DMEM; #41965-039, ThermoFisher) and Ham's F12 Nutrient Mixture (Ham's F12; #21765-029, ThermoFisher), supplemented with 0.01 mg/ml insulin (#783811004, Humulin 30/70, Lilly), 20 ng/ml human epidermal growth factor (EGF; #236-GMP, R&D Systems), 100 ng/ml Cholera toxin (#C8052, Sigma-Aldrich) and 500 ng/ml

hydrocortisone (#H9611, LKT Laboratories). The BT-549 cells were cultured in Roswell Park Memorial Institute media (RPMI; #52400-025, ThermoFisher), supplemented with 0.01 mg/ml of insulin. The MDA-MB-231 cells were cultured in DMEM.

All three cell lines were cultured in complete media, consisting of the aforementioned media and supplements, with the addition of 10% foetal bovine serum (FBS; #FBS-GI-12A, Capricorn Scientific) and 1% Penicillin-Streptomycin (PenStrep; #15140-122, ThermoFisher). This was in line with the specifications issued by the leading global bioresource centre (ATCC, 2020).

All cell lines were maintained in incubators at 37°C, a relative humidity of 95%, 21% oxygen and 5% carbon dioxide. Cells were cultured in T75 flasks until they reached a confluence of approximately 70-80%, whereafter they were passaged using 0.25% trypsin-EDTA (#25200-072, ThermoFisher) and seeded in new flasks, or in the appropriate plate for experimental purposes.

2.2.3 Treatment conditions

In order to mimic starvation *in vitro*, cells were cultured in low-glucose media (which contained approximately 70% less glucose than standard media), with reduced FBS (1% as opposed to 10%) for the duration of the starvation period. This is in line with previous studies (Raffaghello, *et al.,* 2008; Lee, *et al.*, 2012; Safdie, *et al.*, 2012; Bianchi, *et al.,* 2015; D'Aronzo, *et al.,* 2015).

Since low-glucose Hams' F12 media was not available, glucose-free DMEM (#11966-025, ThermoFisher) was purchased and mixed with standard Ham's F12 to yield a low-glucose DMEM/F12 solution. This was repeated with glucose-free and standard DMEM for the MDA-MB-231 cells, and glucose-free RPMI (#11879-020, ThermoFisher) and standard RPMI for the BT-549 cells. All other supplements were added as per usual to the media of each respective cell line. Cells were starved for either 3, 6, or 24 hours, while the control group was not starved, and received standard media only. Treatment with doxorubicin hydrochloride (#D5794, LKT Laboratories) commenced at a concentration of 2.5 µM for a period of 24 hours.

2.2.4 Incubation with bafilomycin

Where autophagic outcomes were assessed, cells were incubated in 400 nM Bafilomycin A1 (#B1793, Sigma-Aldrich) for one hour prior to imaging with fluorescent microscopy, or for four hours prior to the harvesting of cells for western blotting. Bafilomycin A1 is a macrolide antibiotic isolated from *Streptomyces griseus* that prevents the acidification of the lysosome, consequently inhibiting its fusion with autophagosomes. As this results in the accumulation of autophagosomes, short-term treatment with bafilomycin A1 enables the quantification of autophagic flux using various techniques.

2.3 Experimental techniques

2.3.1 Western blotting

In order to examine the change in the expression of specific target proteins, western blotting was performed following experimental treatments. This provided insight into the cellular response to starvation at specific time points.

2.3.1.1 Cell harvesting and protein extraction

Cells were seeded in T25 flasks and treated according to their experimental group. After the completion of the treatment period, culture medium was removed, and cells were washed three times with ice-cold PBS (See Appendix A) to remove traces of culture media. Thereafter, cells were harvested, while working on ice to minimise protein degradation, by using a cell scraper and a modified radio-immunoprecipitation (RIPA) buffer (1% NP-40, 1% Na-deoxycholate, 5 mM EDTA, 5 mM EGTA, 0.1% SDS) supplemented with cOmplete™ Protease Inhibitor Cocktail (#11697498001, Roche), 1 mM Na_3VO_4, 1 mM NaF, and 1 mM PMSF.

After the cells from each treatment group had been harvested and transferred to ice-cold Eppendorf tubes, cells were sonicated (Misonix Sonicator, S-4000-010, QSonica) for five seconds at five amplitude and incubated on ice in a refrigerator until the foam had settled. Centrifugation for two minutes at 16.3 g and 4°C allowed for the separation

of insoluble cellular debris from the supernatant. The latter was then collected to serve as the protein sample.

2.3.1.2 Protein determination and the Bradford Assay

The protein concentration of each sample was determined through the use of a Bradford colorimetric assay (Bradford, 1976). Using a bovine serum albumin (BSA) stock solution to generate a standard curve, absorbance values were read at 595 nm using a CE2021 Spectrophotometer (Cecil Instrumentation Services Ltd., Lasec). The protein concentration of each sample was established using the Bradford standard curve and this was used to calculate the volumes required to yield 50 µg of protein. Hereafter, the appropriate volume of protein sample was added to the relevant volume of sample buffer, boiled, vortexed and prepared for loading.

2.3.1.3 SDS-PAGE and electro-transfer

Protein samples were separated using sodium dodecyl sulphate polyacrylamide gel electrophoresis (SDS-PAGE; Mini Protean System, Biorad) with self-cast gels and Tris/Glycine/SDS Running Buffer (#1610772, BioRad). Based on the size of the proteins being detected, either 12% or 15% gels were used. Equal amounts of protein (50 µg) were loaded into each lane, along with a protein marker ladder in the first lane. This molecular marker served as a guideline to locate each protein on the gel according to its molecular weight.

Following electrophoresis, the separated proteins were activated on the Bio-Rad ChemiDoc MP, and transferred to a polyvinylidene fluoride (PVDF) membrane using the Trans-Blot Turbo RTA Transfer Kit, LF PVDF (#1704275, BioRad). A mixed molecular weight transfer was selected due to the broad range of molecular weights of the target proteins. Hereafter, the membrane was labelled and rinsed in 100% methanol and washed in Tris-buffered saline Tween (TBS-T).

2.3.1.4 Immunodetection

After the washing step, the membrane underwent a blocking step in 5% milk or BSA for one hour to prevent non-specific binding, followed by another washing step in TBS-T. Hereafter the membrane was incubated overnight in the relevant primary antibody at 4°C. The proteins of interest during the first part of the study included Atg5, p62 and LC3-II to quantify autophagic flux, as well as PI3K and total and phosphorylated Akt.

This provided insight into the change in cellular behaviour over time when confronted with nutrient deprivation, and also illustrated the roles played by intracellular signalling molecules in the adaptation of the cell to nutrient stress.

After overnight incubation in the primary antibody, the membranes were washed in TBS-T and incubated for one hour in the appropriate secondary antibody. After a final washing step in TBS-T, a thin layer of Clarity™ Western ECL Substrate (#170-5061, BioRad) was evenly distributed over the membrane and an appropriate exposure setting was selected, in order to visualise the protein bands on a Bio-Rad ChemiDoc MP. Exposed bands were quantified using Image Lab v6.1 (BioRad). To account for variations in protein loading, these bands were normalised against the total protein within its respective lane. The relative target protein expression was quantified using densitometry software (Quantity One 1-D Analysis Software, BioRad) and presented as a percentage of the control.

For a comprehensive protocol, please see Appendix B.

.

The following primary antibodies were obtained from Abcam:

Protein of interest	Primary Antibody	Catalogue number	Concentration	Secondary antibody	Catalogue number	Concentration	Molecular weight	% gel
PI3K	Mouse anti-PI3K p85	#ab86714 Abcam	1:1000	Anti-mouse	(#7076S, CST),	1:10 000	85kDa	12%
Akt	Rabbit anti-Akt	#ab32505 Abcam	1:1000	Anti-rabbit	(#7074S, CST)	1:10 000	60kDa	12%
Phosphorylated Akt	Rabbit anti-phosphorylated Akt Ser473	#4060 Cell Signaling Technology	1:1000	Anti-rabbit	(#7074S, CST)	1:10 000	60kDa	12%
Atg5	Rabbit anti-Atg5	#2630 Cell Signaling Technology	1:1000	Anti-rabbit	(#7074S, CST)	1:10 000	55kDa	15%
p62	Rabbit anti-p62	#ab109012 Abcam	1:10 000	Anti-rabbit	(#7074S, CST)	1:10 000	62kDa	15%
LC3-II	Rabbit anti-LC3B	#3868 Cell Signaling Technology	1:1000	Anti-rabbit	(#7074S, CST)	1:10 000	14-16kDa	15%

Table 2.1: Primary and secondary antibodies, and their relevant concentrations for the detection of the target proteins.

2.3.2 Immunocytochemistry

For the first part of the study, immunocytochemistry was used to determine the effect of different periods of starvation on the autophagic flux of three different cell lines.

Immunocytochemistry is a technique whereby specific proteins and/or organelles are visualised using fluorescent probes and a specialised fluorescent microscope, with the goal of gaining insight into intracellular processes. Autophagic flux refers to the rate of protein degradation through autophagic pathways (Mizushima & Komatsu, 2011). In order to quantify autophagic flux within a cell, both the number of autophagosomes and lysosomes must be established, as well as the co-localisation thereof, thus indicating autolysosomes. Autophagosomes may be visualised in a number of ways, but this study employed the transfection of cells with a plasmid, namely eGFP-LC3 (#21073, Addgene). LC3 is a protein found in the membranes of autophagosomes and the visualisation thereof using a fluorescent microscope is used to determine of the number of these autophagic vesicles within a cell. Similarly, LysoTracker™ Red DND-99 (#L7528, ThermoFisher) is a fluorescent probe that labels lysosomes, enabling the visualisation of these organelles. By staining cells transfected with eGFP-LC3 with LysoTracker Red, both autophagosomes and lysosomes may be visualised, respectively. The formation of autolysosomes is thus observed by the co-localization of the green and red fluorescent signals.

Each cell line was seeded and cultured in a T25 flask until a confluence of approximately 60-70% was attained. The Lipofectamine™ 3000 Transfection Reagent (#L3000-001, ThermoFisher) was used to transfect the cells with the eGFP-LC3 plasmid. The eGFP-LC3 plasmid was originally donated by Tamotsu Yoshimori, and obtained from Addgene (Addgene plasmid #21073; http://n2t.net/addgene:21073; RRID:Addgene_21073).

Thereafter, successfully transfected cells were selected by the addition of G418 disulfate salt (A1720-1G, Sigma-Aldrich), an aminoglycoside antibiotic that kills non-transfected cells. The continual selection of successfully transfected cells ensured a population suitable for fluorescent microscopy. These cells were then seeded in an 8-well chamber slide and each experimental group was treated accordingly. LysoTracker Red, at a concentration of 80 nM, was added to each well three hours prior to imaging on the Carl Zeiss LSM 780 confocal microscope.

A 488 nm laser was used for the imaging of eGFP, which has excitation and emission wavelengths of 488/510 nm. A 561 nm laser was used for the visualisation of LysoTracker Red (577/590 nm). Triplicate images in the form of z-stacks, visualising one cell per image, were obtained per group. The experiment was repeated in triplicate, yielding a total of nine cells imaged per group. The images were processed using the Zeiss ZEN 3.2 Blue Edition software. Data were presented as the mean number of autophagosomes per cell.

For a comprehensive protocol, please see Appendix B.

2.3.3 Cell cycle analysis

For the first part of the study, cell cycle analysis was performed using flow cytometry to establish the effect of starvation on the cell cycle in both malignant and normal cell lines. For the second part, the effect of starvation on chemosensitivity was determined by establishing whether cells that were starved prior to receiving doxorubicin displayed a greater extent of growth arrest.

By permeabilising the cell membrane with 70% ethanol prior to the addition of a fluorescent dye (such as propidium iodide), the dye may permeate the cell membrane and stain all nucleic acids within the cell. However, with the addition of ribonuclease (RNase), propidium iodide stains only cellular DNA. The intensity of the fluorescent signal is thus directly proportional to the amount of DNA within the cell, which enables the flow cytometer to determine which stage of the cell cycle the cell is in. Cells in the G_2/M phase have twice the amount of DNA as those in G_0/G_1, with everything in between falling within the S-phase category. This determination of cell cycle was achieved by using the BD FACSMelody to perform flow cytometry.

For the analysis of the cell cycle, cells were seeded in T25 flasks at an appropriate density and given their respective treatments. At the end of the treatment period, cells were harvested, permeabilised with ethanol, resuspended in a solution of Ribonuclease A from bovine pancreas (#R4642-10mg, Sigma-Aldrich) and propidium iodide (PI; #P4170-10mg, Sigma-Aldrich) in phosphate buffered saline (PBS), and analysed using the BD FACSMelody cell sorter. By utilising the BD FlowJo™ v10.6 software, debris and doublets were excluded from the sample, the appropriate

parameters were set, and the data were extracted. Data were presented as the percentage of cells within each phase of the cell cycle.

For a comprehensive protocol, please see Appendix B.

2.3.4 Cell viability assay

In order to determine the effect of starvation on cell viability over time, as well as the effect of starvation on chemosensitivity, a cell viability assay was conducted using a water-soluble tetrazolium salt 1 (WST1; #05015944001, Roche).

WST1 is often employed to quantify the effects of a given treatment on cytotoxicity and cell proliferation. A WST1 assay is a colorimetric assay, as the tetrazolium salt is cleaved in the presence of viable cells to form yellow formazan. This reduction reaction relies predominantly of the production of NAD(P)H, which only occurs in metabolically active cells. The amount of formazan is therefore directly proportional to the level of activity of mitochondrial dehydrogenases, which generally corresponds with the number of live cells, and is thus used as a proxy for cell viability.

Once cells had reached a confluence of 70-80%, cells were trypsinised and seeded at an appropriate density in 48-well plates. For the first part of the study, a viability assay was performed utilising a control group, and three starvation groups of varying durations (3, 6 and 24 hours). For the second part of the study, the groups comprised of a control group, a doxorubicin treatment group, a 24-hour starvation group, and a combination group.

Each group consisted of triplicate wells, and each experiment was performed three times to account for both technical and biological replicates, respectively. At the end of the treatment periods, 10 µl of WST1 reagent was added to each well containing 200 µl of growth medium, and the plates were incubated for two hours at 37°C. The absorbance values were read at 450 nm using the EL800 Universal Microplate Reader (Bio-Tek Instruments, Inc.). Cell viability was calculated and expressed as a percentage of the control values.

For a comprehensive protocol, please see Appendix B.

2.3.5 Live cell count with trypan blue

In order to determine the effect of starvation, doxorubicin and the combination thereof on live cell number and proliferation, the number of live cells was determined through the use of a live cell count with trypan blue. Trypan blue is generally excluded from viable cells, due to its inability to permeate intact cell membranes.

Cells were seeded in T25 flasks at an appropriate density and given their respective treatments. At the end of the treatment period, growth medium was removed and discarded. Adherent cells were harvested using 0.25% trypsin-EDTA, neutralised with growth medium, and the T25 flasks rinsed with PBS to collect any remaining cells. The tube, containing PBS and cells in a trypsin suspension, was centrifuged for five minutes at 1500 rpm. The supernatant was discarded, and the cell pellet resuspended in 1000 µl warm PBS. In a labelled Eppendorf tube, 100 µl of this cell suspension was added to 100 µl of 0.1% trypan blue solution. This was prepared in advance from trypan blue and PBS. A volume of 10 µl from this suspension was loaded onto the grids of three Neubauer counting chambers and the number of viable (unstained) cells were counted. This was repeated in triplicate for each group, with the experiment also repeated in triplicate, thus accounting for technical and biological replicates. Data were presented as a percentage of the control.

For a comprehensive protocol, please see Appendix B.

2.3.6 Flow cytometry with propidium iodide

For the second part of the study, cell viability was determined by using flow cytometry and propidium iodide. Notably, this did not involve a permeabilization step, as propidium iodide is intended to penetrate permeable, and therefore, non-viable cells, only. This determined the percentage of non-viable cells within the population.

For the determination of cell viability, cells were seeded in T25 flasks at an appropriate density and given their respective treatments. At the end of the treatment period, cells were harvested, centrifuged, resuspended in a solution of propidium iodide in PBS and analysed using the BD FACSMelody cell sorter. By utilising the BD FlowJo™ v10.6 software, debris and doublets were excluded from the sample, the appropriate

parameters were set, and the data were extracted. Data are presented as the percentage of non-viable cells.

2.4 Statistical analysis

All data were captured and analysed using Statistica Version 13.6. Data are expressed as the mean ± standard error of the mean (SEM). Data were assessed for normality using the Kolmogorov-Smirnov test, and the following tests were used to establish significance: one-way ANOVA, Kruskal-Wallis test, Pearson's correlation matrix. Data were considered statistically significant at a p-value <0.05.

Chapter 3: Results

Part 1: Cellular characterization of starvation

3.1 The cellular response to starvation over time

A normal breast epithelial cell line, MCF-12A, was selected as a control to determine the effects of starvation on benign cell behaviour. Two triple negative breast cancer (TNBC) cell lines, BT-549 and MD-MB-231, were selected to represent cancers with limited available therapeutic interventions. For the first part of the study, cells were seeded in the appropriate plates or flasks and treated according to their respective treatment group. Where autophagic outcomes were not assessed, four experimental groups were involved: 1) the control group, which received standard, fully supplemented media (Con); 2) a three-hour starvation period (3h); 3) a six-hour starvation period (6h); and 4) a 24-hour starvation period (24h). For experiments assessing autophagic outcomes, additional groups corresponding to those listed above, but supplemented with bafilomycin, were included, resulting in eight experimental groups.

3.1.1 Metabolic signalling pathways in starvation

In order to determine the effect of starvation on signalling pathways involved in growth and proliferation, western blotting was employed to quantify relative target protein expression. Membranes were visualised using the Image Lab™ software from Bio-Rad™. Protein expression was normalised according to the total protein and expressed as a percentage of the control.

3.1.1.1 The effect of starvation on Phosphatidylinositol 3-Kinase (PI3K)

PI3K is a lipid kinase and oncoprotein that forms part of the PI3K/Akt/mTOR signalling pathway. This pathway is activated through receptor binding of multiple growth signals and is upregulated to promote cellular survival, growth and proliferation (Hemmings &

Restuccia, 2012). There were no significant differences in any of the groups in any of the cell lines. While the expression of PI3K increased with starvation in the MDA-MB-231 cell line, none of the groups reached significance. Only the 24-hour starvation group approached significance (p=0.1).

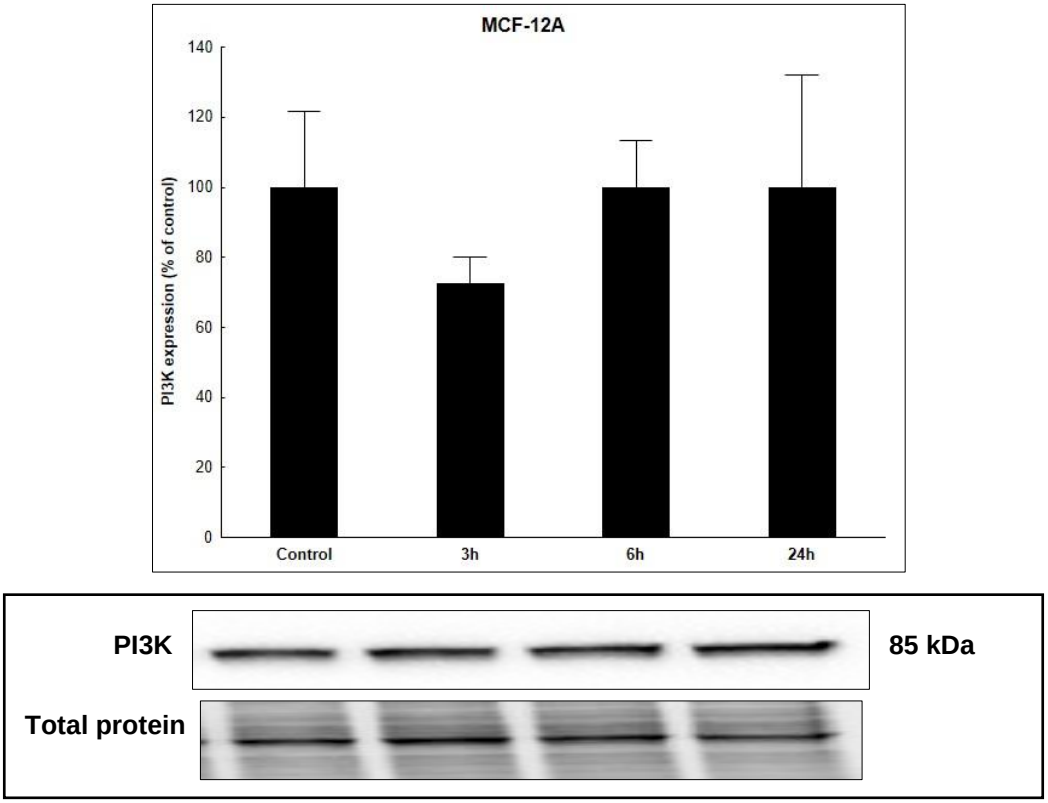

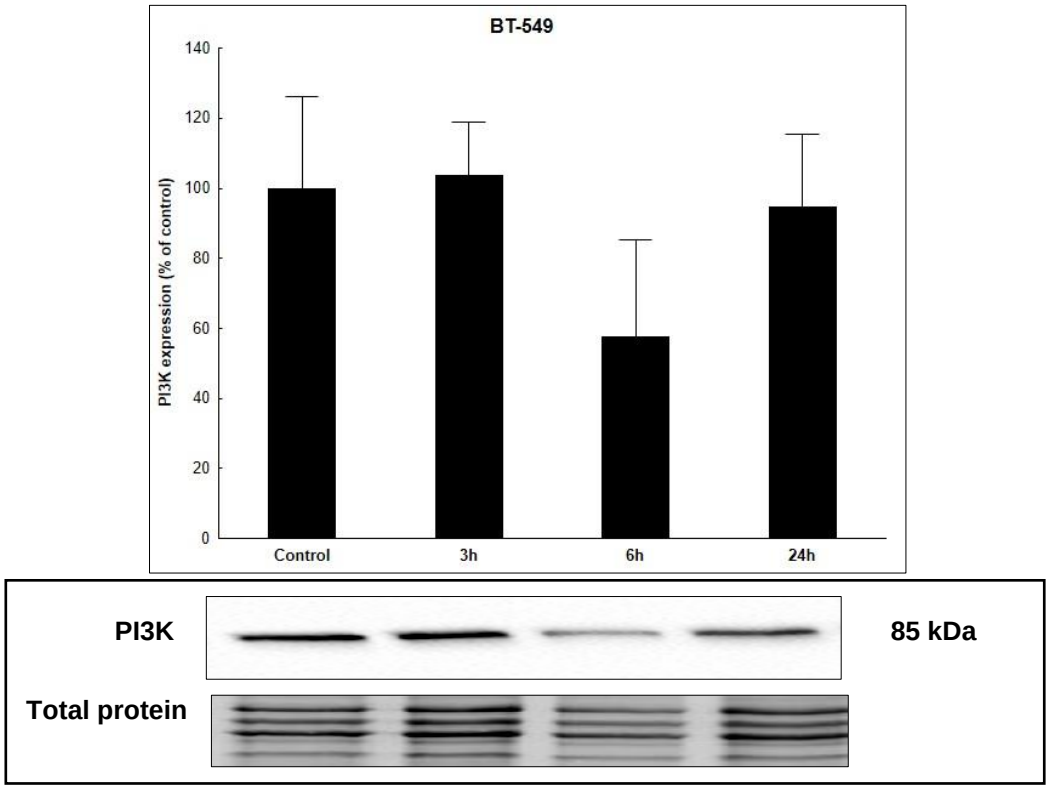

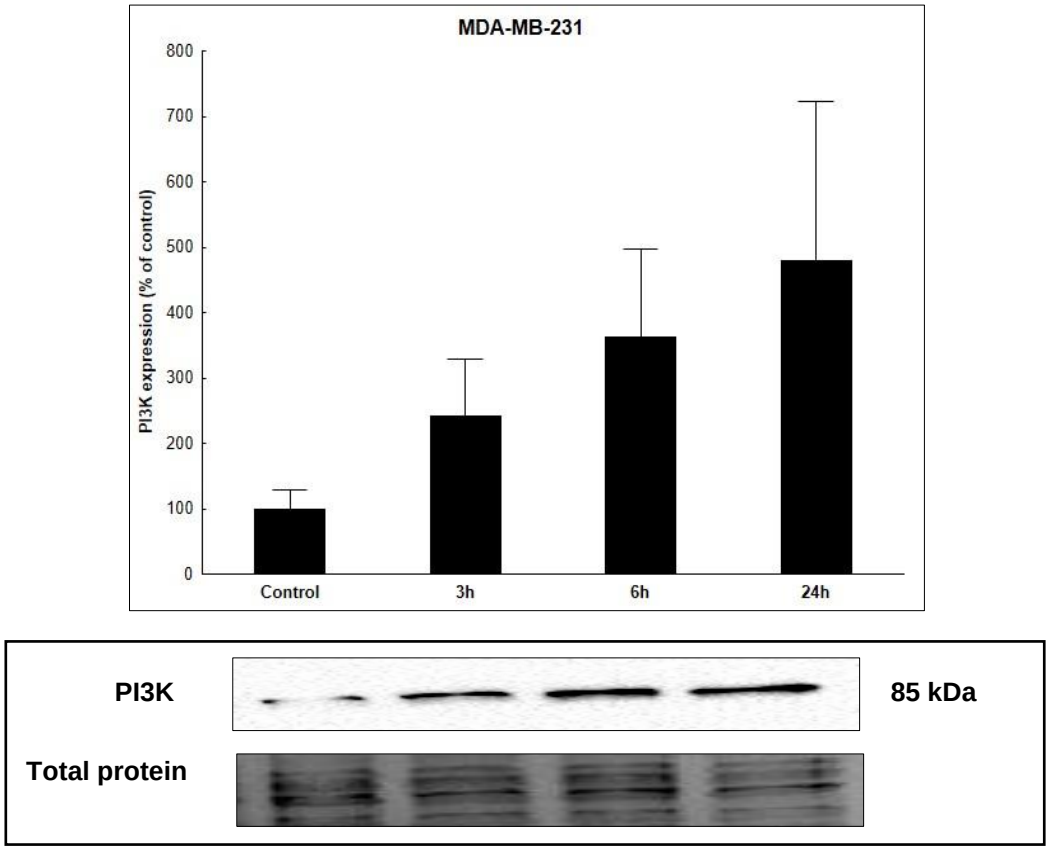

Figure 3.1: The effect of starvation over time on PI3K expression. *PI3K expression, as determined by western blotting, in MCF-12A cells, BT-549 cells and MDA-MB-231 cells. Results are presented as a percentage of the control ± SEM (n=3). * = p<0.05 when compared to the control.*

3.1.1.2 The effect of starvation on total Akt expression

Akt, also known as protein kinase B (PKB), is a serine/threonine kinase that is a downstream target of PI3K. Akt promotes cell survival, growth and proliferation (Cantley, 2002).

In the MCF-12A cell line, the three-hour starvation group had significantly lower Akt expression than the control group ($p<0.01$). The 24-hour group approached but did not reach significance ($p=0.08$). There were no significant differences between any of the groups in the BT-549 cells. In the MDA-MB-231 cell line, there was a significant increase in Akt expression at six hours ($p<0.05$) and 24 hours ($p<0.01$) of starvation.

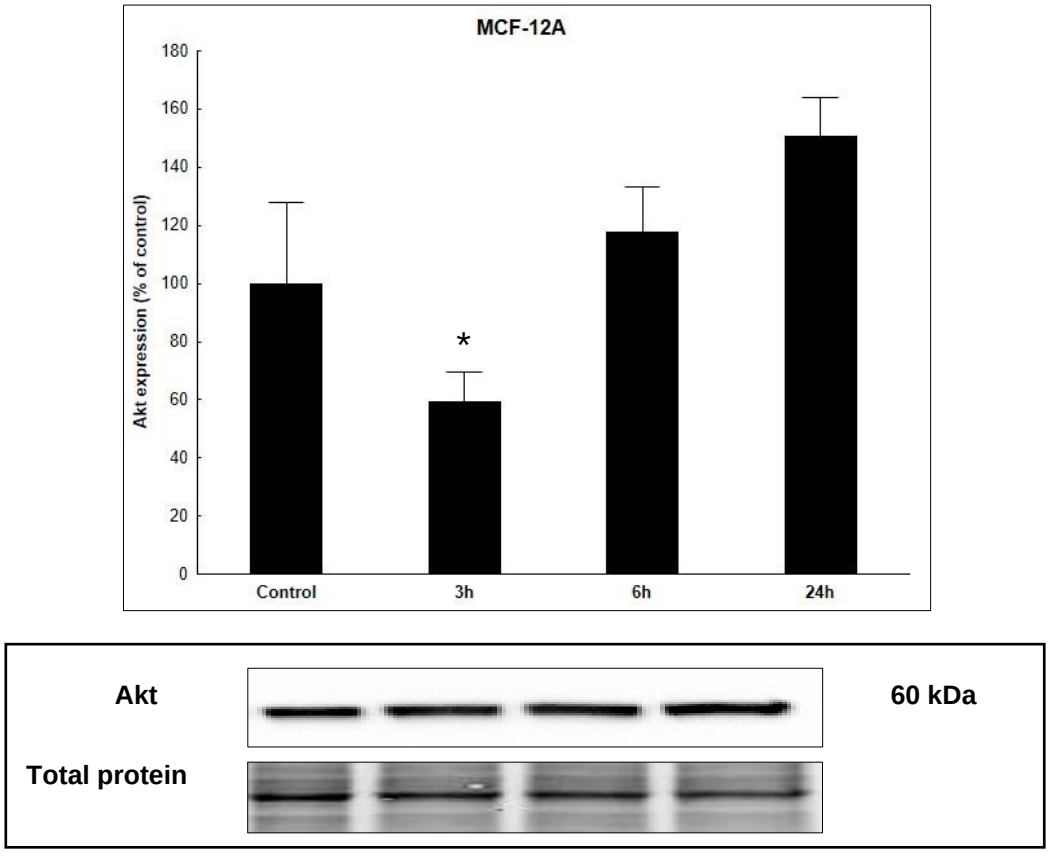

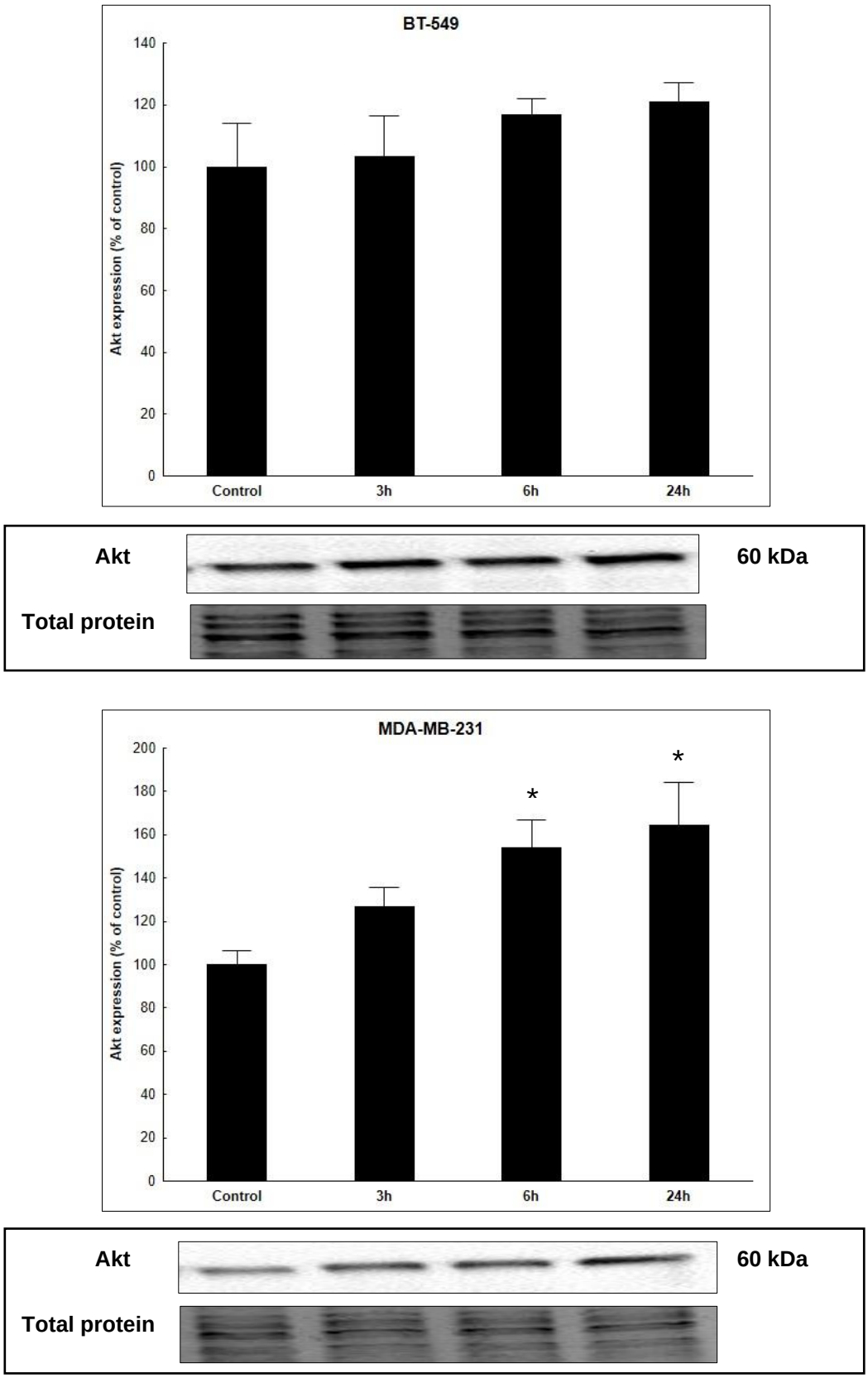

Figure 3.2: The effect of starvation over time on Akt expression. *Akt expression, as determined by western blotting, in MCF-12A cells, BT-549 cells and MDA-MB-231 cells. Results are presented as a percentage of the control ± SEM (n=3). * = p<0.05 when compared to the control.*

3.1.1.3 The effect of starvation on Akt phosphorylation

For Akt to be activated, it must be phosphorylated, both on Thr308 and at Ser473. The latter is executed by either mTOR or DNA-dependent protein kinases, and this stimulates full Akt activity (Hemmings & Restuccia, 2012).

There were no significant differences between any of the groups in the MCF-12A cells. Only the three-hour group neared significance (p=0.1). There were also no significant differences between any of the groups in the BT-549 cells or the MDA-MB-231 cells.

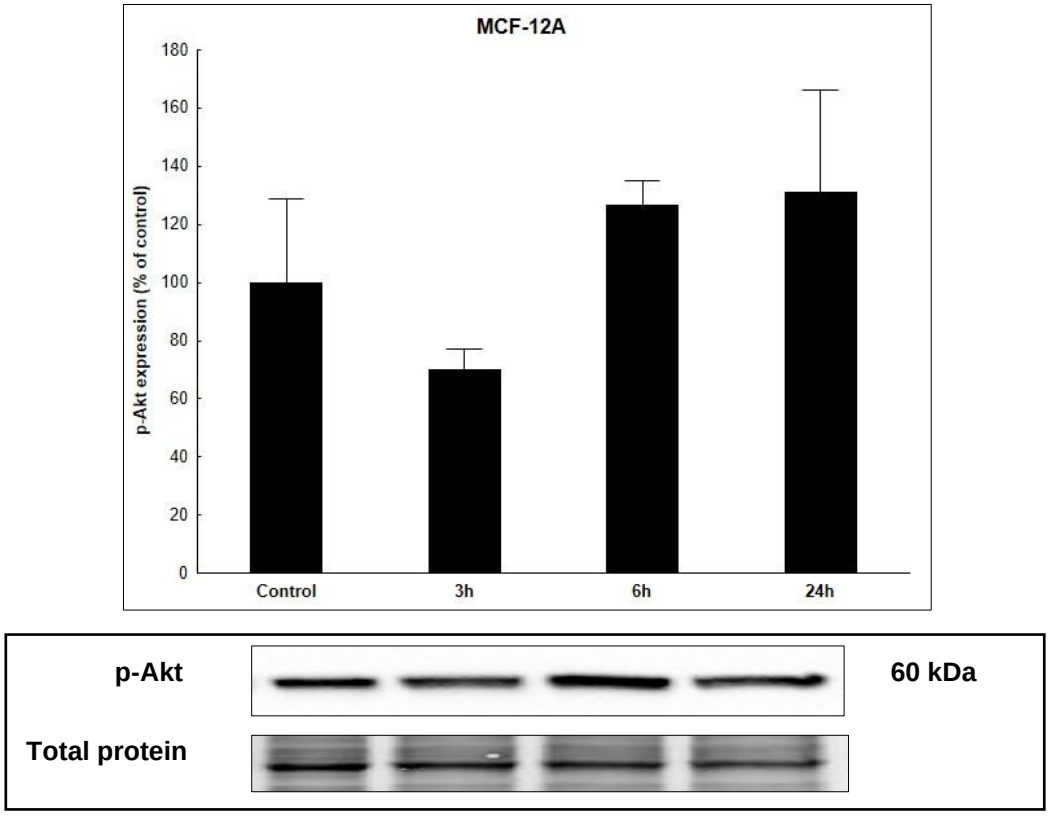

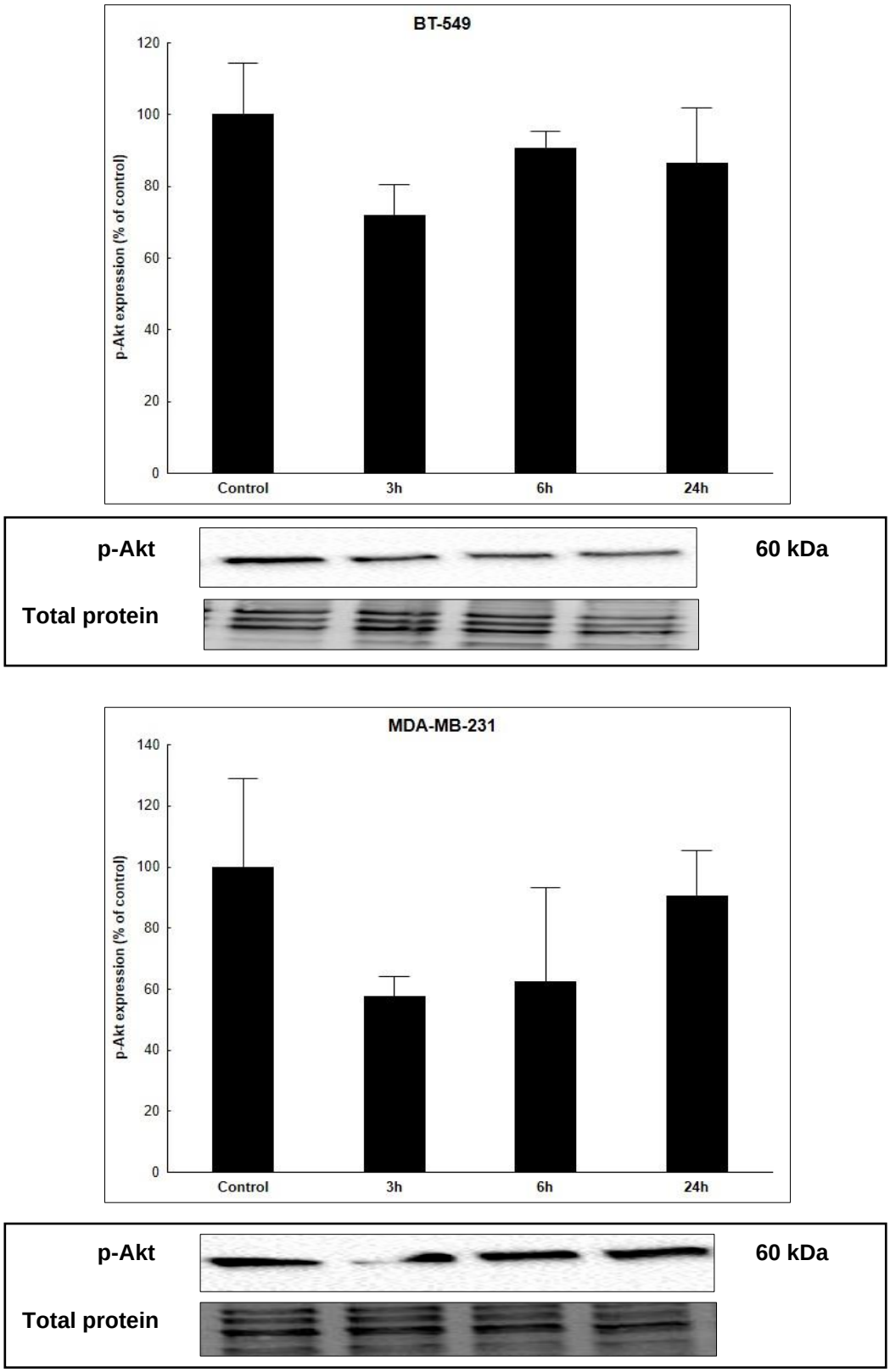

Figure 3.3: The effect of starvation over time on phosphorylated Akt (Ser473). *Phosphorylated Akt, as determined by western blotting, in MCF-12A cells, BT-549 cells and MDA-MB-231 cells. Results are presented as a percentage of the control ± SEM (n=3). * = p<0.05 when compared to the control.*

3.1.2 Autophagic flux in starvation

In order to determine the effect of starvation on autophagy, Western blotting was employed to quantify the expression of Atg5, p62 and LC3-II. Immunocytochemistry was used to quantify autophagic puncta.

3.1.2.1 The effect of starvation on Autophagy-related protein 5 (Atg5) expression

Autophagy-related proteins (ATG) are key players in the autophagy pathway. ATG5 serves as a key factor and an integral part of the ATG5-ATG12-ATG16L1 complex that catalyses the ATG8 lipidation essential for autophagosome formation and expansion. ATG5 is also indispensable for the fusion of autophagosomes with lysosomes in both canonical and noncanonical autophagy (Glick, *et al.*, 2010). In the MCF-12A cell line, there was a near-significant difference in Atg5 expression between the control group and the 24-hour group ($p=0.052$). There were no significant differences between any of the groups in the BT-549 cells. In the MDA-MB-231 cell line, there were significant differences in the control ($p<0.05$), three-hour ($p<0.05$), six-hour ($p<0.01$) and 24-hour ($p<0.01$) groups when compared to their corresponding bafilomycin-treated groups.

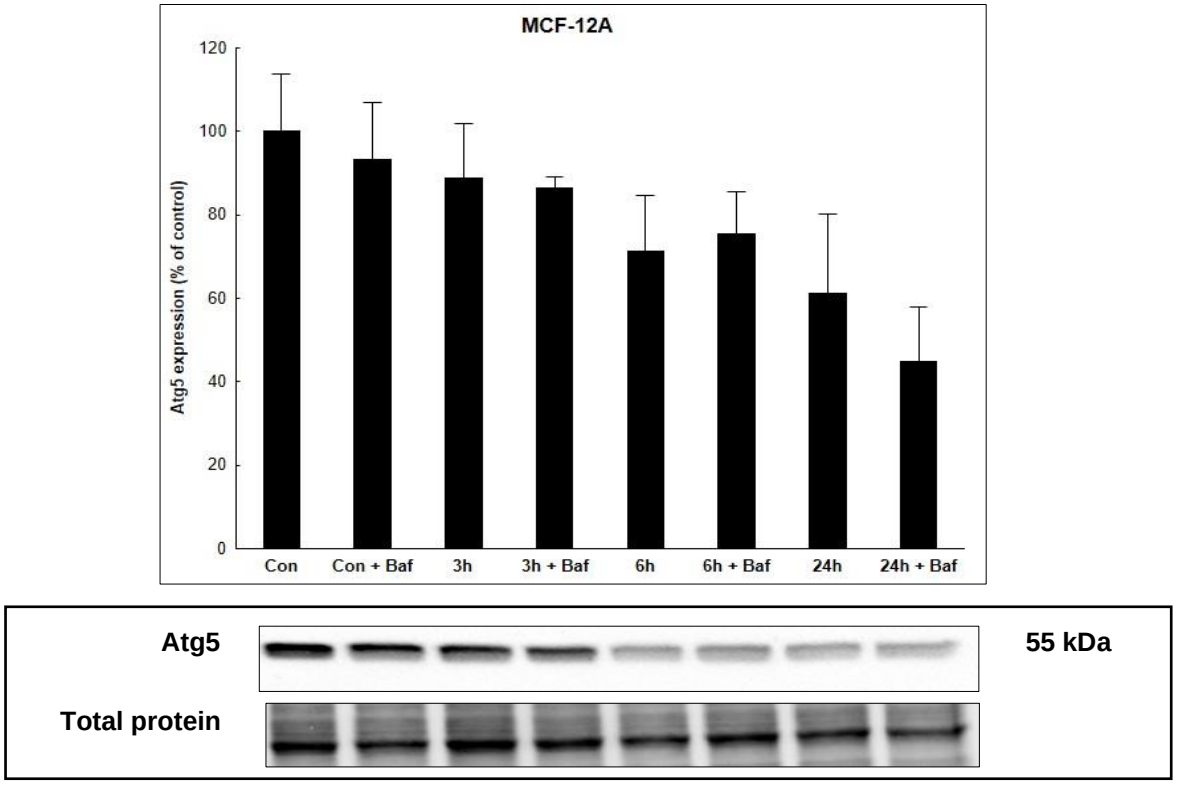

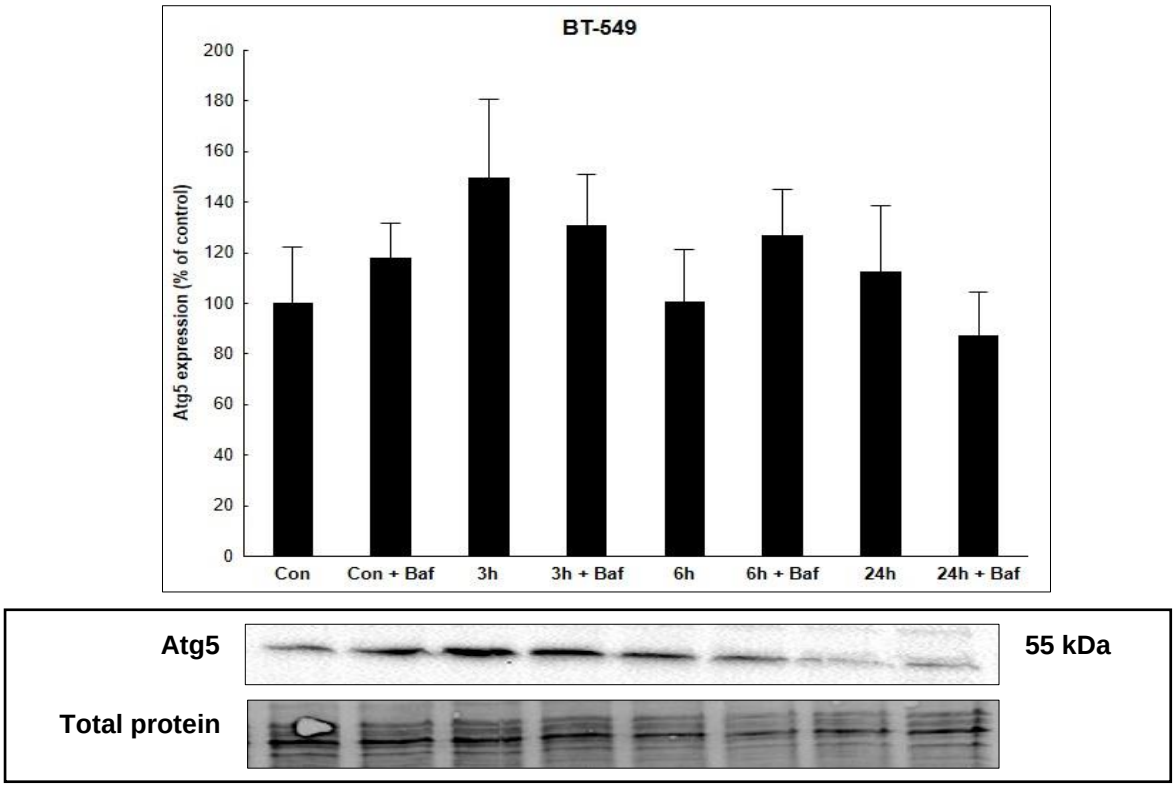

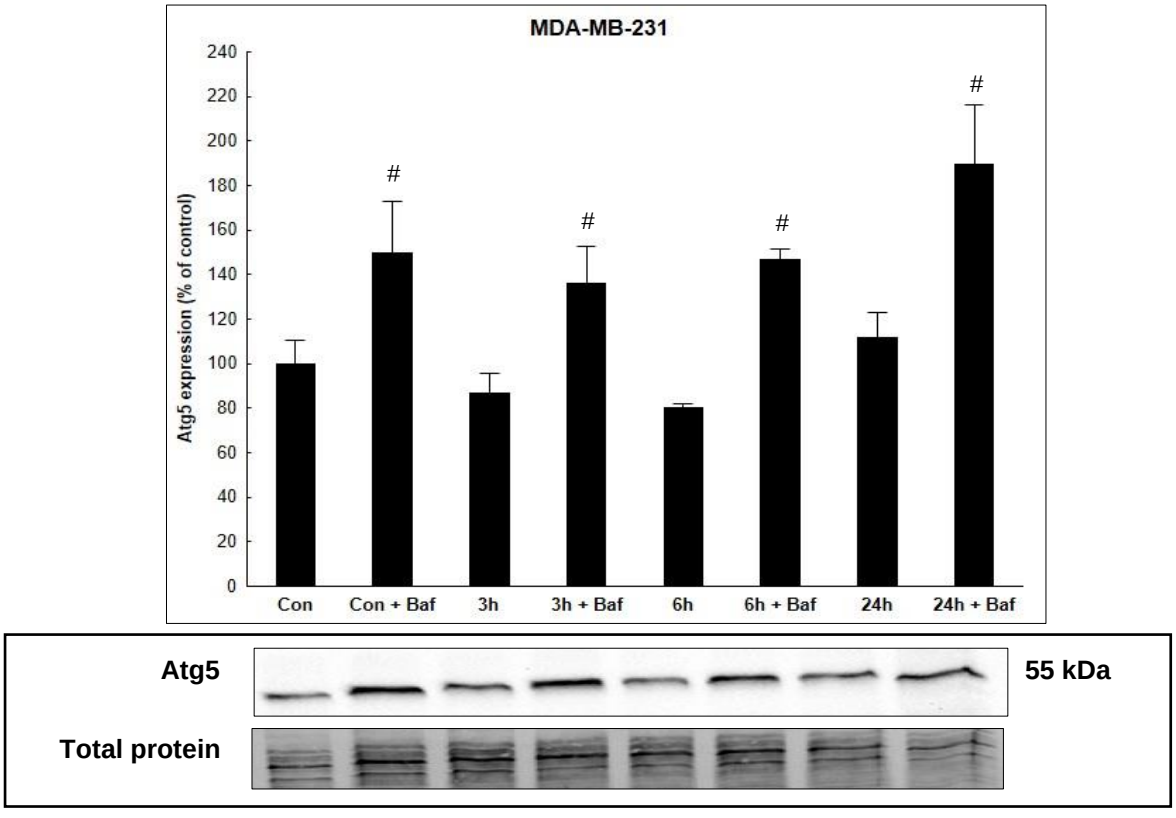

Figure 3.4: The effect of starvation over time on Atg5 expression. *Atg5 expression, as determined by western blotting, in MCF-12A cells, BT-549 cells and MDA-MB-231 cells. Results are presented as a percentage of the control ± SEM (n=3). * = p<0.05 when compared to the control; # = p<0.05 when the group treated with bafilomycin is compared to the corresponding untreated time point.*

3.1.2.2 The effect of starvation on p62 expression

p62, also known as Sequestosome 1 (SQSTM1) is a protein that is required for selective macroautophagy. It is commonly used as a marker for autophagic degradation, displaying an inverse relationship with levels of autophagy and LC3-II, unless bafilomycin treatment induces its accumulation (Mizushima & Komatsu, 2011).

There was a significantly greater expression of p62 in the respective bafilomycin-treated groups than in the control ($p<0.01$), three-hour ($p<0.001$), six-hour ($p<0.001$) and 24-hour ($p<0.01$) groups in the MCF-12A cell line. In the BT-549 cells, there were no significant differences between groups. There was a significantly greater expression of p62 in the respective bafilomycin groups than the the six-hour group ($p<0.05$) as well as the 24-hour group ($p<0.01$) in the MDA-MB-231 cells.

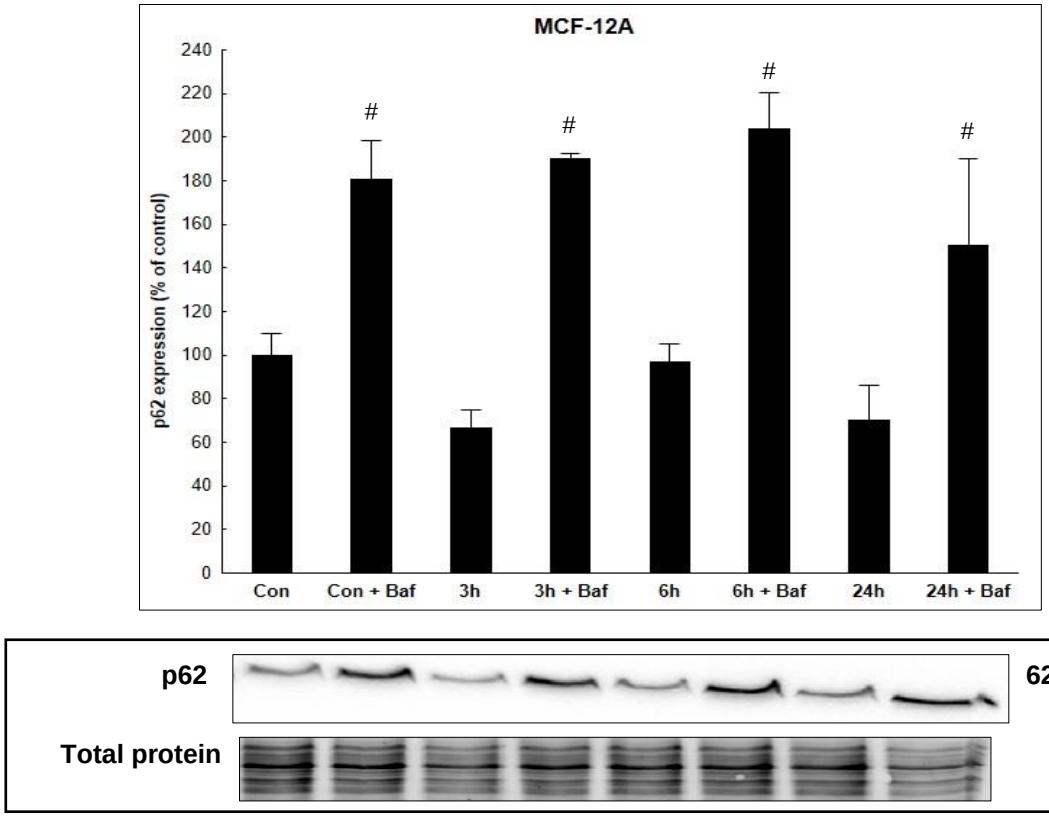

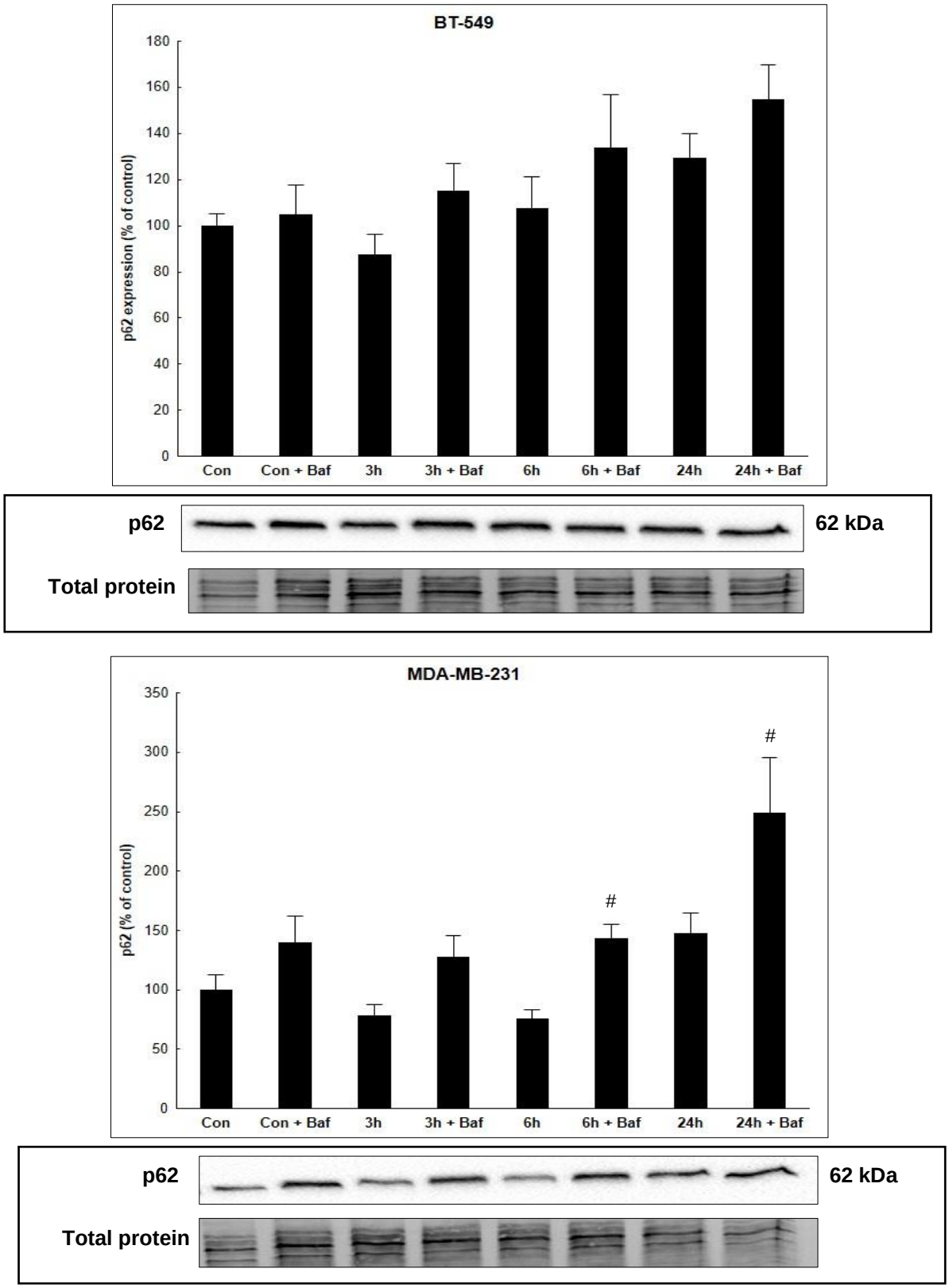

Figure 3.5: The effect of starvation over time on p62 expression. *p62 expression, as determined by western blotting, in MCF-12A cells, BT-549 cells and MDA-MB-231 cells. Results are presented as a percentage of the control ± SEM (n=3). * = p<0.05 when compared to the control; # = p<0.05 when the group treated with bafilomycin is compared to the corresponding untreated time point.*

3.1.2.3 The effect of starvation on LC3-II expression

LC3-I is converted to LC3-II during the maturation of autophagosomes. Quantifying the relative expression of LC3-II serves as an indicator of autophagic flux when combined with bafilomycin treatment (Mizushima & Komatsu, 2011).

Treatment with bafilomycin significantly increased levels of LC3-II in the control, three-hour, six-hour and 24-hour groups ($p<0.0001$) in the MCF-12A cells. The BT-549 cells, however, showed no significant differences when treated with bafilomycin. The MDA-MB-231 cells only showed a significant increase in LC3-II with bafilomycin treatment at the 24-hour time-point ($p<0.001$).

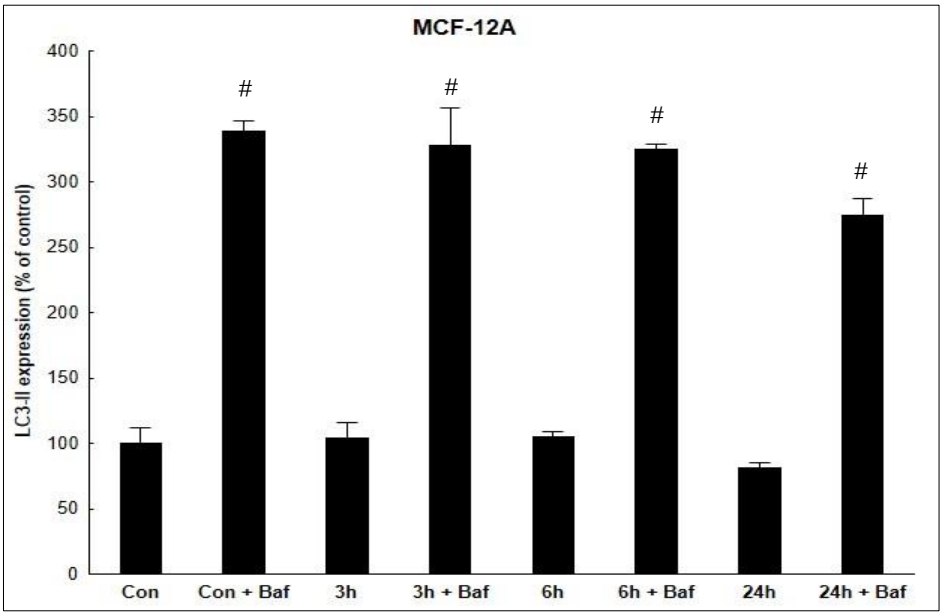

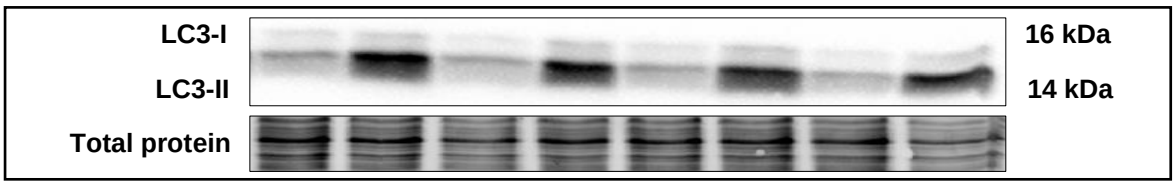

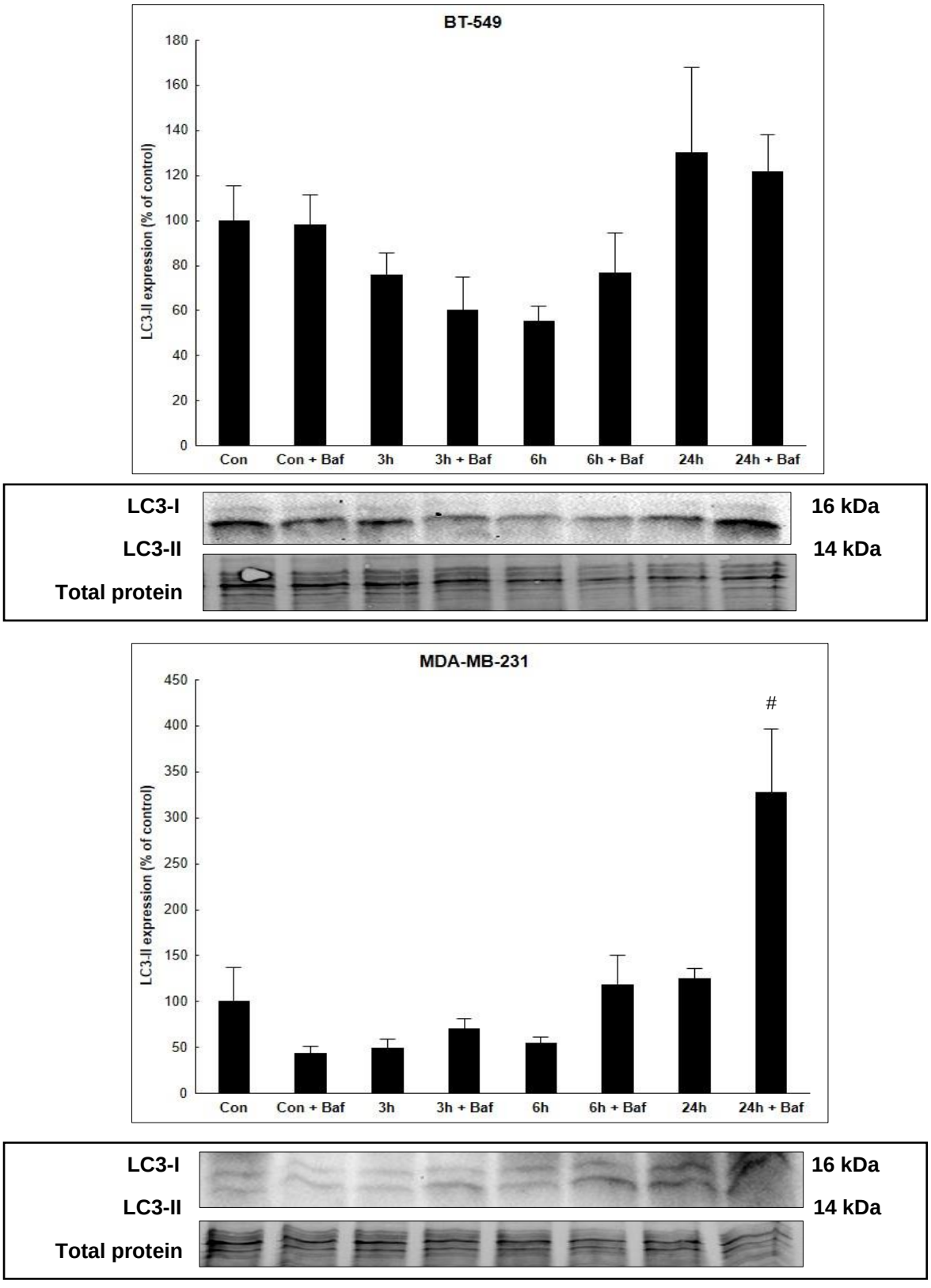

Figure 3.6: The effect of starvation over time on LC3-II expression. *LC3-II expression, as determined by western blotting, in MCF-12A cells, BT-549 cells and MDA-MB-231 cells. Results are presented as a percentage of the control ± SEM (n=3). * = p<0.05 when compared to the control; # = p<0.05 when the group treated with bafilomycin is compared to the corresponding untreated time point.*

3.1.2.4 The effect of starvation on the number of autophagosomes

Another means of quantifying autophagy is by determining the average number of autophagosomes per cell. Cells were transfected with an eGFP-LC3 plasmid and stained with LysoTracker Red™. After z-stack images were obtained using the Carl Zeiss LSM 780 confocal microscope, individual puncta representing autophagosomes were counted. Data is presented as a percentage of the control.

Bafilomycin treatment increased the number of autophagosomes in the control ($p<0.001$), six-hour ($p<0.001$), and 24-hour ($p<0.0001$) groups of the MCF-12A cells. In the BT-549 cells, bafilomycin increased the number of autophagosomes in the control ($p<0.0001$), three-hour ($p<0.001$), and six-hour ($p<0.0001$) group. Additionally, there was a significant difference between the control and three-hour group ($p<0.05$). In the MDA-MB-231 cell line, there was a significant increase in the three-hour ($p<0.01$), six-hour ($p<0.0001$) and 24-hour ($p<0.0001$) group when compared to the control group. Additionally, the control, three-hour and six-hour groups had a significantly higher number of autophagosomes when treated with bafilomycin ($p<0.0001$).

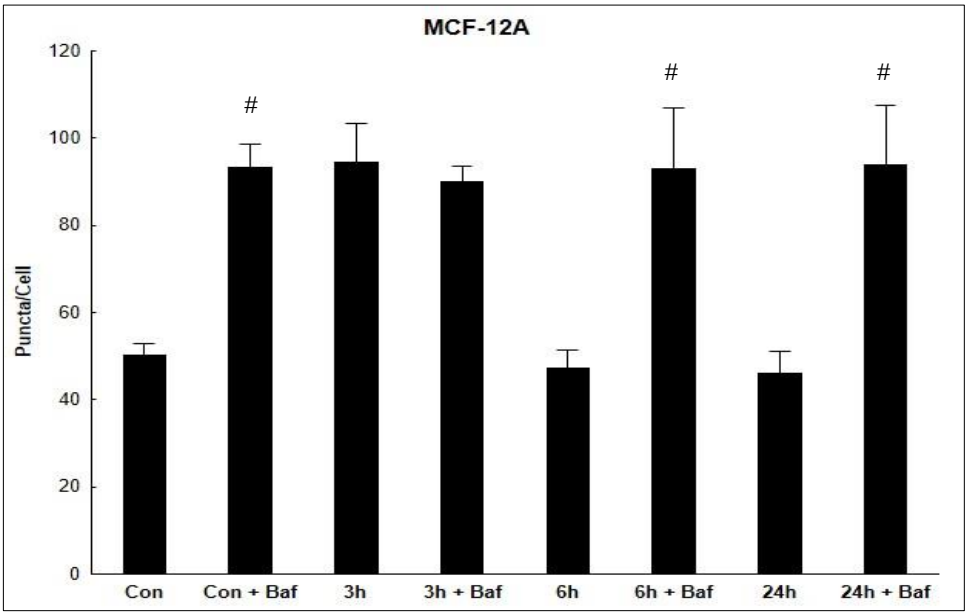

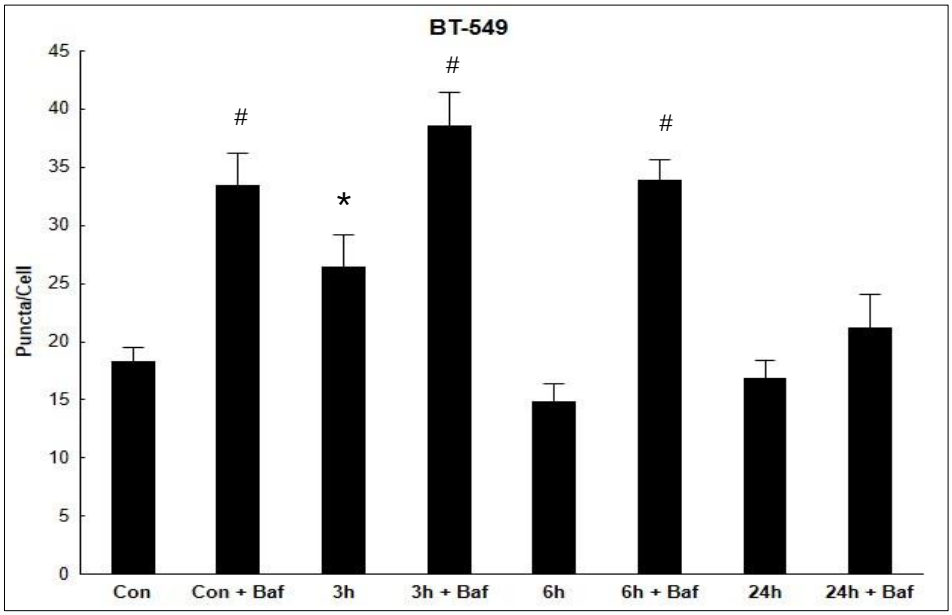

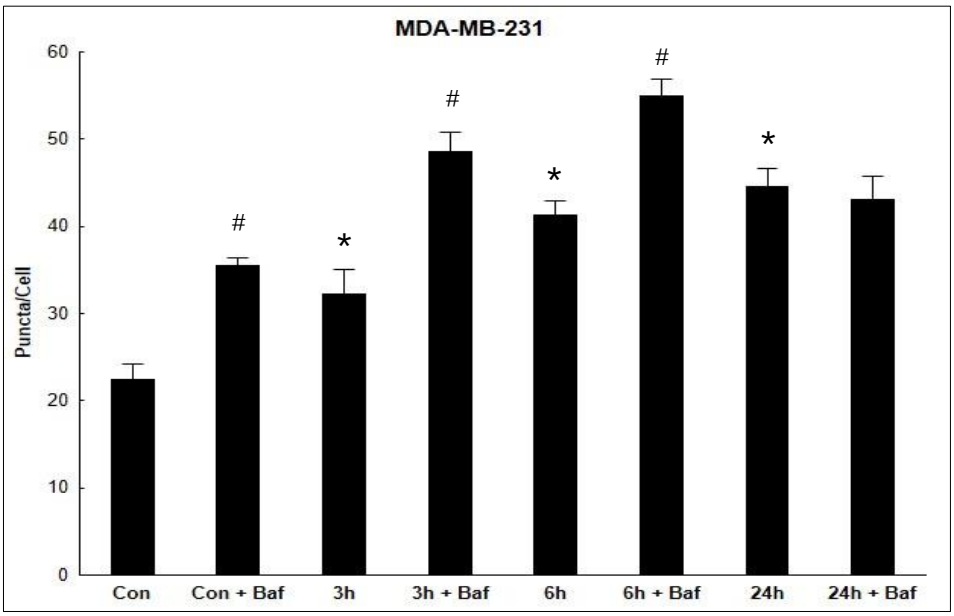

Figure 3.7: The effect of starvation over time on the number of autophagosomes. *The number of autophagosomes, as determined by fluorescent microscopy, in MCF-12A cells, BT-549 cells and MDA-MB-231 cells. Results are presented as the mean number of puncta per cell ± SEM (n=3). * = p<0.05 when compared to the control; # = p<0.05 when the group treated with bafilomycin is compared to the corresponding untreated time point.*

3.1.2.5 Representative images for LC3 puncta quantification

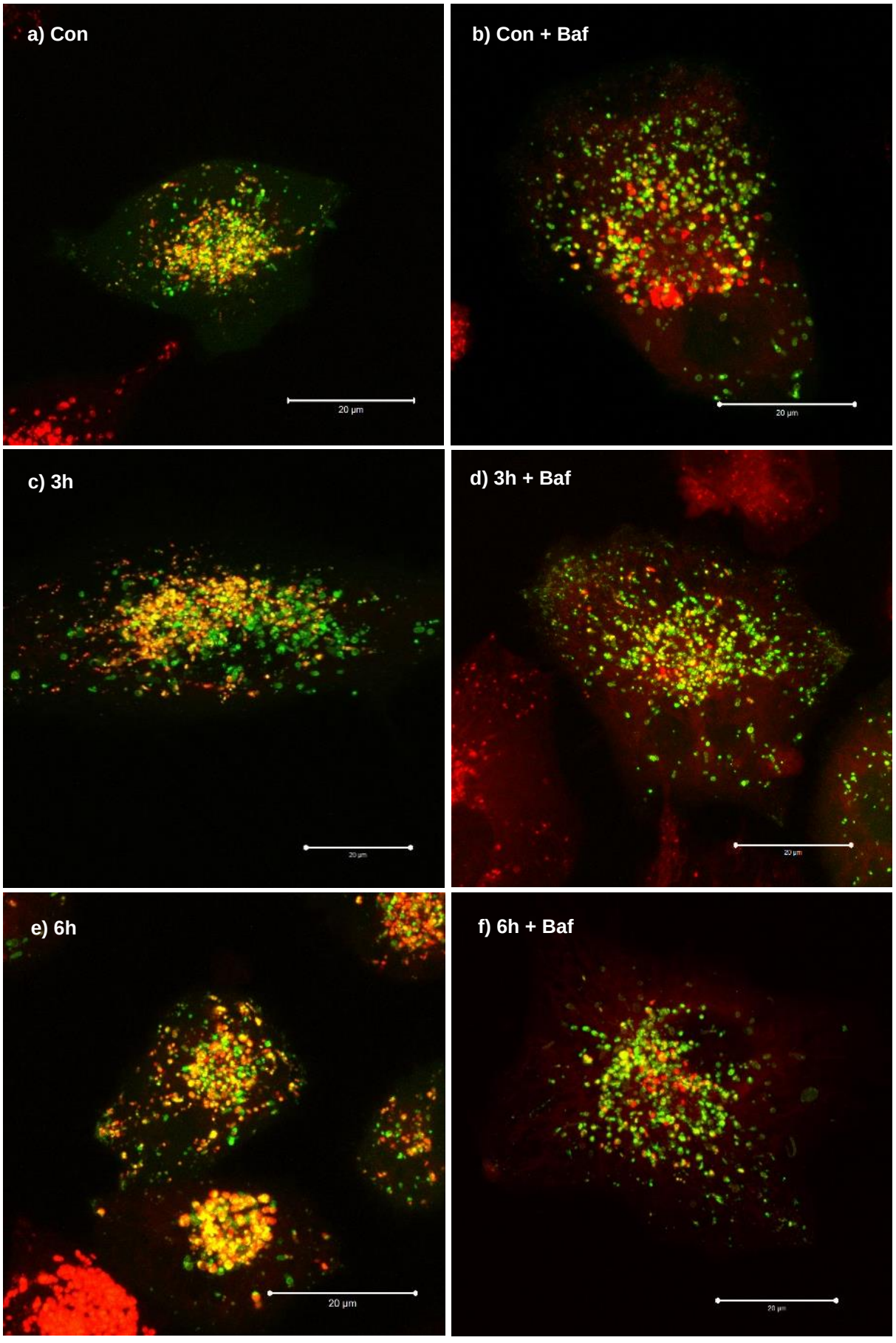

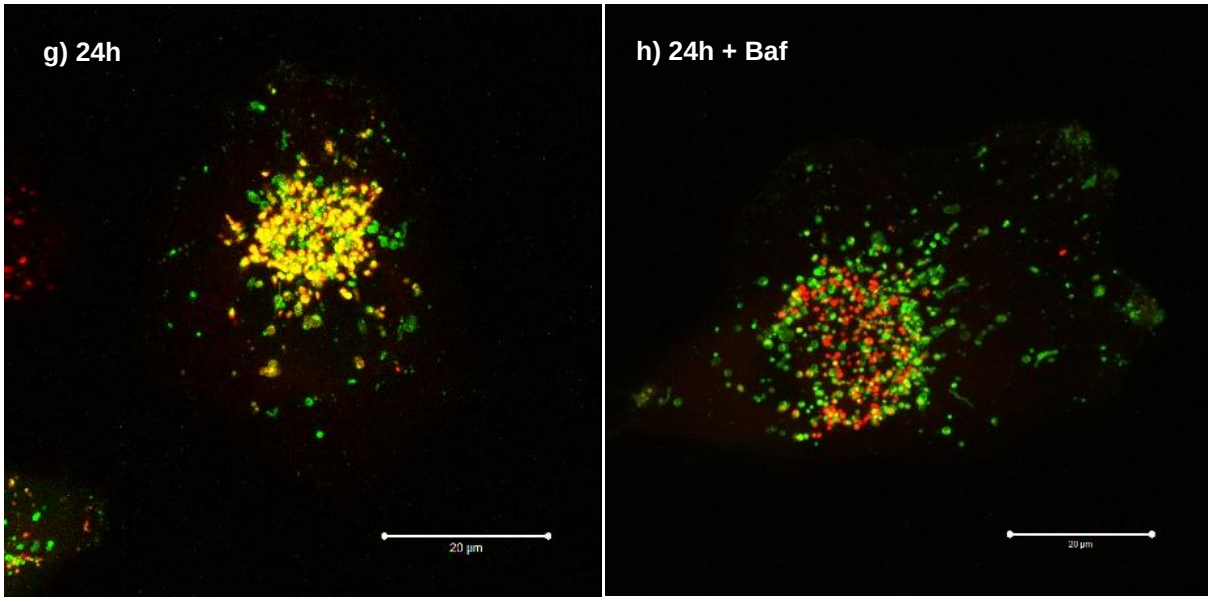

Figure 3.8: Representative images for visualisation of autophagosomes and lysosomes in MCF-12A cells following different periods of starvation. *eGFP-LC3 transfected MCF-12A cells were seeded and starved for 3-, 6- and 24-hours, and stained with LysoTracker Red. Bafilomycin was added at a concentration of 400 nM one hour prior to imaging on the Carl Zeiss LSM 780 confocal microscope. The scale bar represents 20 µm.*

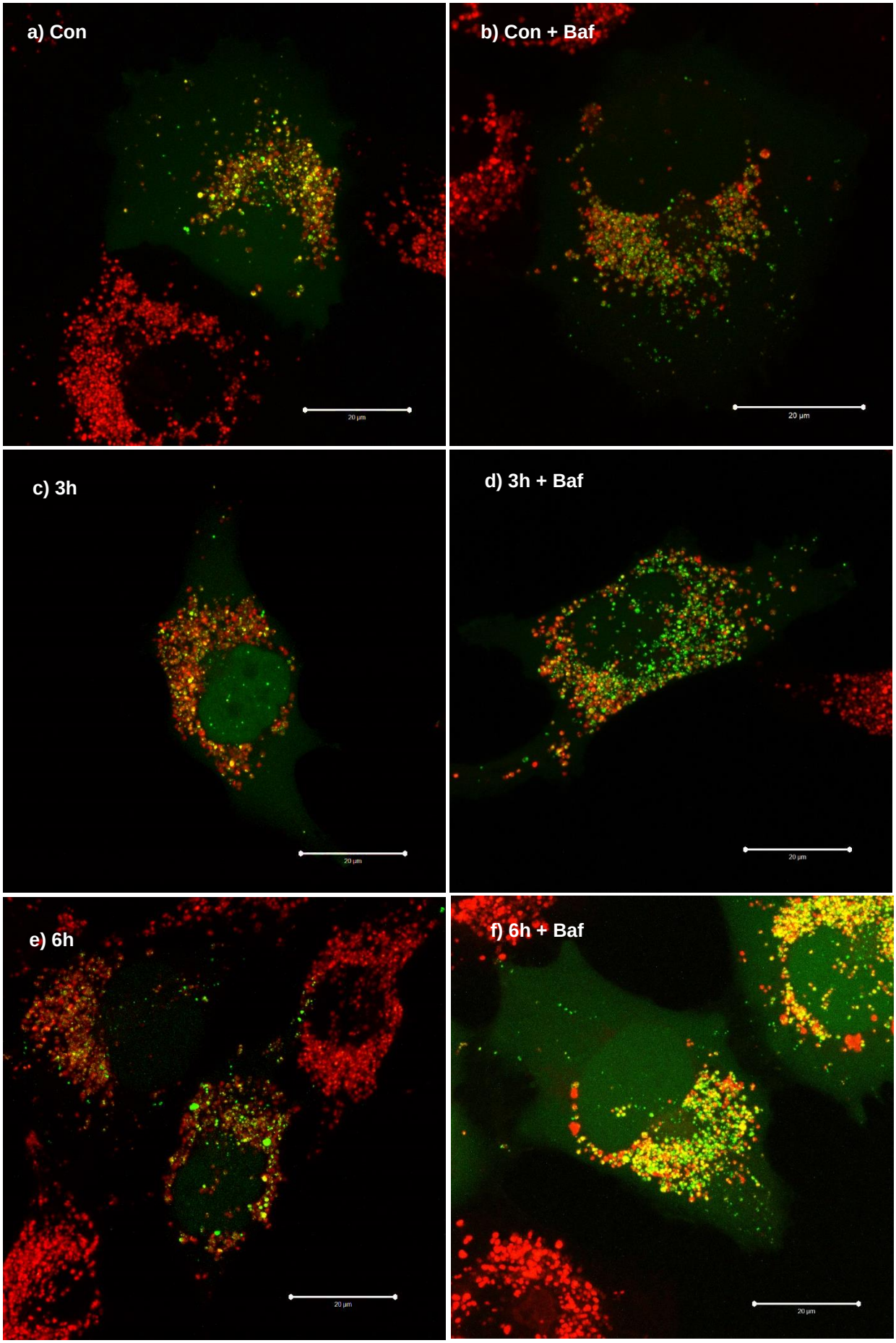

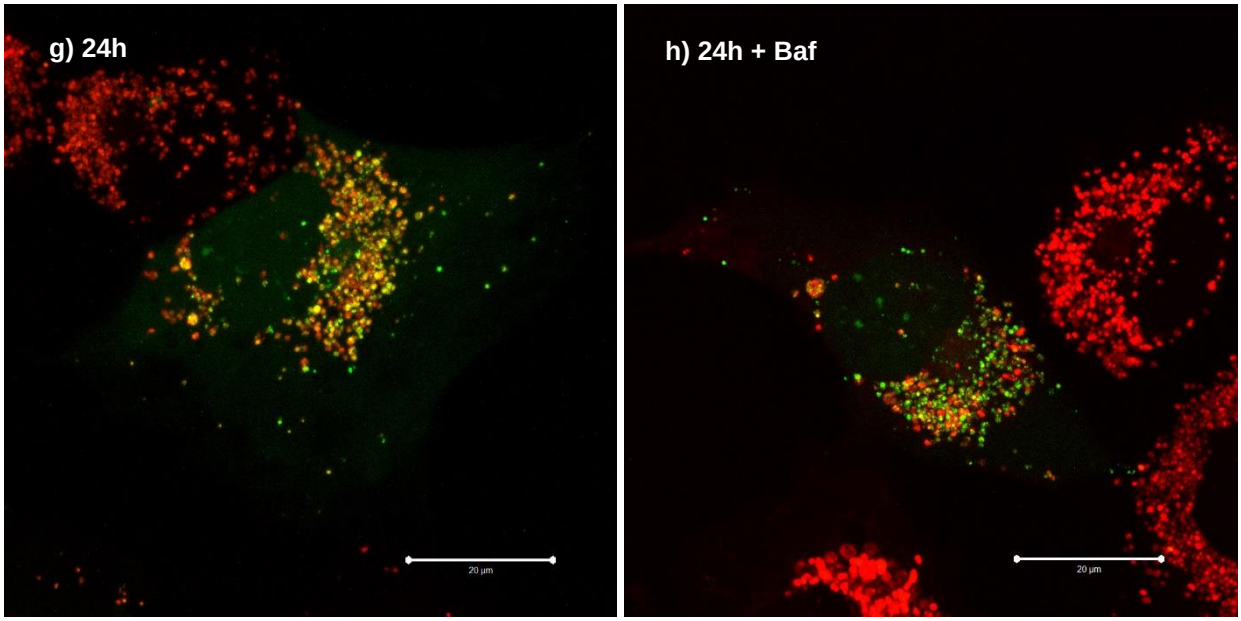

Figure 3.9: Representative images for visualisation of autophagosomes and lysosomes in BT-549 cells following different periods of starvation. *eGFP-LC3 transfected BT-549 cells were seeded and starved for 3-, 6- and 24-hours, and stained with LysoTracker Red. Bafilomycin was added at a concentration of 400 nM one hour prior to imaging on the Carl Zeiss LSM 780 confocal microscope. The scale bar represents 20 µm.*

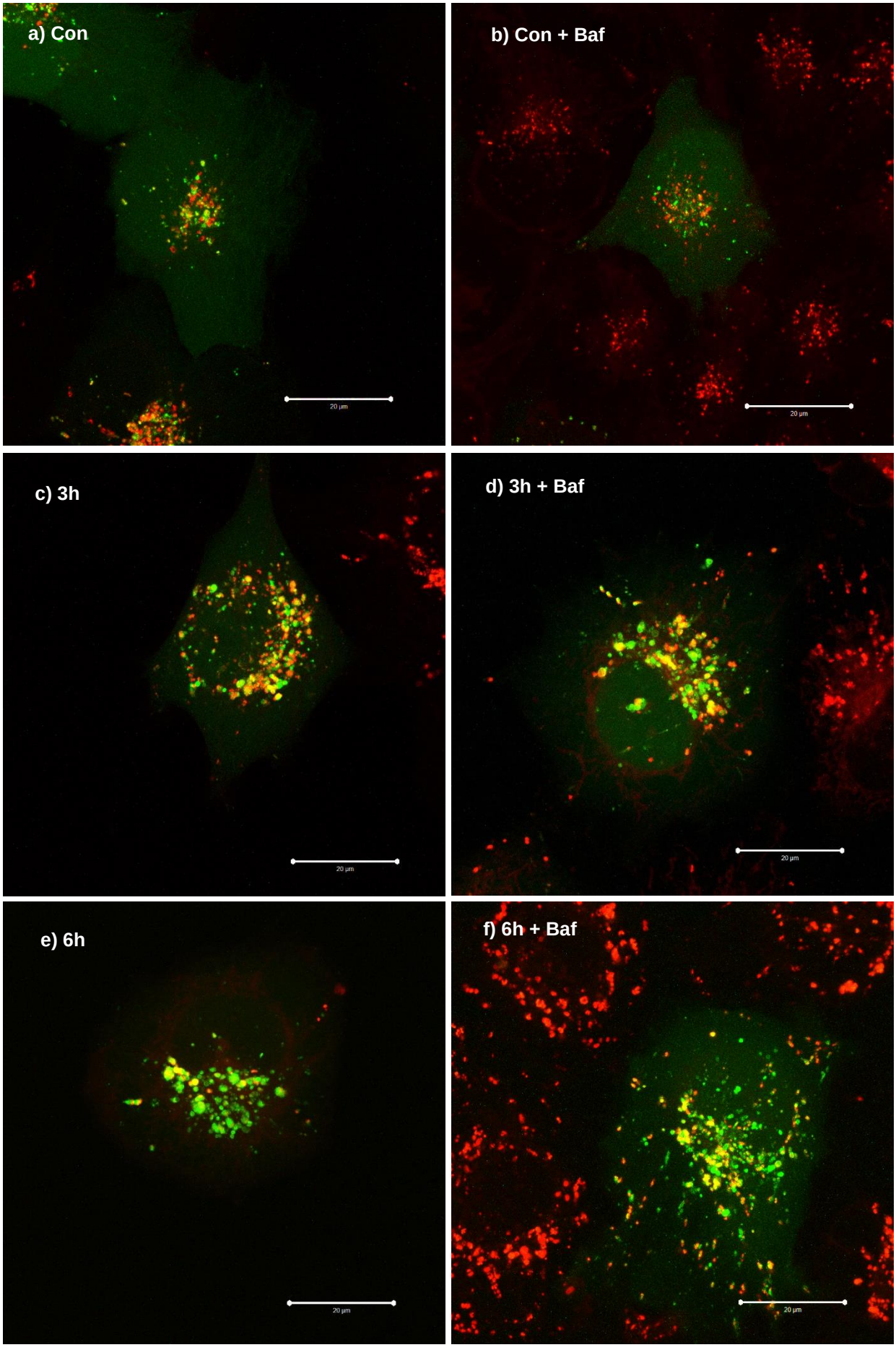

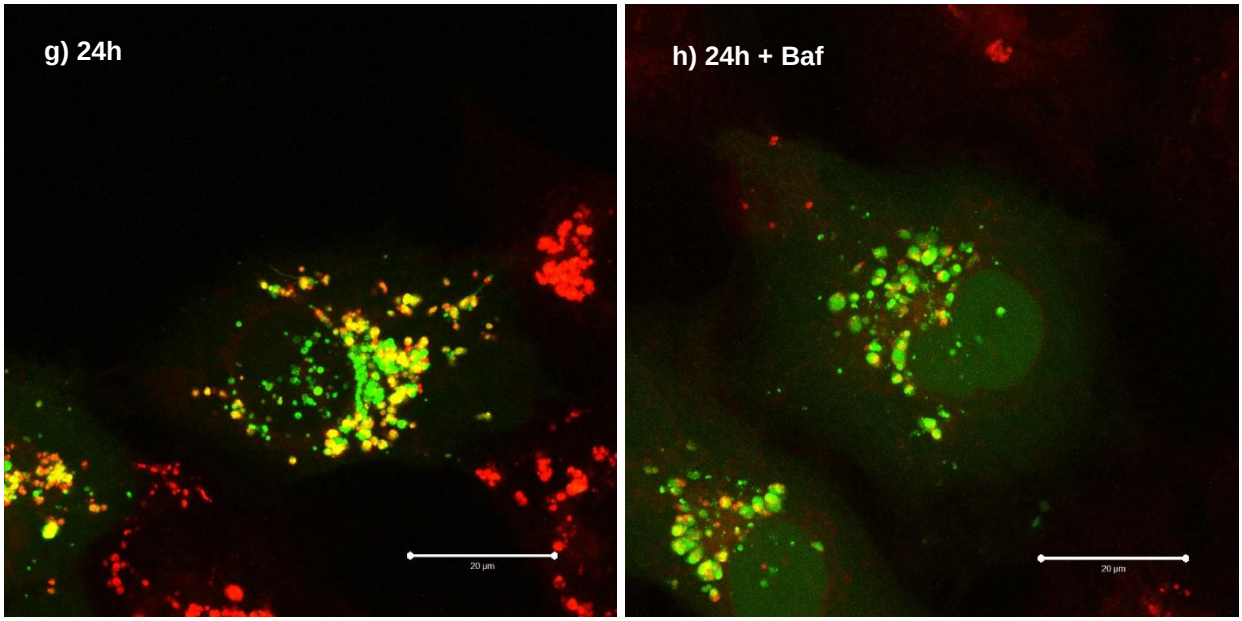

Figure 3.10: Representative images for visualisation of autophagosomes and lysosomes in MDA-MB-231 cells following different periods of starvation. *eGFP-LC3 transfected MDA-MB-231 cells were seeded and starved for 3-, 6- and 24-hours, and stained with LysoTracker Red. Bafilomycin was added at a concentration of 400 nM one hour prior to imaging on the Carl Zeiss LSM 780 confocal microscope. The scale bar represents 20 µm.*

3.1.3 The effect of starvation on cell cycle progression

To establish the effect of starvation over time on cell cycle progression and growth arrest, cell cycle analysis was performed.

In the MCF-12A cell line, the proportion of cells in the G_0/G_1 phase increased with starvation, with significantly higher percentages in the six-hour ($p<0.05$) and 24-hour ($p<0.01$) groups. All three starvation periods reduced the proportion of cells in the S-phase ($p<0.05$). There were no significant differences between any of the groups in the percentage of cells in the G_2/M phase.

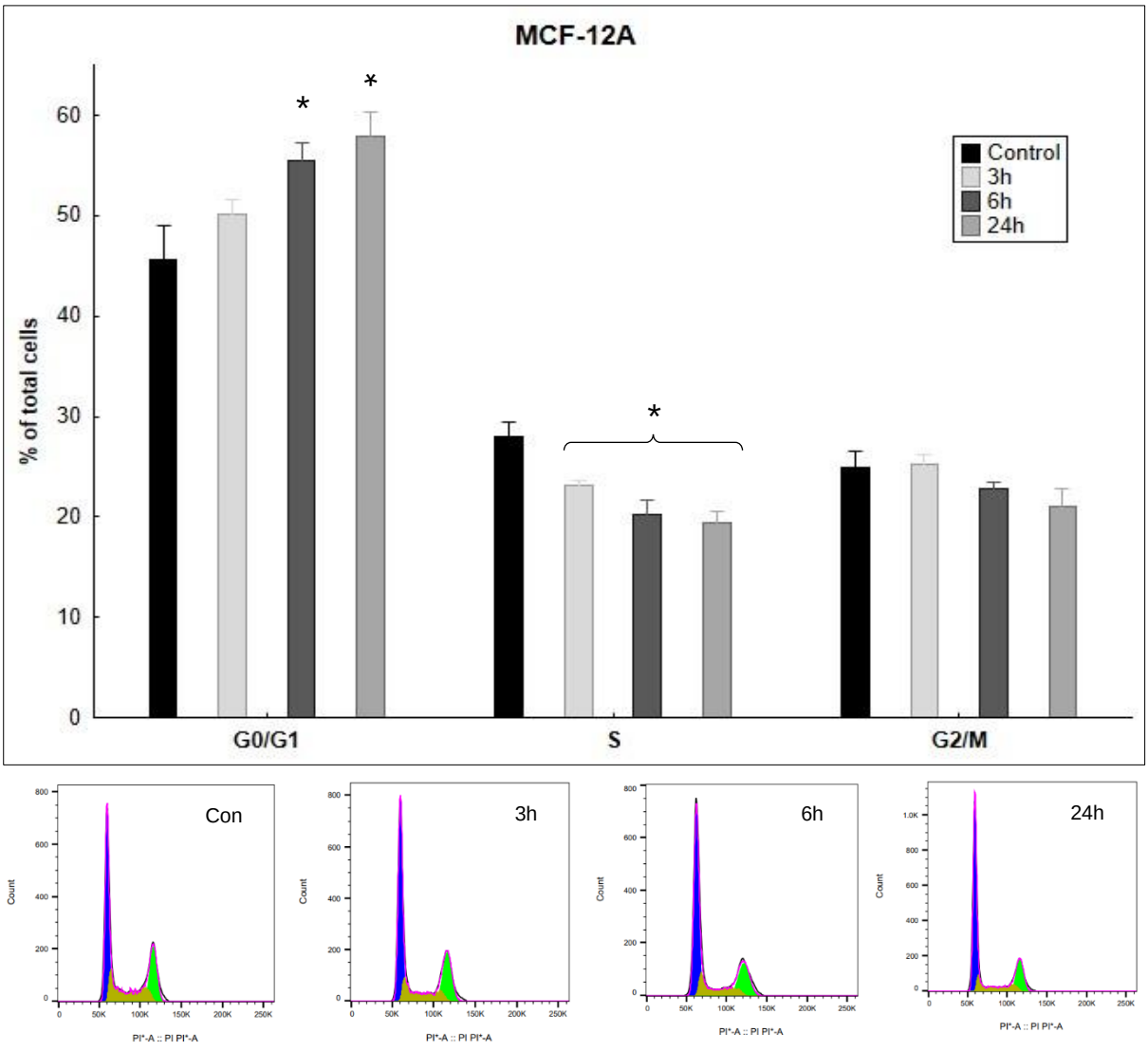

Figure 3.11: The effect of starvation over time on cell cycle progression in MCF-12A cells. *The percentage of cells in the G_0/G_1 phase, S phase and G_2/M phase, as determined by flow cytometry, in MCF-12A cells. Results are presented as the mean percentage of cells per group ± SEM (n=3). * = $p<0.05$ when compared to the control.*

Only a starvation period of 24-hours significantly increased the percentage of cells in the G_0/G_1 phase ($p<0.0001$) in the BT-549 cells when compared to the control. There were significantly fewer cells in the S phase in the six-hour ($p<0.05$) and 24-hour ($p<0.0001$) groups. The three-hour ($p<0.001$), six-hour ($p<0.001$) and 24-hour ($p<0.05$) had a significantly higher percentage of cells in the G_2/M phase than the control group.

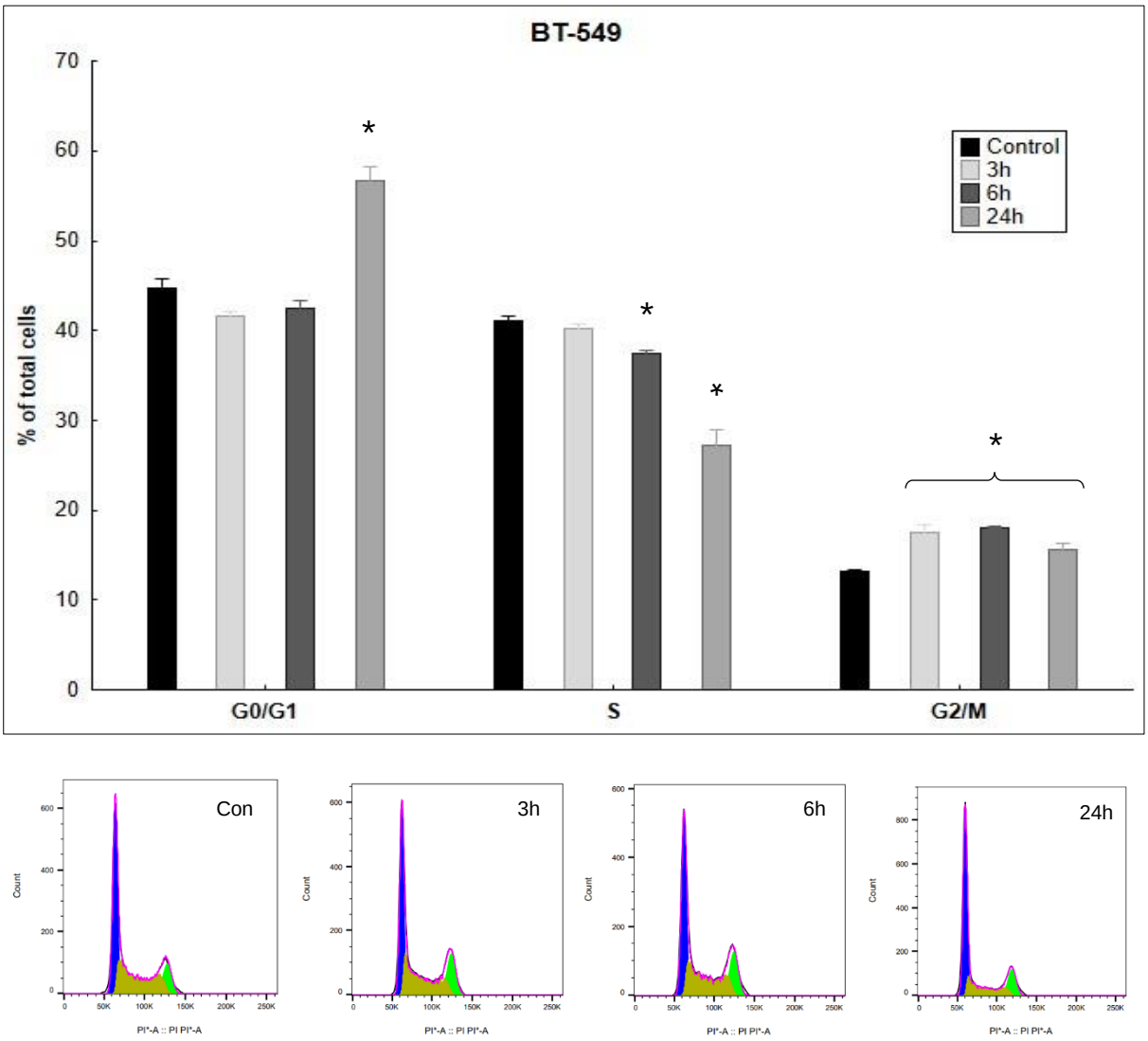

Figure 3.12: The effect of starvation over time on cell cycle progression in BT-549 cells. *The percentage of cells in the G_0/G_1 phase, S phase and G_2/M phase, as determined by flow cytometry, in BT-549 cells. Results are presented as the mean percentage of cells per group ± SEM (n=3). * = $p<0.05$ when compared to the control.*

In the MDA-MB-231 cell line, there were significantly more cells in the G_0/G_1 phase in the six-hour and 24-hour groups ($p<0.05$). Starvation significantly reduced the proportion of cells in the S phase in the six-hour and 24-hour groups ($p<0.01$). Only the three-hour group displayed a significant increase in the percentage of cells in the G_2/M phase ($p<0.05$).

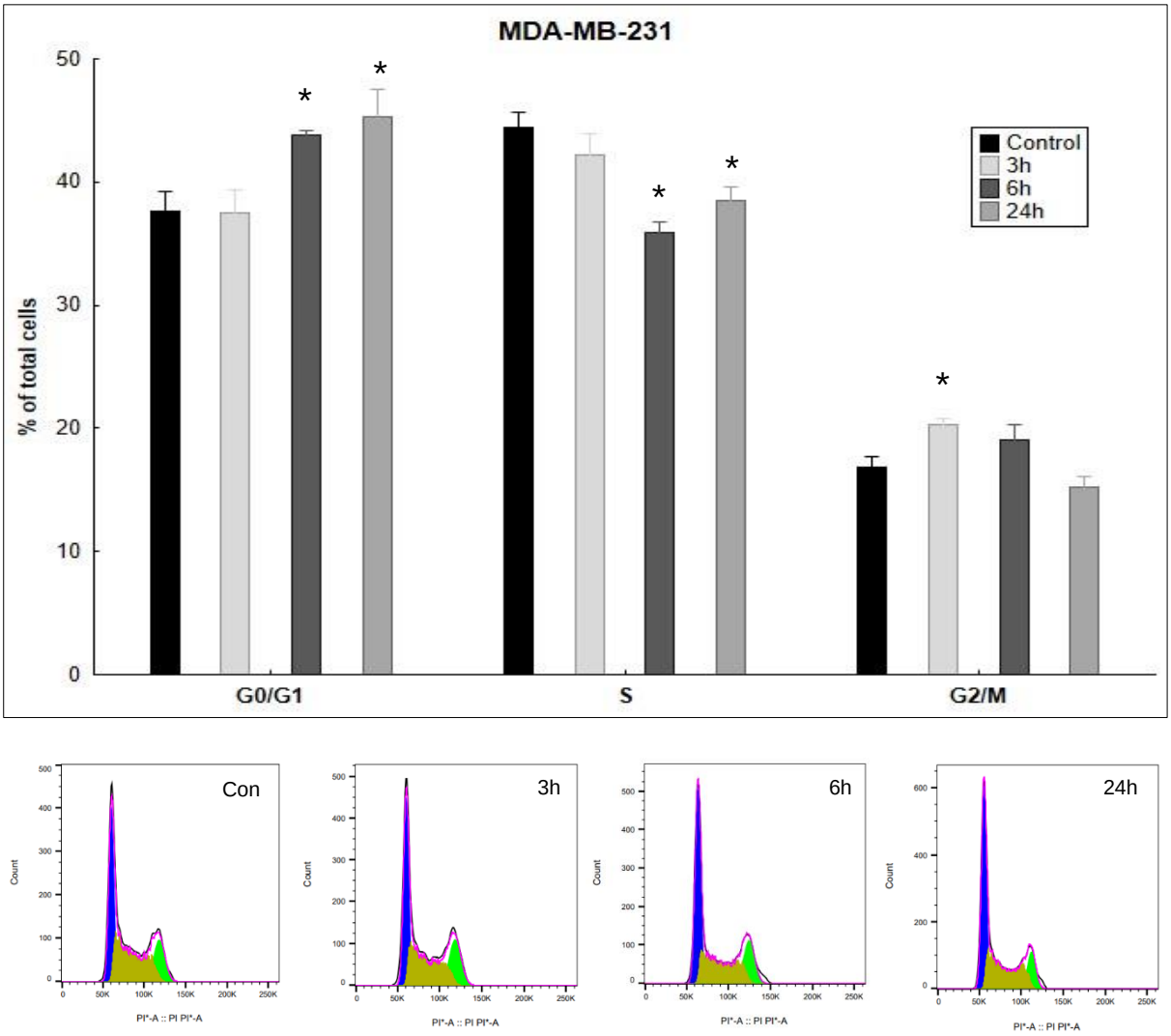

Figure 3.13: The effect of starvation over time on cell cycle progression in MDA-MB-231 cells. *The percentage of cells in the G_0/G_1 phase, S phase and G_2/M phase, as determined by flow cytometry, in MDA-MB-231 cells. Results are presented as the mean percentage of cells per group ± SEM (n=3). * = $p<0.05$ when compared to the control.*

3.1.4 The effect of starvation on cell viability

In order to determine the effect of starvation over time on cell viability, a WST1 assay was conducted. WST1 is reduced to formazan through the production of NAD(P)H, which only occurs in metabolically active cells. The level of mitochondrial activity therefore determines the amount of formazan produced. This generally corresponds with the number of live cells and is thus used as a proxy for cell viability (Van den Berghe, *et al.*, 2013). There was a small but significant increase in cell viability in the three-hour ($p<0.01$) and six-hour ($p<0.001$) starvation groups in the MCF-12A cells, but not in the 24-hour group. In the BT-549 cell line, there was a significant reduction in cell viability following three and six hours of starvation ($p<0.0001$). Compared to the control group, the three-hour ($p<0.001$) and six-hour ($p<0.01$) groups displayed significantly higher viability in the MDA-MB-231 cells, while 24 hours of starvation resulted in a small but significant reduction in cell viability ($p<0.05$).

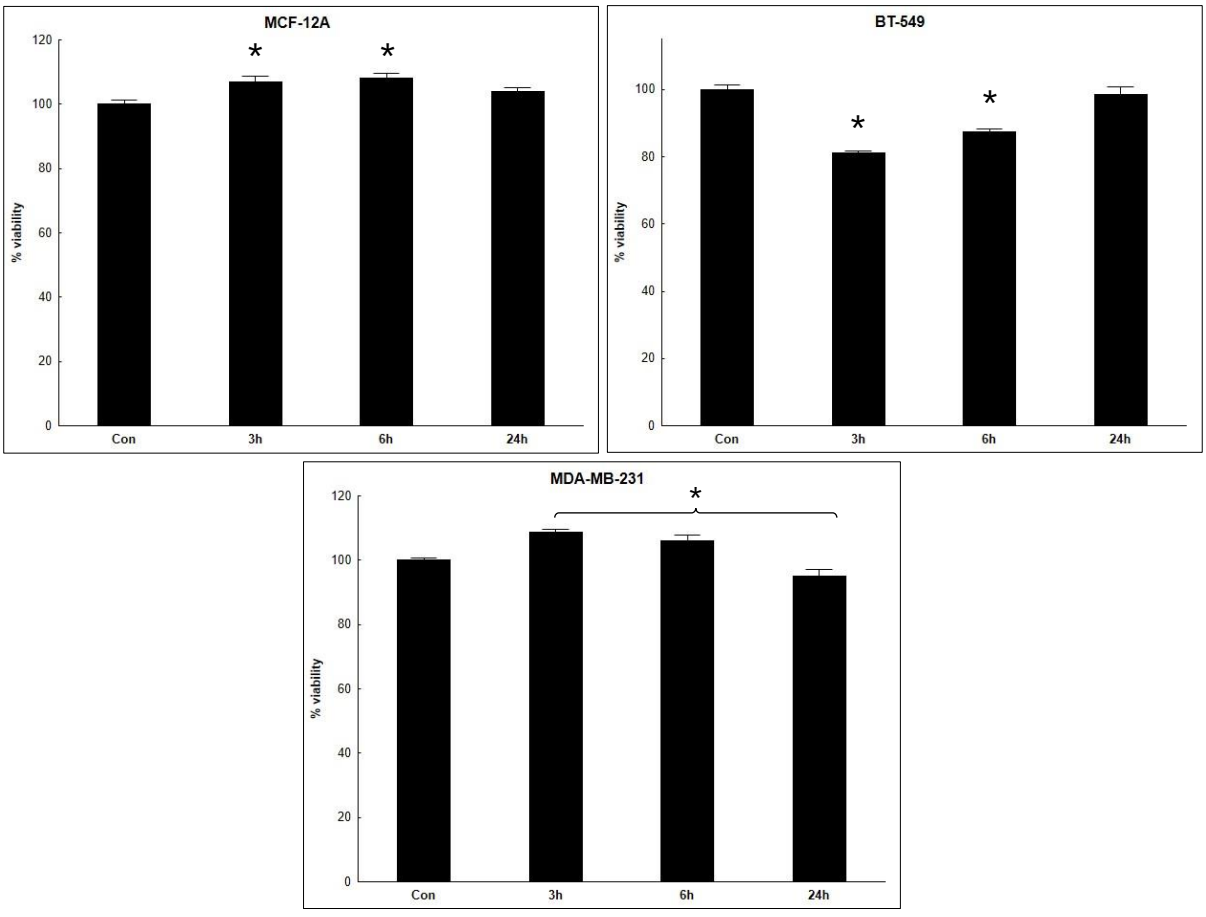

Figure 3.14: The effect of starvation over time on cell viability. *Cell viability, as determined by WST1 assay, in MCF-12A cells, BT-549 cells and MDA-MB-231 cells. Results are presented as the mean percentage of viable cells per group ± SEM (n=3). * = p<0.05 when compared to the control.*

3.1.5 Selection of a starvation period

Based on the above data, a starvation period of 24 hours was selected for the remainder of the study. By 24 hours, the difference from the control group was often the most notable but did not significantly reduce cell viability. Additionally, this period of starvation was commonly used in the literature (Raffaghello, *et al.,* 2008; Safdie, *et al.*, 2012; D'Aronzo, *et al.,* 2015). Lastly, this time point reflects *ex vivo* conditions most accurately (Safdie, *et al.*, 2009).

Part 2: The effect of starvation on chemosensitivity

3.2.1 Doxorubicin dose-response viability study

A dose-response viability study was first conducted to select an appropriate concentration for treatment with doxorubicin. A WST1 assay was used to establish the effect of different concentrations on cell viability. In the MCF-12A cell line, all five concentrations of doxorubicin were able to significantly reduce cell viability ($p<0.001$). However, this effect became more pronounced with concentrations higher than 5 µM. The BT-549 cell line only showed a significant reduction at 2.5 µM ($p<0.001$), and for both concentrations thereafter. The MDA-MB-231 cells showed a small but significant reduction in cell viability from 2.5-10 µM ($p<0.01$). Based on these results, a concentration of 2.5 µM was selected to serve as the concentration for doxorubicin treatment for the remainder of this study. This concentration significantly reduced cell viability by approximately 17% in the MCF-12A cells, 15% in the BT-549 cells and 9% in the MDA-MB-231 cells. This was considered sufficient to illustrate either enhanced or reduced chemosensitivity with short-term starvation (STS) in any of the cell lines.

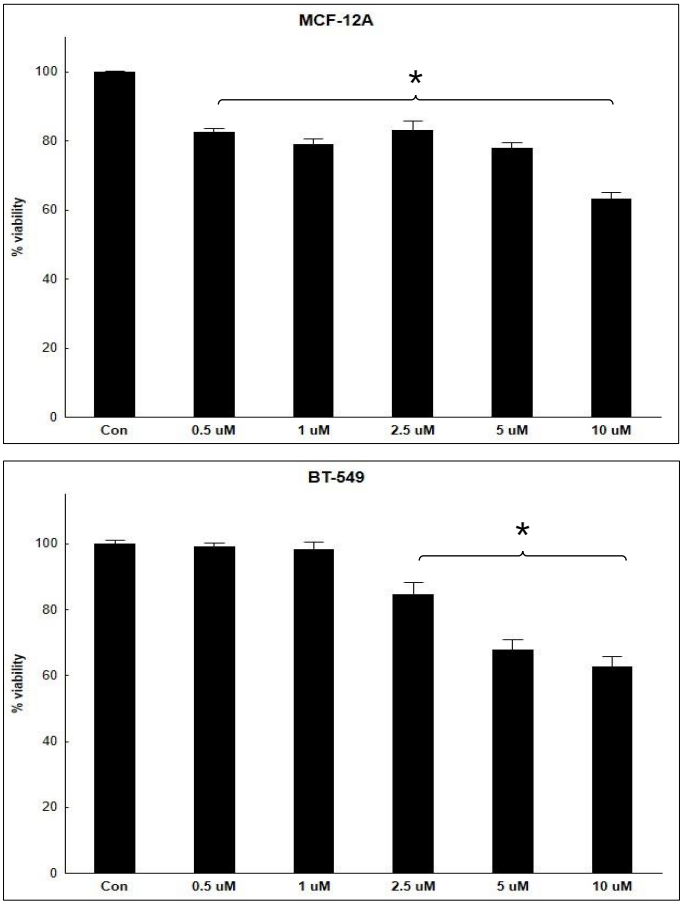

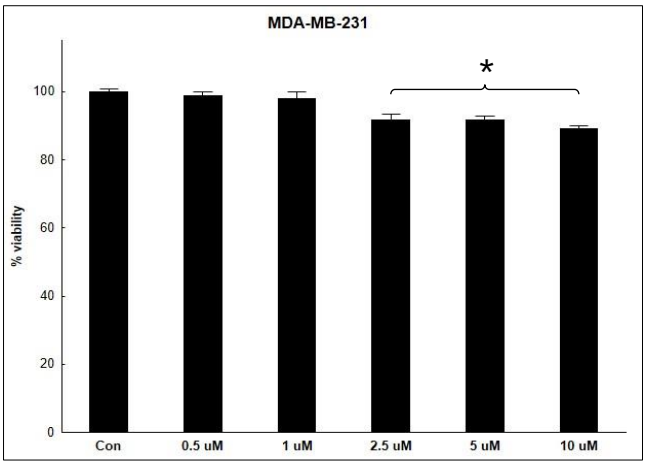

Figure 3.15: Doxorubicin dose-response viability studies. *Cell viability, as determined by a WST1 assay, in MCF-12A cells, BT-549 cells and MDA-MB-231 cells. Results are presented as a percentage of the control ± SEM (n=3). * = p<0.05 when compared to the control.*

3.2.2 Treatment conditions

For the second part of the study, cells were seeded in plates or flasks and treated according to their respective treatment group. A total of four experimental groups were included: 1) a control group (Con); 2) a 24-hour starvation period (St); 3) a 24-hour treatment period with doxorubicin (Dox); 4) a 24-hour starvation period followed by a 24-hour treatment period with doxorubicin (StDox).

Cells were starved using low-glucose media with reduced FBS (1% as opposed to 10%). Doxorubicin treatment was administered at a concentration of 2.5 µM in standard media. All cells not receiving treatment were refreshed with fully supplemented standard media.

All data were assessed for normality using the Kruskal-Wallis test. Data were analysed using one-way ANOVAs. In terms of statistical significance, * = $p<0.05$ when compared to the control; # = $p<0.05$ when compared to the doxorubicin treatment group.

3.2.3 The effect of starvation and doxorubicin on live cell number

A live cell count was employed to establish the effects of starvation, doxorubicin and the combination thereof on the total number of viable cells. Cells undergoing stress may respond in a variety of ways which, among others, may include either a reduction in their rate of proliferation, or the induction of cell death. Both of these mechanisms would result in a lower live cell count, and it was later established through viability studies and cell cycle analysis which accounted for the changes in cell number.

In the MCF-12A cell line, both the doxorubicin ($p<0.001$) and combination treatment ($p<0.001$) significantly reduced the number of live cells when compared to the control. There was no significant difference between the doxorubicin and combination groups. This trend was also observed in the BT-549 cell line, with significantly fewer live cells in both the doxorubicin treatment group ($p<0.001$) and the combination group ($p<0.01$). While there were a greater number of live cells in the combination group than the doxorubicin treatment group, this did not achieve statistical significance ($p=0.155$). In the MDA-MB-231 cells, there was a significant reduction in live cell number between the control group and the doxorubicin treatment group ($p<0.05$), as well as the combination group ($p<0.01$). While there were fewer cells in the combination group than the doxorubicin treatment group, this was also not significant ($p=0.238$).

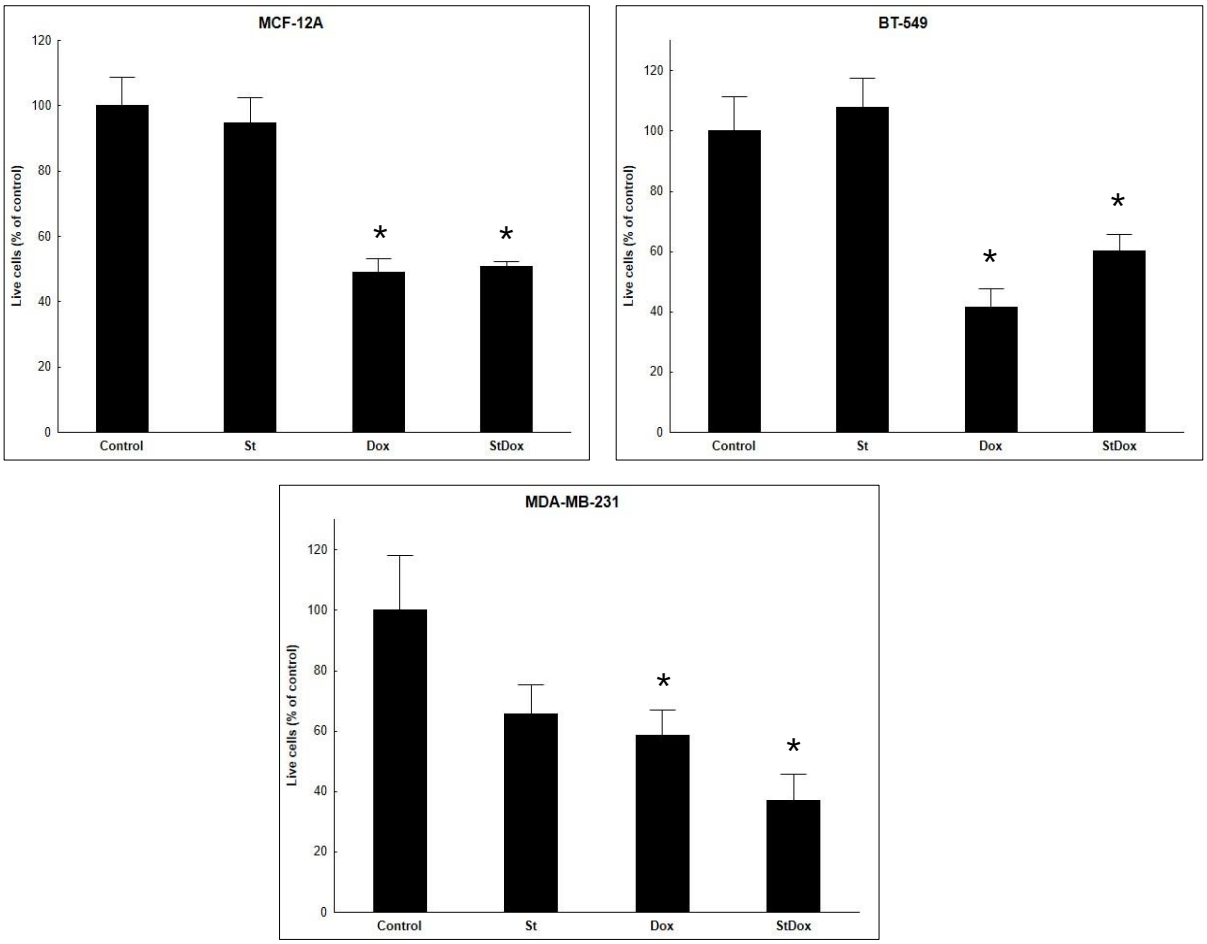

Figure 3.16: The effect of starvation, doxorubicin and the combination thereof on live cell counts. *Total number of live cells, as determined by a cell count with trypan blue, in MCF-12A cells, BT-549 cells and MDA-MB-231 cells. Results are presented as a percentage of the control ± SEM (n or N=3). * = p<0.05 when compared to the control.*

3.2.4 The effect of starvation and doxorubicin treatment on cell viability using flow cytometry with a propidium iodide stain

To further examine the effect of starvation on chemosensitivity, cell viability was assessed through the use of flow cytometry with propidium iodide. Propidium iodide is generally excluded from viable cells due to its inability to permeate intact cell membranes. When cells become non-viable, membrane integrity is lost. This allows the dye to enter the cell and bind to nucleic acids, serving as a marker for non-viable cells.

In both the MCF-12A and MDA-MB-231 cell lines, there were no significant differences in the percentage of dead cells between any of the groups. However, in the BT-549 cells, there was a small, but significant difference between the combination group and both the control group ($p<0.001$), and the doxorubicin group ($p<0.01$).

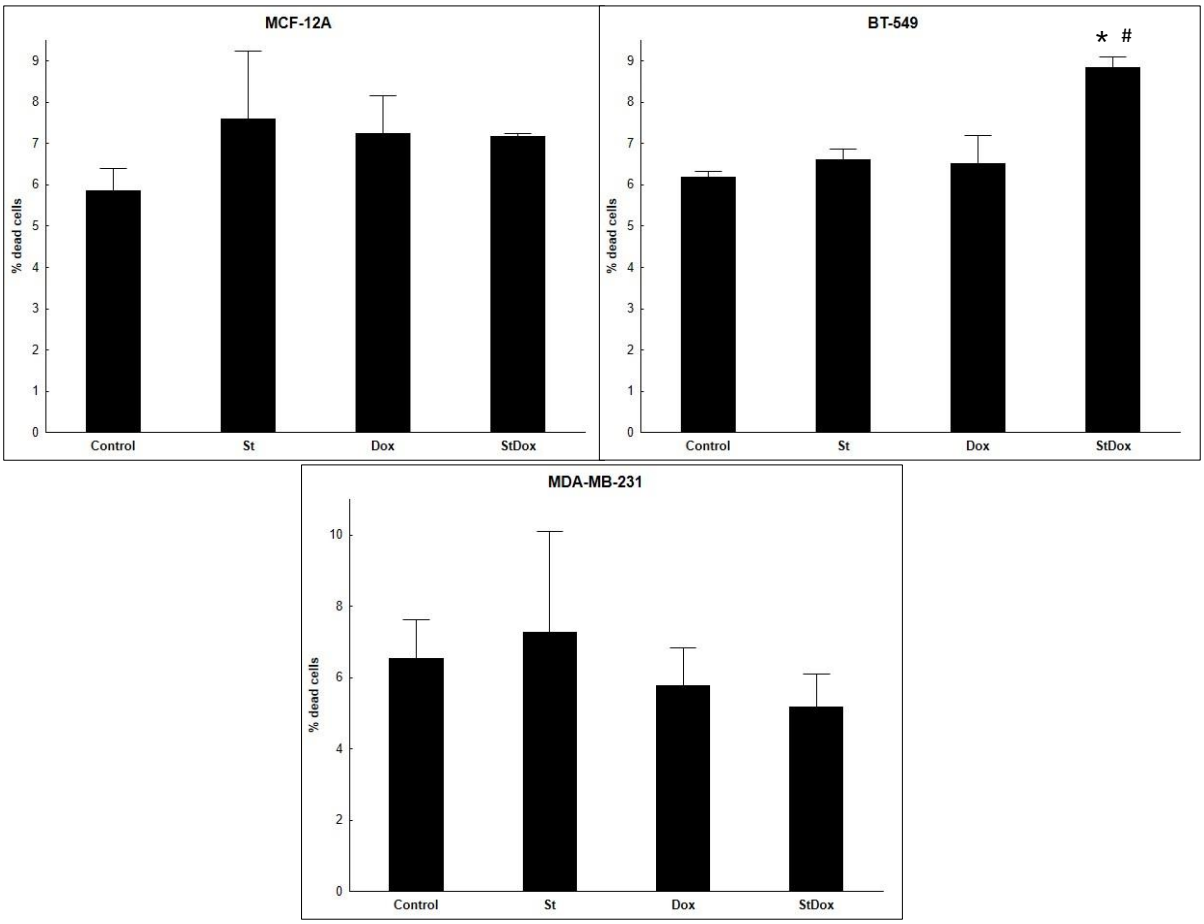

Figure 3.17: The effect of starvation, doxorubicin, and the combination thereof on cell death. *Percentage of dead cells, determined using flow cytometry with propidium iodide, in MCF-12A cells, BT-549 cells and MDA-MB-231 cells. Results are presented as the mean percentage of non-viable cells per group ± SEM (n=3). * = p<0.05 when compared to the control; # = p<0.05 when compared to the doxorubicin treatment group.*

3.2.5 The effect of starvation and doxorubicin treatment on cell viability

In order to determine the effect of starvation on chemosensitivity, a WST1 assay was conducted. There was a small but significant reduction in cell viability following starvation in the MCF-12A cell line ($p<0.05$). However, there was a greater reduction in viability following the doxorubicin ($p<0.0001$) and combination ($p<0.0001$) treatments. There was also a small but significant difference between the doxorubicin and combination groups ($p<0.01$). In the BT-549 cell line, there was a small but significant reduction in cell viability when comparing the control group to the starvation ($p<0.01$), doxorubicin ($p<0.05$) and combination groups ($p<0.0001$). There was also a significant difference between the doxorubicin and combination group ($p<0.05$). In the MDA-MB-231 cells, a small but significant reduction in cell viability followed starvation ($p<0.01$), doxorubicin ($p<0.01$) and the combination treatments ($p<0.0001$). There was also a significant difference between the doxorubicin and combination group ($p<0.05$).

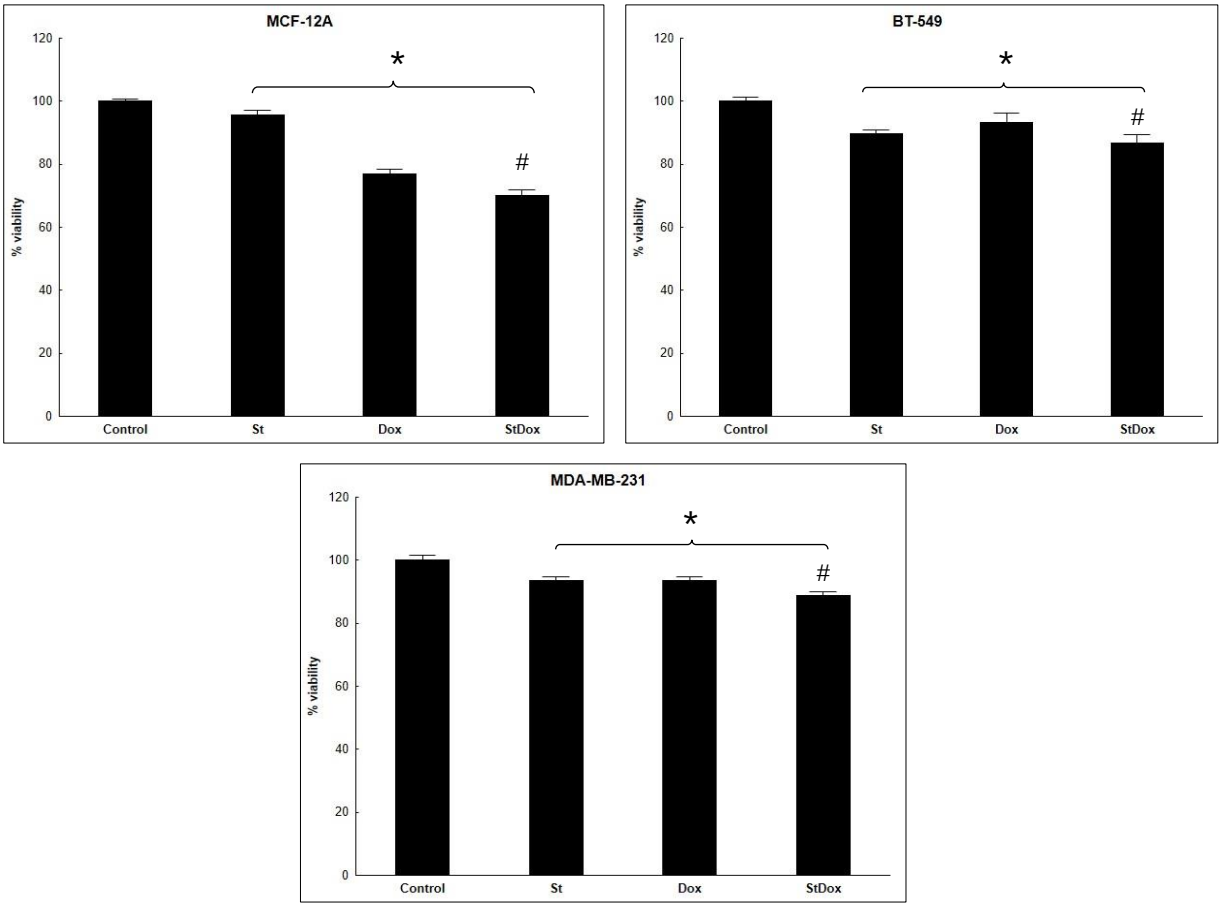

Figure 3.18: The effect of starvation, doxorubicin, and the combination thereof on cell viability. *Cell viability, as determined by WST1 assay in MCF-12A cells, BT-549 cells, and MDA-MB-231 cells. Results are presented as the mean percentage of viable cells per group ± SEM (n=3). * = p<0.05 when compared to the control; # = p<0.05 when compared to the doxorubicin treatment group.*

3.2.6 The effect of starvation and doxorubicin treatment on cell cycle progression

To establish the effect of starvation on chemosensitivity in terms of cell cycle progression and growth arrest, cell cycle analysis was performed. This involves the permeabilization of the cell membrane and the addition of a fluorescent dye (such as propidium iodide). When combined with ribonuclease, propidium iodide stains only cellular DNA, with the intensity of the fluorescent signal reflecting the amount of DNA within the cell. This illustrates which stage of the cell cycle the cell is in. Cells in the G_2/M phase have twice the amount of DNA as those in G_0/G_1, with everything between falling within the S-phase category. This determination of cell cycle was achieved by using the BD FACSMelody to perform flow cytometry.

Compared to the control group in the MCF-12A cell line, there were significantly fewer cells in the G_0/G_1 phase in both the starvation group ($p<0.05$) and the doxorubicin treatment group ($p<0.0001$). There were, however, significantly more in the combination group than in the control ($p<0.05$), or in the group that received doxorubicin alone ($p<0.0001$). A significantly greater proportion of cells were found to be in the S phase in the doxorubicin group than in the control group ($p<0.001$) or the combination group ($p<0.01$). In terms of cells in the G_2/M phase, when compared to the control group, both the starvation group and the doxorubicin treatment group approached but did not achieve significance ($p=0.07$). The combination group had significantly fewer cells in the G_2/M phase than either the control group ($p<0.01$) or the doxorubicin treatment group ($p<0.001$).

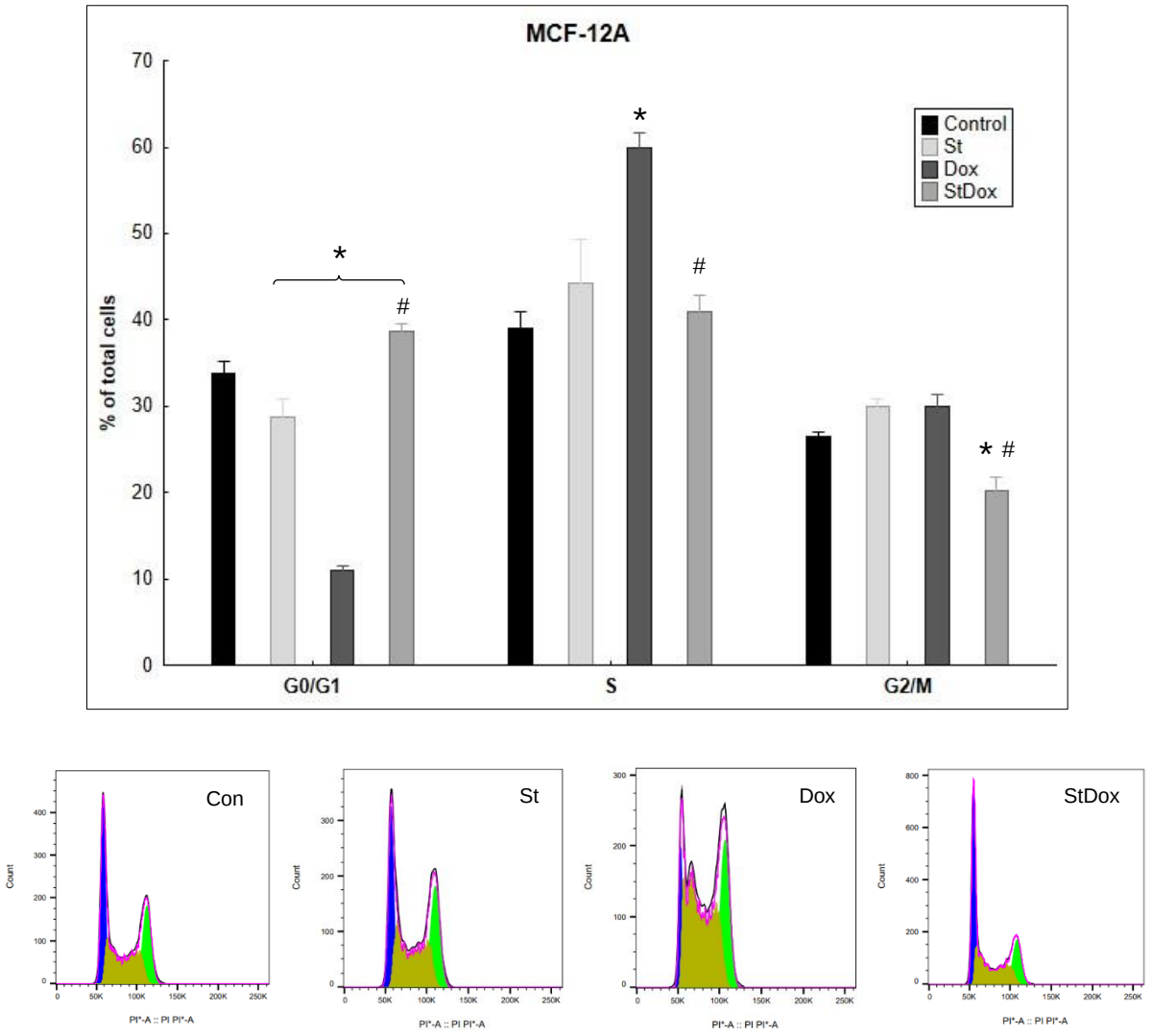

Figure 3.19: The effect of starvation, doxorubicin, and the combination thereof on cell cycle progression in MCF-12A cells. *The percentage of cells in the G_0/G_1 phase, S phase and G_2/M phase, as determined by cell cycle analysis, in MCF-12A cells. Results are presented as the mean percentage of cells in each phase per group ± SEM (n=3). * = p<0.05 when compared to the control; # = p<0.05 when compared to the doxorubicin treatment group.*

In the BT-549 cell line, there were significant differences in the proportion of cells in the G_0/G_1 phase between the control group and both the doxorubicin treatment group ($p<0.001$), and the combination group ($p<0.001$), but not between the doxorubicin treatment group and the combination group ($p=0.4229$). There were significantly more cells in the S phase in the doxorubicin treatment group than in both the control group ($p<0.0001$) or the combination group ($p<0.01$). There was also a significant difference between the control group and the combination group ($p<0.001$). In terms of the proportion of cells in the G_2/M phase, there were no statistically significant differences between groups. Only the combination group achieved a near-significant difference when compared to the control group ($p=0.065$).

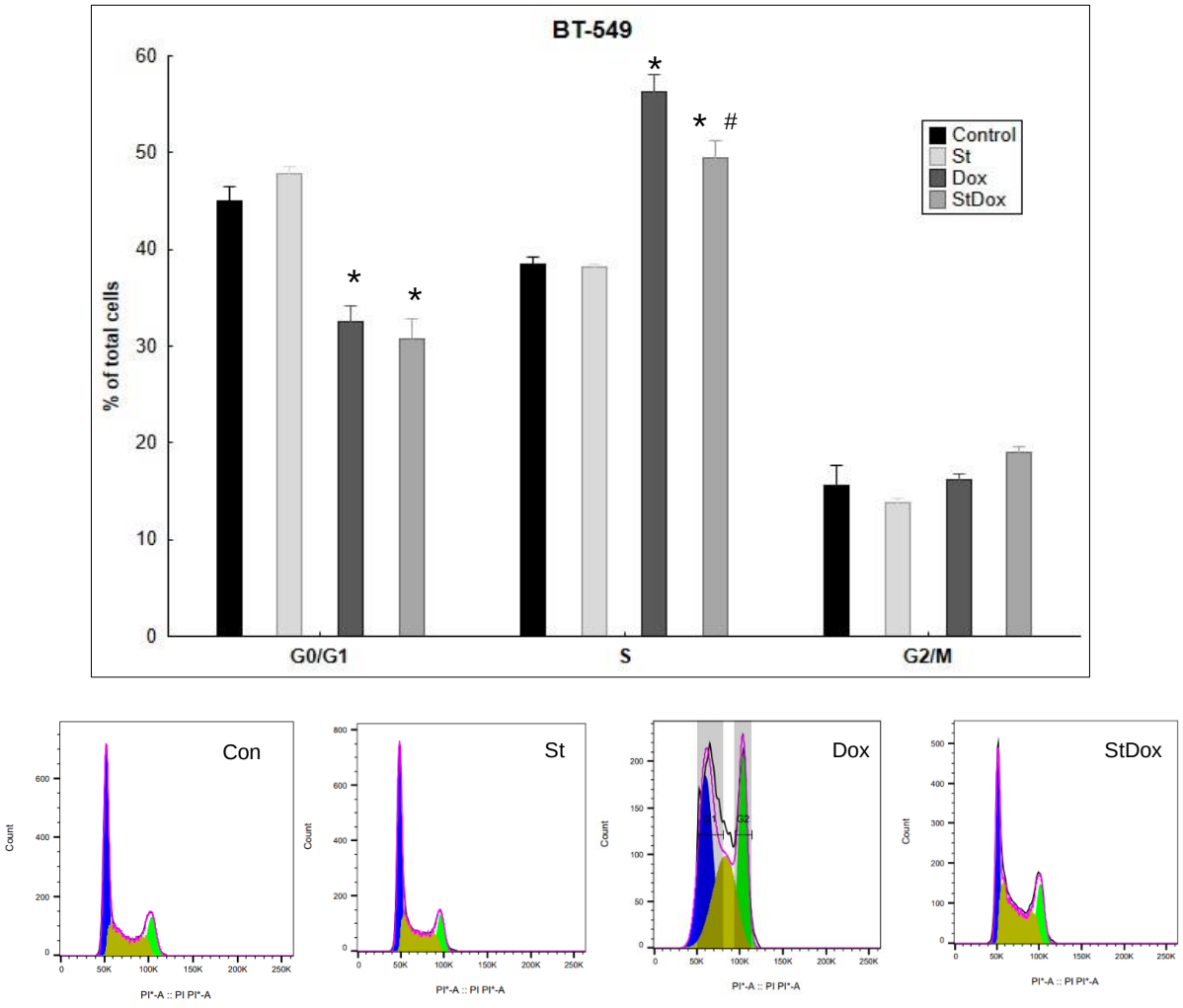

Figure 3.20: The effect of starvation, doxorubicin, and the combination thereof on cell cycle progression in BT-549 cells. *The percentage of cells in the G_0/G_1 phase, S phase and G_2/M phase, as determined by cell cycle analysis, in BT-549 cells. Results are presented as the mean percentage of cells in each phase per group ± SEM (n=3). * = $p<0.05$ when compared to the control; # = $p<0.05$ when compared to the doxorubicin treatment group.*

In the MDA-MB-231 cell line, there were small but significant differences in the proportion of cells in the G_0/G_1 phase between the control group and the starvation group ($p<0.01$), as well as the combination group ($p<0.01$). There were more pronounced differences when comparing the doxorubicin treatment group to both the control ($p<0.0001$), and combination treatment groups ($p<0.0001$). There were significantly more cells in the S phase in the doxorubicin treatment group than in the control group ($p<0.001$) or the combination group ($p<0.05$). There were also small but significant differences between the control group and both the starvation group ($p<0.05$), and the combination group ($p<0.05$). Lastly, the doxorubicin group had a significantly greater proportion of cells in the G_2/M phase than either the control group ($p<0.01$) or the combination group ($p<0.01$).

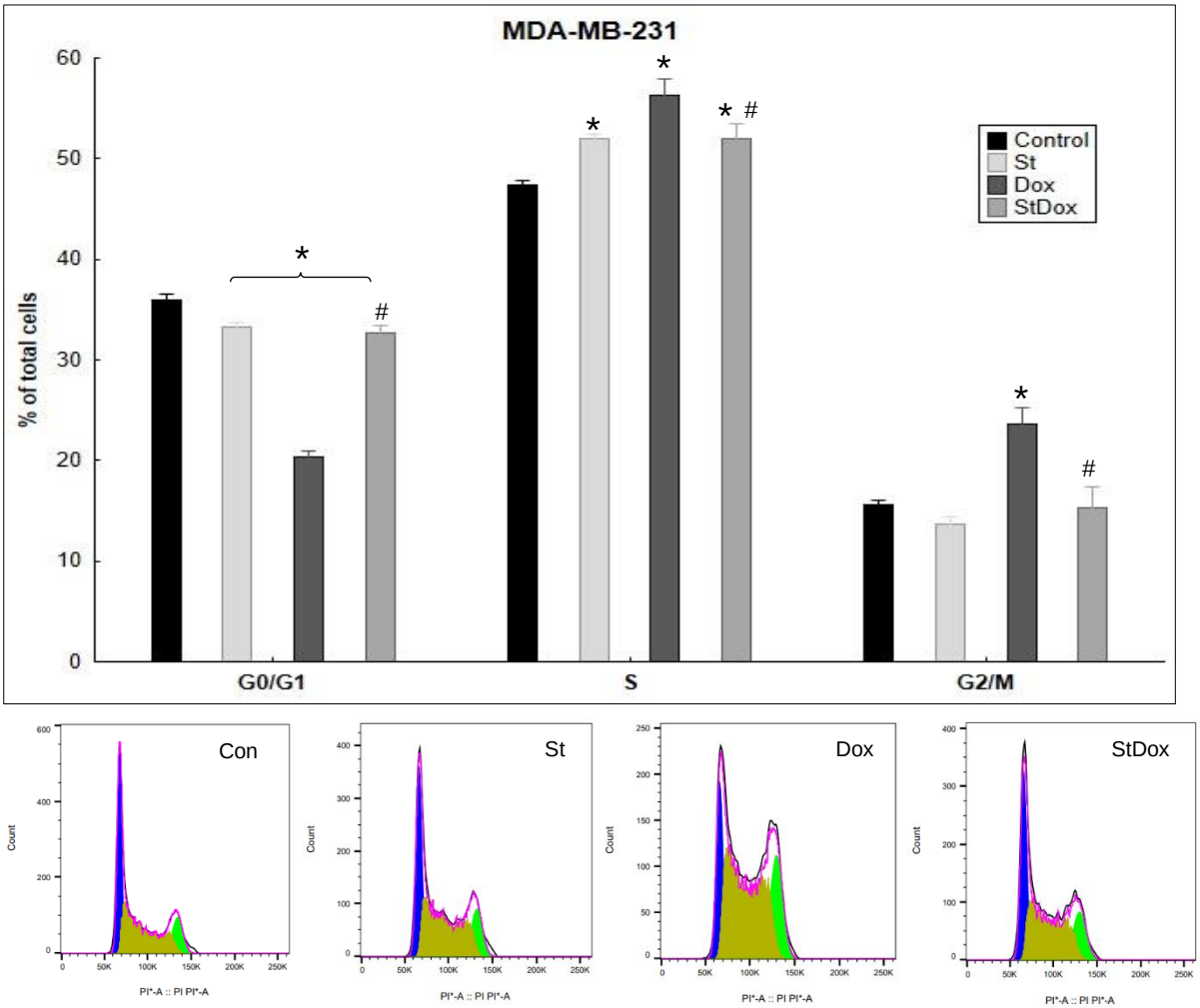

Figure 3.21: The effect of starvation, doxorubicin, and the combination thereof on cell cycle progression in MDA-MB-231 cells. *The percentage of cells in the G_0/G_1 phase, S phase and G_2/M phase, as determined by cell cycle analysis, in MDA-MB-231 cells. Results are presented as the mean percentage of cells in each phase per group ± SEM (n=3). * = $p<0.05$ when compared to the control; # = $p<0.05$ when compared to the doxorubicin treatment group.*

Chapter 4: Discussion

Breast cancer currently accounts for 25.4% of female cancer diagnoses globally. It is therefore the most common cancer among women in both developed and developing countries (WHO, 2018). Treatment resistance is an increasing challenge in the management of the disease, posing a threat to patient outcome and prognosis (Foulkes, *et al.,* 2010). Of all the different types of breast cancer, TNBC is the most aggressive and has the worst prognosis as drug-resistance is common among this subtype (Foulkes, *et al.,* 2010). As a result, extensive research is being conducted in order to find adjuvant therapies that may improve drug sensitivity.

While there are many unique hallmarks of cancer that distinguish it from benign tissue, its high metabolic rate and excessive consumption of nutrients make it an ideal target for metabolic adjuvant therapies (Berger, 2014). We therefore set out to investigate the effect of STS on the growth, viability, and metabolism of TNBC cells and a benign breast epithelial cell line. We also investigated the effect of STS on chemosensitivity in these cells to see whether it offers any potential in the face of current treatment regimes.

We hypothesised that STS prior to doxorubicin treatment would selectively enhance treatment efficacy in cancer cells, while offering protection to non-malignant cells. Our aims were as follows: firstly, to explore the effect of starvation over time on intracellular signalling pathways, autophagic flux, cell cycle progression, and viability in BT-549 and MDA-MB-231 breast cancer cells, as well as in MCF-12A breast epithelial cells; secondly, to determine the effects of starvation, doxorubicin treatment, and the combination thereof on live cell number, cell viability, and cell cycle progression to establish chemosensitivity.

4.1 Part one: the cellular response to starvation over time

The first part of the study investigated the effect of starvation over time on intracellular signalling pathways, autophagic flux, cell cycle progression and viability.

4.1.1 Starvation reduces growth and proliferation signalling in MCF-12A, but not in BT-549 or MDA-MB-231 cells

In order to determine the effect of starvation on signalling pathways involved in growth and proliferation, western blot analyses were employed to quantify relative target protein expression. Two core proteins involved in the promotion of cell growth and proliferation were selected: PI3K and Akt, with phosphorylated Akt also quantified.

PI3K is a lipid kinase that forms part of the PI3K/Akt/mTOR pathway (Hemmings & Restuccia, 2012). It is downstream of multiple growth signals and is upregulated to promote cellular survival, growth and proliferation. When phosphorylated, PI3K is activated and converts PIP_2 to PIP_3, thereby recruiting PDK1 and Akt to the cell membrane for phosphorylation and activation (Hemmings & Restuccia, 2012). Akt, also known as protein kinase B (PKB), is a serine/threonine kinase that is a downstream target of PI3K, as well as other growth-promoting pathways. When activated through phosphorylation, Akt has multiple downstream effects, such as the inhibition of autophagy, and the promotion of glycolysis, protein synthesis, cell survival and proliferation (Kuhajda, 2008).

While it may seem that nutrient- and serum-deprivation would attenuate growth and proliferation pathways, this was the case in only the benign cell line. Although the 6- and 24-hour time points yielded no significant changes, the MCF-12A cells displayed a significant decrease in Akt expression after three hours of starvation ($p<0.01$) (Figure 3.2). PI3K and phosphorylated Akt also appeared to diminish. However, the former was not significant (Figure 3.1), and the latter only approached significance ($p<0.10$) (Figure 3.3). These findings are similar to those obtained by Muranen, *et al.* (2017), who found that MCF-10A breast epithelial cells reduced phosphorylated Akt expression when cultured for 24 hours in media free from serum, insulin and EGF. While this model of starvation differs from ours in that we did not restrict insulin and EGF, but glucose instead, it represents the principle that benign cells may reduce Akt signalling when faced with serum and nutrient deprivation.

Contrarily, the BT-549 cell line displayed no significant reduction in any of these growth signalling proteins at any of the starvation time points (Figure 3.1; Figure 3.2; Figure 3.3). This is concurrent with the findings of Zhang, *et al.* (2017) who found no significant changes in phosphorylated Akt expression when BT-549 cells were

incubated in serum-free media overnight. These findings may, in part, be explained by a PTEN mutation in BT-549 cells (Torbett, *et al.*, 2008). PTEN plays an essential role in the suppression of the PI3K/Akt pathway, and this loss of PTEN function may cause dysregulations in the cell's response to starvation, thereby preventing the appropriate downregulation under conditions of nutrient deprivation (Torbett, *et al.*, 2008).

Interestingly, the MDA-MB-231 cells showed an increase in PI3K expression with increasing duration of starvation (Figure 3.1). However, this was not significant, and only the 24-hour group approached significance ($p=0.1$). This lack of significance may be partially due to variability in the data, and we recommend a higher number of replicates for future experiments to reduce variability. The MDA-MB-231 cells displayed a similar trend between PI3K and Akt expression, which increased as starvation duration increased (Figure 3.2). Variability in Akt expression was less, and the 6- and 24-hour time points displayed significantly higher Akt expression ($p<0.05$ and $p<0.01$, respectively). However, this trend was not maintained when examining phosphorylated Akt, as none of the groups illustrated significant changes (Figure 3.3). In a study by Yi, *et al.* (2013), serum-starved MDA-MB-231 cells also showed no significant changes in the expression of phosphorylated Akt when compared to the control group. However, MDA-MB-436 and HCC-1937 cells showed significantly higher expressions of total Akt following serum starvation (Yi, *et al.*, 2013). Both of these cell lines carry *BRCA1* mutations, which are associated with hyperactivated PI3K/Akt pathways (Elstrodt, *et al.,* 2006). While BT-549 and MDA-MB-231 cells do not carry this mutation, it has been reported that these cells contain an allelic loss at *BRCA1* (Elstrodt, *et al.,* 2006). In summary, these findings suggest that some breast cancer cell lines may either resist the downregulation of pro-growth pathways in response to starvation, or even upregulate them, and that this may be influenced by mutations within their genome.

4.1.2 Starvation upregulates autophagy in MCF-12A and MDA-MB-231 cells, but not BT-549 cells

Western blot analyses were utilised to assess changes in autophagy over time during starvation. Total Atg5, p62 and LC3-II expression were quantified. Thereafter, immunocytochemistry was employed to further examine autophagy. eGFP-LC3-transfected cells were treated and stained with LysoTracker Red™, and images were obtained using a confocal microscope. The average number of autophagosomes per cell was calculated and presented by group.

LC3-II is produced through the modification of LC3-I during the maturation of autophagosomes. It is therefore an indicator of the rate of autophagosome initiation (Mizushima & Komatsu, 2011). When cells are treated with bafilomycin, which impairs the fusion of autophagosomes with lysosomes, LC3-II accumulates and may serve as an indicator of autophagic flux (Gottlieb, *et al.*, 2015). p62, also known as Sequestosome 1 (SQSTM1), is a protein that acts as a substrate during autophagic degradation (Mizushima & Komatsu, 2011). p62 displays an inverse relationship with LC3-II, unless autolysosomal fusion is inhibited. Under such circumstances, p62 will not undergo degradation, but accumulate within the cell (Gottlieb, *et al.*, 2015). Besides LC3-II and p62, other autophagy-related proteins may be used to measure autophagy, such as Atg5. Quantifying these proteins provides support to findings from LC3-II and p62 determination. Atg5 is an intracellular protein that forms part of the Atg5-Atg16-Atg12 complex, which is essential for the elongation of the phagophore. It is upregulated when autophagic activity increases (Glick, *et al.*, 2010).

In the MCF-12A cell line, there were no significant differences in Atg5 expression between any of the group (Figure 3.4). However, there was a significantly greater expression of p62 in the respective bafilomycin-treated groups than in the control ($p<0.01$), three-hour ($p<0.001$), six-hour ($p<0.001$) and 24-hour ($p<0.01$) groups, with the largest difference at three hours. Levels of LC3-II in the control, three-hour, six-hour and 24-hour groups all increased significantly with bafilomycin treatment ($p<0.0001$). Lastly, bafilomycin treatment increased the number of autophagosomes in the control ($p<0.001$), six-hour ($p<0.001$), and 24-hour ($p<0.0001$) groups in these cells. These findings are corroborated by those of Thomas, *et al.* (2020) who found that complete amino acid starvation led to a significant increase in LC3-II expression

in MCF-12A cells, and that this was increased with the addition of bafilomycin. This may indicate that autophagic flux is upregulated in benign cells in response to nutrient deprivation.

There were no significant differences between any of the groups in the BT-549 cells in terms of Atg5, p62 or LC3-II expression (Figure 3.4; Figure 3.5; Figure 3.6). There are currently limited studies examining the effects of starvation on markers of autophagic flux in BT-549 cells. However, in response to other stressors, these cells have been reported to display a weaker upregulation of autophagic flux than MDA-MB-231 cells. These stressors include doxorubicin (Zhu, *et al.*, 2015) and a bacterial enterotoxin (Masso-Welch, *et al.*, 2019). However, when utilising fluorescent microscopy, it was observed that the three-hour starvation group had a significantly higher number of autophagosomes per cell than the control group ($p<0.05$) (Figure 3.7). Additionally, bafilomycin treatment increased the number of autophagosomes in the control ($p<0.0001$), three-hour ($p<0.001$), and six-hour ($p<0.0001$) group, indicating upregulated autophagic flux at these time points. Notably, very few puncta were observed per cell, which may suggest low baseline levels of autophagy in these cells. Therefore, more sensitive techniques, such as fluorescent microscopy, may be needed to detect changes in autophagic activity.

In the MDA-MB-231 cell line, there were significant differences in Atg5 expression between the control ($p<0.05$), three-hour ($p<0.05$), six-hour ($p<0.01$) and 24-hour ($p<0.01$) groups and their corresponding bafilomycin-treated groups (Figure 3.4). There was also a significantly greater expression of p62 in the respective bafilomycin groups than the the six-hour group ($p<0.05$) as well as the 24-hour group ($p<0.01$) (Figure 3.5), suggesting increased autophagic flux at these time points. LC3-II expression, however, was only significantly increased at the 24-hour time point with bafilomycin treatment ($p<0.001$) (Figure 3.6). Zhu, *et al.* (2017) demonstrated that MDA-MB-231 cells increased the expression of both p62 and LC3-II when incubated in serum-free media for 24 hours and treated with bafilomycin. This supports the notion that autophagic flux is upregulated in these cells after 24 hours of starvation. Lastly, fluorescent microscopy illustrated a significant increase in the number of autophagosomes at the three-hour ($p<0.01$), six-hour ($p<0.0001$) and 24-hour ($p<0.0001$) group when compared to the control group (Figure 3.7), indicating high baseline levels of autophagy in these cells. This is also in agreement with the findings

of Zhu, *et al.* (2017) who found that the number of autophagosomes per cell were significantly upregulated at 24 hours of incubation in serum-free media. Additionally, the control, three-hour and six-hour groups had a significantly higher number of autophagosomes when treated with bafilomycin ($p<0.0001$).

4.1.3 Starvation increases the proportion of cells in the G_0/G_1 phase in MCF-12A, BT-549 and MDA-MB-231 cells

To establish the effect of starvation over time on cell cycle progression and growth arrest, cell cycle analysis was performed using propidium iodide, ribonuclease, and the BD FACSMelody flow cytometer.

In the MCF-12A cell line, the proportion of cells in the G_0/G_1 phase increased with the duration of starvation, with significantly higher percentages in the six-hour ($p<0.05$) and 24-hour ($p<0.01$) groups (Figure 3.11). This is commonly seen in cultured cells in response to serum-starvation, especially in those of benign origins (Felice, *et al.*, 2009; Yao, 2014). There were no significant differences between any of the groups in the percentage of cells in the G_2/M phase, but all three starvation periods significantly reduced the proportion of cells in the S-phase ($p<0.05$) (Figure 3.11). As data from cell cycle analysis are represented as percentages of the total number of cells, rather than crude values, an increase in one category would naturally result in a decrease in another. Thus, we suspect that the relative decrease in the proportion of cells in the S-phase is the result of the G_0/G_1 portion expanding, rather than an active upregulation of cells within the S-phase.

In the MDA-MB-231 cell line, a similar trend was observed as in the MCF-12A cells, with significantly more cells in the G_0/G_1 phase of the six-hour and 24-hour groups ($p<0.05$) (Figure 3.13). This is concurrent with a study by Barascu, *et al.* (2006) as a 24-hour period of serum starvation was used to induce G_0/G_1 arrest in these cells. While the model for starvation may differ, Thomas, *et al.* (2020) also illustrated a significant increase in the proportion of cells in the G_0/G_1 phase after 24 hours of amino acid starvation, but not at six or 12 hours. This may indicate that longer periods of nutrient deprivation are needed to influence cell cycle progression in these cells.

In the BT-549 cells, a significant increase in the percentage of cells in the G_0/G_1 phase was only observed at 24-hours when compared to the control ($p<0.0001$) (Figure 3.12). This significant change was only observed at a later stage than in the other cell lines. BT-549 cells are reported to have mutations in the *PTEN*, *Rb* and *TP53* genes, all of which regulate the cell cycle (ATCC, 2020). Additionally, Furnari, *et al.* (1998) illustrated that the passage of serum-starved Glioma cells into G_1 growth arrest was mediated by PTEN. If these mechanisms are similar in other types of cancer, the BT-549 cells may have been able to resist G_0 growth arrest for longer than the other cell lines, or otherwise were able to adapt to the shorter time points of starvation better than the other cell lines could. There were significantly fewer cells in the S phase in the six-hour ($p<0.05$) and 24-hour ($p<0.0001$) groups. The three-hour ($p<0.001$), six-hour ($p<0.001$) and 24-hour ($p<0.05$) had a significantly higher percentage of cells in the G_2/M phase than the control group (Figure 3.12).

These results illustrate that cancer cells may also enter G_0 (quiescence) or G_1 growth arrest in sub-optimal nutrient availability, as benign cells do. However, the mutations in genes that regulate the cell cycle may influence the conditions under which these states are entered, and whether they are permanent or not. For future studies, it may be worth investigating whether conditions of starvation result in a permanent exit from the cell cycle by quantifying markers of senescence (p21, RB and p53).

4.1.4 Starvation has varied effects when using bio-reductive capacity as an indicator of cell viability

In order to determine the effect of starvation over time on cell viability, a WST1 assay was conducted. In the benign breast epithelial cell line, there was a small but significant increase in cell viability in the three-hour ($p<0.01$) and six-hour ($p<0.001$), but not in the 24-hour starvation group (Figure 3.14). This is in contrast with the findings of Govender (2013) who found that viability in MCF-12A cells was significantly decreased by both six and 24 hours of starvation. However, starvation was simulated using Hank's Balanced Salt Solution (HBSS), in contrast to our low-glucose and reduced-serum media. HBSS represents a more severe state of nutrient deprivation, as it lacks most metabolites, and may thus explain the difference in findings. Thomas, *et al.* (2020), on the other hand, illustrated that total amino acid deprivation as a form

of starvation was not sufficient to significantly reduce cell viability in MCF-12A cells. This supports our findings that MCF-12A cells are able to withstand less severe forms of nutrient deprivation over a 24-hour period. While it may be possible that STS promotes cell proliferation in some cell lines, none of the proliferative pathways were significantly upregulated in MCF-12A cells, which makes it unlikely that proliferation was responsible for the increase in viability. On the contrary, starvation significantly increased the proportion of cells within the G_0/G_1 phase at six and 24 hours. This is characteristic of benign cells in response to serum- and nutrient-deprivation, and potentially indicates a temporary state of quiescence in response to suboptimal nutrient availability. It is more likely that this reported increase in viability may reflect cellular activity rather than live cell number. WST1 is a tetrazolium salt that is reduced by the production of NAD(P)H at the respiratory chain of the mitochondria. While viable cells are metabolically active, the level of metabolic activity may change in response to certain stressors, especially in the context of nutrient deprivation where autophagy and other compensatory pathways may be upregulated. This may lead to overestimations of cell viability in assays which use metabolic activity as a proxy for cell viability (Van den Berghe, *et al.*, 2013). A WST1 assay is therefore a direct indicator of bio-reductive capacity, and only an indirect measure of viability. In this case, the MCF-12A cells may have displayed increased cellular metabolism in the early stages of starvation, which was later reduced as the cell achieved homeostasis.

In the BT-549 cell line, there was a significant reduction in cell viability following three and six hours of starvation ($p<0.0001$) (Figure 3.14), which may indicate reduced metabolic activity in response to starvation, rather than reduced viability (Van den Berghe, *et al.*, 2013). These cells displayed a weaker upregulation of autophagy in response to starvation than the other cell lines. Thus, reduced, rather than increased, metabolic activity may follow starvation (Van den Berghe, *et al.*, 2013).

Compared to the control group, the three-hour ($p<0.001$) and six-hour ($p<0.01$) groups displayed significantly higher viability in the MDA-MB-231 cells, while 24 hours of starvation resulted in a small but significant reduction in cell viability ($p<0.05$) (Figure 3.14). The former may again be the result of increased metabolic activity, while the latter may reflect the G_0/G_1 shift in response to starvation. Alternatively, these findings are similar to those of Thomas, *et al.* (2020) who demonstrated that total amino acid deprivation for 24 hours significantly reduced cell viability in MDA-MB-231 cells.

4.2 Part two: the effect of starvation on chemosensitivity

The second part of the study investigated the effect of starvation on chemosensitivity. The outcomes included the total number of live cells, cell death, bio-reductive capacity as an indicator of viability, and cell cycle progression.

4.2.1 Doxorubicin reduces cell viability in MCF-12A, BT-549 and MDA-MB-231 cells

A dose-response curve was conducted to select an appropriate concentration for doxorubicin treatment. A WST1 assay was used to establish the effect of different concentrations of doxorubicin on cell viability.

A concentration of 2.5 µM was able to significantly reduce cell viability in the MCF-12A, BT-549 and MDA-MB-231 cells (Figure 3.15). These findings are confirmed by those of Aroui, *et al.* (2009), who illustrated a significant reduction in viability, as determined by an MTT assay, when MDA-MB-231 cells were treated at a concentration of 2.5 µM. Although the concentrations tested by Inao, *et al.* (2009) differed from that which we tested (0-1 µM vs 0-10 µM), they indicated greater sensitivity to doxorubicin in BT-549 cells than in MDA-MB-231 cells, as was seen in our study (Inao, *et al.*, 2009).

Based on these results, a concentration of 2.5 µM was selected for doxorubicin treatment for the remainder of this study, as this was considered sufficient to illustrate either enhanced or reduced chemosensitivity with starvation in any of the cell lines. Additionally, this does not exceed the peak plasma concentration of patients receiving standard bolus infusions (5 µM) (Minotti, *et al.*, 2004).

4.2.2 Doxorubicin, but not starvation, reduces live cell number in MCF-12A, BT-549 and MDA-MB-231 cells

A live cell count was employed to establish the effects of starvation, doxorubicin and the combination thereof on the total number of viable cells. Cells undergoing stress may respond in a variety of ways which, among others, may include either a reduction in their rate of proliferation, or the induction of cell death (Terzi, *et al.*, 2016). Both of these mechanisms would result in a lower live cell count, and it was later established through viability studies and cell cycle analysis which accounted for the changes in cell number.

In the MCF-12A cell line, both the doxorubicin ($p<0.001$) and combination treatments ($p<0.001$) significantly reduced the number of live cells when compared to the control (Figure 3.16). This is in line with findings from Thomas, *et al.* (2020) which showed that doxorubicin was able to significantly reduce total live cell number in MCF-12A cells. Although the model of starvation differed, Thomas, *et al.* also showed no significant reduction in live cell number when MCF-12A cells were subjected to 24 hours of amino acid deprivation, suggesting that starvation is well-tolerated in these cells. However, in our findings, there was no significant difference between the doxorubicin and combination groups, which contradicts those of Thomas, *et al.* This may be ascribed to the model of starvation used, as total amino acid deprivation may elicit slightly different intracellular processes to our model, which may explain the difference in findings. Ultimately, the findings from our study suggest that starvation does not increase chemosensitivity in terms of total live cells in this benign cell line.

In the BT-549 cell line there were significantly fewer live cells in both the doxorubicin treatment group ($p<0.001$) and the combination group ($p<0.01$) than in the control group (Figure 3.16). In the MDA-MB-231 cells, there was also a significant reduction in live cell number in the doxorubicin treatment group ($p<0.05$), as well as the combination group ($p<0.01$) (Figure 3.16). Bar-On, *et al.*, (2007) reported similar findings in MDA-MB-231 cells, as well as MCF-7 breast cancer cells. A 72-hour incubation period in doxorubicin of differing concentrations (10-100 nM) resulted in significant reductions in total cell number. While the concentrations tested were lower than in our study (2.5 µM), the incubation period was three times longer. Ultimately,

the principle was illustrated that doxorubicin is able to reduce live cell counts in these cells.

Lastly, while there was a reduction of nearly 20% between the doxorubicin and the combination group in the MDA-MB-231 cell line, this did not achieve significance. This may, in part, have been due to variations in the data.

In summary, all three cell lines showed a significant reduction in the total number of live cells when treated with doxorubicin, with or without a preceding starvation period. However, starvation was not able to significantly reduce the number of live cells when administered prior to doxorubicin treatment.

4.2.3 Starvation increases doxorubicin-induced cell death in BT-549, but not MCF-12A or MDA-MB-231 cells

To further examine the effect of starvation on chemosensitivity, cell death was assessed through the use of flow cytometry with propidium iodide. Propidium iodide is excluded from viable cells due to its inability to permeate intact cell membranes. When cells become non-viable, membrane integrity is lost, which allows the dye to enter the cell and serve as a marker for cell death.

In both the MCF-12A and MDA-MB-231 cell lines, there were no significant differences in the percentage of dead cells between any of the groups (Figure 3.17). Interestingly, Aroui, *et al.* (2009) also indicated that in the latter, doxorubicin was not able to significantly increase the proportion of dead cells at a concentration of 2.5 µM. This was established using flow cytometry to determine the fraction of sub-G_1 cells and was followed by fluorescent microscopy with Hoescht staining as an additional measure of cell death. However, these findings are in contrast with a study by Pilco-Ferreto & Calaf (2016), wherein it was reported that doxorubicin induces apoptosis in MCF-10A, MCF-7 and MDA-MB-231 cells. Treatment with doxorubicin was accompanied by a significant increase in the expression of Bax, caspase 3 and caspase 8, and decreased Bcl-2. However, the number of non-viable cells was never directly assessed. This suggests that the technique used to quantify cell death may affect the reported efficacy of doxorubicin to cause apoptotic cell death. For the present study, we selected flow cytometry to quantify cell death as it is a direct measure of cell death

(as opposed to techniques which use proxies or indicators, such as MTT assays and western blotting, respectively), reduces the risk for bias as the cell count is performed by the flow cytometer, and is generally accepted as an accurate technique. However, this technique does not provide insight into apoptotic signalling pathways, should they be upregulated in response to treatment.

In the BT-549 cells, the only group with a significantly higher proportion of dead cells than the control was the combination group ($p<0.001$) (Figure 3.17). Interestingly, while doxorubicin treatment alone resulted in approximately 6.5% cell death, a starvation period administered prior to doxorubicin treatment significantly increased this to approximately 8.9% ($p<0.01$). The latter, when represented as a percentage of original cell death, resulted in 35.5% more cell death than doxorubicin was able to induce alone. Ultimately, this finding suggests that a period of starvation prior to doxorubicin treatment significantly increased drug sensitivity in these cells. Furthermore, if a higher concentration of doxorubicin or a different technique to quantify cell death were used (such as western blotting for markers of apoptosis), these effects may have been more pronounced. As autophagy is reported to play a role in treatment resistance in breast and other types of cancer cells (Park, *et al.*, 2016; Jiang, *et al.,* 2017; Jung, *et al.*, 2017; Rupniewska, *et al.*, 2018), we suspect that the lack of autophagic upregulation at the 24-hour starvation time point may have rendered this specific cell line more susceptible to chemotherapy-induced cytotoxicity. At 24-hours, the BT-549 cells did not display an increase in autophagic flux, as illustrated by the quantification of Atg5 (Figure 3.4), p62 (Figure 3.5), LC3-II (Figure 3.6) or autophagic puncta (Figure 3.7).

In summary, a starvation period of 24 hours prior to treatment was able to significantly improve chemosensitivity in the BT-549 cells. Additionally, our findings also indicate that doxorubicin acts through various mechanisms to reduce cell viability, which may or may not include the induction of apoptosis. This is probably dose-, duration- and cell-dependent. Additionally, there may be other mechanisms by which the changes in total live cell number are mediated, such as through cell cycle arrest.

4.2.4 Starvation sensitises MCF-12A, BT-549 and MDA-MB-231 cells to doxorubicin when using bio-reductive capacity as an indicator of cell viability

A WST1 viability assay was conducted to further examine the effect of starvation on chemosensitivity.

In the MCF-12A, BT-549 and MDA-MB-231 cell lines, there was a significant reduction in cell viability following incubation with doxorubicin ($p<0.0001$; $p<0.05$; $p<0.01$, respectively) (Figure 3.18). This is in agreement with a study by Pilco-Ferreto & Calaf (2016) where an MTT assay was used to illustrate that 2 µM of doxorubicin significantly reduced cell viability in MCF-10A, MCF-7 and MDA-MB-231 cells.

The effect of doxorubicin treatment was significantly enhanced in the MCF-12A, BT-549 and MDA-MB-231 cells when preceded by a 24-hour starvation period ($p<0.01$; $p<0.05$; $p<0.05$, respectively) (Figure 3.18). In a study by Lee, *et al.* (2012), similar findings were reported. After a 24-hour period in starvation-mimicking media, the following cell lines all showed increased chemosensitivity to doxorubicin: MCF-7 breast adenocarcinoma, 4T1 mouse mammary carcinoma, HeLa and A431 cervix squamous cell carcinoma, C42B human prostatic carcinoma, GL26 mouse glioma cells, ACN neuroblastoma cells and MZ2-MEL malignant skin melanoma. Starvation conditions were simulated using low-glucose media and reduced serum (1% as opposed to 10%), and viability assessed by MTT assays (Lee, *et al.*, 2012).

However, as previously elucidated, a WST1 assay is only an indirect indicator of cell viability, but a direct indicator of bio-reductive capacity as it relies on reduction by NAD(P)H at the mitochondria (Milanese & Mastroberardino, 2020). The changes in viability estimated by WST1 assay in Figure 3.18 do not correspond to the changes in live cell number seen in Figure 3.16. It may therefore be possible that the effect of cellular stress on metabolic activity may influence the reduction of tetrazolium salts used in viability assays. This is especially true in the context of doxorubicin: DNA damage has been reported to upregulate the production of NAD(P)H, which increases cellular bio-reductive capacity (Milanese & Mastroberardino, 2020). This notion is supported by Van den Berghe, *et al.* (2013), who noted that many conditions and treatments can enhance or reduce respiratory activity within the cell, compromising the accuracy of techniques which rely on this as an indicator of cell viability. Their final

recommendations are that these viability assays be accompanied by other indicators of cell viability or cell death. Ultimately, when supported by a live cell count, or other indicators of cell viability, this technique may provide some insight into cellular metabolic activity in response to stress (Van den Berghe, *et al.*, 2013).

4.2.5 Starvation reverses doxorubicin-induced G_2/M arrest in MCF-12A and MDA-MB-231, but not BT-549 cells

To establish the effect of starvation on chemosensitivity in terms of cell cycle progression and growth arrest, cell cycle analysis was performed using the BD FACSMelody flow cytometer.

Compared to the control group in the MCF-12A cell line, the doxorubicin treatment group had significantly fewer cells in the G_0/G_1 phase ($p<0.0001$), significantly more in the S phase ($p<0.001$), and more cells in the G_2/M phase, although this did not achieve significance ($p=0.07$) (Figure 3.19). The former was observed by both Harvey, *et al.* (2019) and Ibiyeye, *et al.* (2019) in MCF-10A cells in response to doxorubicin treatment. However, as previously described, when results are presented as percentages of a total, rather than as crude values, a loss in one category may yield a natural increase in another. This may explain the increase in the proportion of cells in the S phase, as it may not be the result of an active upregulation of cells in this phase.

When compared to the doxorubicin group, the combination group had significantly more cells in G_0/G_1 ($p<0.0001$) and significantly fewer cells in G_2/M ($p<0.001$), which could suggest that starvation may have reversed the effects of doxorubicin on the cell cycle of MCF-12A cells. However, the total number of live cells did not recover when doxorubicin was preceded by starvation, and there were no significant changes in cell death, which suggests that this was not the case. Considering that doxorubicin causes G_2/M growth arrest (Bar-On, *et al*., 2007; Martin, *et al*., 2007; Newell, *et al.*, 2019), it might be possible that this specific effect had been ameliorated in the cells that received starvation treatment prior to doxorubicin, and that growth arrest occurred at an earlier point in the cell cycle. Doxorubicin may induce growth arrest at the G_1 checkpoint (Bar-On, *et al.*, 2007) or even senescence (Hou, *et al.*, 2019), which remains a possibility in these cells. Another possible explanation is that a period of

starvation prior to doxorubicin may have shuttled the cells into quiescence (G_0). This could provide partial protection from doxorubicin-induced cell damage, as this affects dividing cells to a greater extent than those in a temporary non-proliferating phase (Terzi, *et al.*, 2016). Ultimately, the total live cell count supports the idea that growth arrest occurred in both the doxorubicin and combination groups. To determine precisely how starvation modulates cell cycle arrest in doxorubicin-treated MCF-12A cells, further investigation would be required. Techniques that quantify cell cycle arrest and senescence would provide insight into whether the decrease in live cell number in the doxorubicin and combination groups are the result of quiescence, G_1 or G_2/M growth arrest, or senescence.

In the BT-549 cell line, incubation with doxorubicin promoted a decrease in the proportion of cells in the G_0/G_1 phase ($p<0.001$) and an increase of those in the S phase ($p<0.0001$). There was no significant change in the proportion of cells in the G_2/M phase. Between the doxorubicin treatment group and the combination group, there were also no significant differences in the percentage of cells in the G_0/G_1 phase or the G_2/M phase (Figure 3.20). Thus, starvation did not significantly alter the effect of doxorubicin on the cell cycle in the BT-549 cells.

In the MDA-MB-231 cell line, doxorubicin caused a significant reduction in the proportion of cells in the G_0/G_1 phase ($p<0.0001$), and a significant increase in the G_2/M phase ($p<0.01$) (Figure 3.21). Bar-On, *et al.* (2007) observed this same trend in MDA-MB-231 cells treated with doxorubicin, as doxorubicin is known to induce G_2/M arrest in these cells (Bar-On, *et al*., 2007; Martin, *et* al., 2007; Newell, *et al.*, 2019). A starvation period prior to doxorubicin treatment significantly increased the proportion of cells in the G_0/G_1 phase ($p<0.0001$) and decreased those in the G_2/M phase ($p<0.01$) (Figure 3.21). Thus, as in the MCF-12A cell line, starvation appeared to reverse the effects of doxorubicin on the cell cycle. However, this was also not the case in MDA-MB-231 cells, as the total number of live cells was lower in the combination group than in the doxorubicin group, although this was not significant. In other words, the reversal of doxorubicin's effect on the cell cycle or growth arrest would have been accompanied by an increase in live cell number. As this was not the case in the combination group, it may be speculated that starvation altered the point at which growth arrest occurred during the cell cycle.

The same possibilities exist in the MDA-MB-231 cell line as in the MCF-12A cell line: a starvation period prior to doxorubicin treatment could have shuttled the cells into either quiescence (G_0), senescence, or G_1 growth arrest, as opposed to G_2/M growth arrest seen in the doxorubicin group. If the MDA-MB-231 cells had entered quiescence, this would compromise treatment efficacy, as quiescence would buffer them against the DNA damage induced by doxorubicin during DNA synthesis and cell division (Terzi, *et al.*, 2016). Senescence, on the other hand, might be a better alternative as doxorubicin is reported to also induce senescence in MDA-MB-231 cells (Inao, *et al.*, 2019). This would reduce the number of cells able to actively divide, thereby reducing tumour volume and growth *in vitro* (Capparelli, *et al*, 2012). Additionally, senescence may be associated with increased susceptibility to apoptotic cell death when the cells are presented with an adjuvant therapy, such as targeted antibody therapies (Inao, *et al.*, 2019). However, senescence may also be accompanied by the senescence-associated secretory phenotype (SASP), which is associated with an increased production of inflammatory cytokines, chemokines and growth factors (Milczarek, 2020). This has been reported to contribute to the stimulation of non-senescent cancer cells within the population, and promote tumour recurrence (Inao, *et al.*, 2019; Milczarek, 2020).

Ultimately, in improving treatment efficacy, an increase in apoptotic cancer cell death is the ultimate goal of any treatment or adjuvant strategy (Inao, *et al.*, 2019). Irreversible growth arrest, in the form of senescence, is sometimes viewed as an adequate alternative, although this is not without challenges of its own (Terzi, *et al.*, 2016). Reversible growth arrest and quiescence are not generally accepted as positive outcomes, as relapse and recurrence are likely (Terzi, *et al.*, 2016). However, in order to thoroughly explore the effect of starvation on doxorubicin-induced growth arrest, markers of cell cycle arrest and senescence would need to be quantified. This would illustrate whether the decrease in live cell number in the doxorubicin and combination groups are the result of quiescence, G_1 or G_2/M growth arrest, or senescence.

Lastly, in a study by Newell, *et al.* (2019), doxorubicin also promoted an increase in the proportion of MDA-MB-231 cells in the G_2/M phase, indicating cell cycle arrest at this point. G_2/M arrest is often induced in response to DNA damage. This arrest either facilitates the repair of DNA or promotes apoptosis, with the latter being the goal of modern cancer therapies. Additionally, in the study by Newell, *et al.*, pre-treatment

with DHA prior to doxorubicin treatment increased the proportion of cells in G_2/M growth arrest. Interestingly, this pre-treatment also decreased cell viability (WST1), upregulated the expression of pro-apoptotic proteins (caspase 10), and apoptotic cell death when compared to the group that received doxorubicin alone (Newell, *et al.*, 2019). This may suggest that the increase in cells within the G_2/M growth arrest phase is an indication of improved drug efficacy and may be accompanied by increased cell death. In this case, our findings may indeed suggest that a period of starvation did not enhance chemosensitivity in these cells but may have compromised treatment efficacy. This may be supported by studies which find that upregulated autophagic processes contribute to treatment resistance in breast and other types of cancer cells (Park, *et al.*, 2016; Jiang, *et al.,* 2017; Jung, *et al.*, 2017; Rupniewska, *et al.*, 2018). In the findings from part one of the present study, it was observed that the MDA-MB-231 cells had significantly higher autophagic flux at the 24-hour starvation time point. This was determined by western blotting for Atg5 (Figure 3.4), p62 (Figure 3.5) and LC3-II (Figure 3.6). This theory is supported by findings from Thomas, *et* al. (2020) who discovered that the inhibition of autophagy through both Atg5 siRNA and bafilomycin treatment significantly increased caspase3/7 expression in MDA-MB-231 when treated with doxorubicin. However, in order to confirm this in our model of starvation, more extensive investigation into the effects of autophagy on chemoresistance would be required.

In summary, all three cell lines showed significant decreases in the proportion of cells in the G_0/G_1 phase when treated with doxorubicin. However, in both the MCF-12A and MDA-MB-231 cell lines, this trend was reversed in the combination group, along with significant reductions in the proportion of cells in G_2/M when compared to the doxorubicin group. However, based on the total live cell counts, it may be suggested growth arrest still occurred in the combination groups of these two cell lines. Since inferences on senescence cannot be made from cell cycle analyses, we recommend future studies examine markers of growth arrest and senescence to determine precisely how starvation and autophagy modulate the effect of doxorubicin on cell cycle arrest.

Chapter 5: Summary and Conclusion

The aims of this study were to investigate the intracellular response of a benign breast epithelial and two breast cancer cell lines to starvation, and to determine how this influences chemosensitivity. We hypothesised that a period of starvation prior to doxorubicin treatment would selectively enhance treatment efficacy in cancer cells, while offering protection to non-malignant cells. Investigations into the intracellular response to starvation demonstrated that the MCF-12A benign cell line downregulated growth and proliferation pathways during starvation, while the MDA-MB-231 cell line showed upregulation instead. The BT-549 cell line showed no significant changes in growth and proliferation signalling during starvation. While the MCF-12A and MDA-MB-231 cell lines had significantly upregulated autophagic activity at 24 hours of starvation, the BT-549 cell line showed no change in autophagic flux at this time point. This may have rendered this cell line vulnerable to doxorubicin-induced cytotoxicity, as the other two cell lines showed no significant increase in cell death when doxorubicin treatment was preceded by a starvation period. In addition, starvation prior to treatment ameliorated doxorubicin-induced G_2/M growth arrest in the MCF-12A and MDA-MB-231 cell lines, although further investigation is required to establish the exact effect of starvation and doxorubicin on cell cycle arrest. In conclusion, our results illustrated that the BT-549 breast cancer cell line was indeed sensitised to doxorubicin when starved for 24 hours prior to administration. However, this did not hold true for the MDA-MB-231 breast cancer cell line. The MCF-12A cells did not display enhanced chemoprotection with starvation but did not experience increased chemosensitivity either.

Chapter 6: Limitations and Future Recommendations

With regards to variability and statistical significance, we recommend an increase in the number of replicates performed for western blotting analyses, as this semi-quantitative technique displays a natural variability. Additionally, there is room for better optimisation of the protocols for each protein. This may also help to reduce variation and improve accuracy of the data obtained from this technique.

To strengthen the insight into metabolic signalling pathways, we recommend that mTOR, AMPK and phosphorylated PI3K be included in future studies. It should be noted that although the total level of PI3K provides insight into intracellular expression, it does not depict activation. In order to fully appreciate the relative amount of active PI3K, phosphorylated PI3K should be quantified as well. However, we were unable to optimise this protocol within the given time constraints as the antibody showed severe non-specific binding, and specific bands were undetectable. We recommended that this protocol be optimised for future studies to include phosphorylated PI3K in the outcomes.

We also recommend that a greater number of cells be imaged during immunocytochemistry. The cells utilised rejected the plasmid quite rapidly, and as such, imaging cells with a strong eGFP signal proved troublesome. For future studies, it may be worthwhile investigating the use of fluorescent antibodies for this purpose.

For future studies, it may also be worth investigating whether starvation and doxorubicin treatment result in a permanent exit from the cell cycle by quantifying markers of senescence (p21, RB and p53). Additionally, we recommend that apoptotic signalling pathways be explored by doing western blot analyses for markers of apoptosis.

This study used an *in vitro* model, and any conclusions should be limited as such, not extrapolated to *in vivo* or *ex vivo* conditions. As a whole, starvation is a difficult metabolic state to accurately replicate under *in vitro* conditions. An *in vivo* model should be considered for future studies, due to the inclusion of systemic factors involved in starvation (e.g. endocrinological involvements), as well as the tumour microenvironment.

References

Adekola, K., Rosen, S.T., Shanmugam, M. (2012) Glucose transporters in cancer metabolism. *Current Opinion in Oncology.* 24(6):650-654.

American Diabetes Association. (2001) *Postprandial blood glucose* [Online] Available at: https://care.diabetesjournals.org/content/24/4/775 (Accessed 19 December 2020)

Aroui, S., Brahim, S., De Waard, M., Bréard, J., Kenani, A. (2009) Efficient induction of apoptosis by doxorubicin coupled to cell-penetrating peptides compared to unconjugated doxorubicin in the human breast cancer cell line MDA-MB-231. *Cancer Letters.* 285:28-38.

Bar-On, O., Shapira, M., Hershko, D.D. (2007) Differential effects of doxorubicin treatment on cell cycle arrest and Skp2 expression in breast cancer cells. *Anti-cancer Drugs.* 18(10):1113-1121.

Barascu, A., Besson, P., Le Floch, O., Bougnoux, P., Jourdan, M. (2006) CDK1-cyclin B1 mediates the inhibition of proliferation induced by omega-3 fatty acids in MDA-MB-231 breast cancer cells. *The International Journal of Biochemistry and Cell Biology.* 38:196-208.

Barnum, K.J., O'Connell, M.J. (2014). Cell cycle regulation by checkpoints. *Methods in Molecular Biology.* 1170:29-40.

Berg, J.M., Tymoczko, J.L., Stryer, L. (2002) *Biochemistry*: 5th edition. New York: W.H Freeman and Company.

Berger, N.A. (2014) Obesity and cancer pathogenesis. *Annals of the New York Academy of Science.* 113:57-76.

Bianchi, G., Martella, R., Ravera, S., Marini, C., Capitano, S., *et al.* (2015) Fasting induces anti-Warburg effect that increases respiration but reduces ATP-synthesis to promote apoptosis in colon cancer models. *Oncotarget.* 6(14):11806-11819.

Blackadar, C.B. (2016) Historical review of the causes of cancer. *World Journal of Clinical Oncology*. 7(1):54-86.

Blagosklonny, M.V. (2011) Cell cycle arrest is not senescence. *Aging.* 3(2):94-101.

Bonuccelli, G., Tsirigos, A., Whitaker-Menezes, D., Pavlides, S., Pestell, R.G., *et al.* (2010) Ketones and lactate "fuel" tumour growth and metastasis: evidence that epithelial cancer cells use oxidative mitochondrial metabolism. *Cell Cycle.* 9(17): 3506-3514.

Bradford, M. M. (1976) A rapid and sensitive method for the quantitation of microgram quantities of protein utilising the principle of protein-dye binding. *Analytical Biochemistry.* 72:248-254.

Brandhorst, S., Wei, M., Wang, S., Morgan, T.E., Longo, V.D. (2013) Short-term calorie and protein restriction provide partial protection from chemotoxicity but do not delay glioma protection. *Experimental Gerontology.* 48(10):1120-1128.

Buono, R., Longo, V.D. (2018) Starvation, stress resistance and cancer. *Trends in Endocrinology and Metabolism.* 29(4):271-280.

Caccuri, F., Sommariva, M., Marsico, S., Giordano, F., Zani, A., Giacomini, A., Fraefel, C., Balsari, A., Caruso, A. (2019) Inhibition of DNA repair mechanisms and induction of apoptosis in triple negative breast cancer cells expressing the Human Herpesvirus 6 U94. *Cancers.* 11(1006):2-20.

Cancer Association of South Africa. (2014) *Fact Sheet on the Top 10 Cancers per Population Group* [Online] Available at: https://www.cansa.org.za/files/2018/07/Fact-Sheet-Top-Ten-Cancers-per-Population-Group-NCR-2014-web-July-2018.pdf (Accessed 26 February 2019)

Cancer Association of South Africa. (2019) *Women and Cancer* [Online] Available at: https://www.cansa.org.za/womens-health/ (Accessed 2 December 2019)

Cangemi, A., Fanale, D., Rinaldi, G., Bazan, V., Galvano, A, *et al.* (2016) Dietary restriction: could it be considered as speed bump on tumour progression road. *Tumour Biology*. 37:7109-7118.

Cantley, L.C. (2002) The phosphoinositide 3-kinase pathway. *Science.* 296:1655-1657.

Capparelli, C., Chiavarina, B., Whitaker-Menezes, D., Pestell, T.G., Pestell, R.G., Hulit, J., Ando, S., Howell, A., Martinez-Outschoorn, U.E., Sotgia, F., Lisanti, M.P. (2012) CDK inhibitors (p16/p19/p21) induce senescence and autophagy in cancer-

associated fibroblasts, “fuelling” tumour growth via paracrine interactions, without an increase in neo-angiogenesis. *Cell Cycle.* 11(19):3599-3610.

Carver, D.K., Barnes, H.J., Anderson, K.E., Petitte, J.N., Whitaker, R., *et al.* (2011) Reduction of ovarian and oviductal cancers in calorie-restricted laying chickens. *Cancer Prevention Research.* 4:562-567.

Cathcart, P., Craddock, C., Stebbing, J. (2017) Fasting: starving cancer. *The Lancet Oncology.* 18:431.

Chew, H.K. (2001) Adjuvant therapy for breast cancer: who should get what? *Western Journal of Medicine.* 174:284-287.

Collins, K., Jacks, T., Pavletich, N.P. (1997) The cell cycle and cancer. *Proceedings of the National Academy of Sciences of the United States of America.* 94:2776-2778.

Cooper, G.M. (2000) *The Cell: A Molecular Approach.* 2nd edition. Massachusetts: Sinauer Associates.

Courtney, K.D., Corcoran, R.B., Engelman, J.A. (2010) The PI3K pathway as a drug target in human cancer. *Journal of Clinical Oncology.* 28(6):1075-1083.

D’Aronzo, M., Vinciguerra, M., Mazza, T., Panebianco, C., Saracino, C., Pereira, S.P., Graziano, P., Pazienza, V. (2015) Fasting cycles potentiate the efficacy of gemcitabine treatment in *in vitro* and *in vivo* pancreatic cancer models. *Oncotarget.* 6(21):18545-18557.

Dai, S., Gocher, A., Euscher, L., Edelman, A. (2016) Serum starvation induces a rapid increase of Akt phosphorylation in ovarian cancer cells. *Federation of American Societies for Experimental Biology.* 30(1):714-719.

De Groot, S., Pijl, H., Van der Hoeven, J.J.M., Kroep, J.R. (2019) Effects of short-term fasting on cancer treatment. *Journal of Experimental and Clinical Cancer Research.* 38:209.

Dumalaon-Canaria, J.A., Hutchinson, A.D., Prichard, I., Wilson, C. (2014) What causes breast cancer? A systematic review of causal attributions among breast cancer survivors and how these compare to expert-endorsed risk factors. *Cancer Causes Control.* 25:771-785.

Elmore, S. (2007) Apoptosis: a review of programmed cell death. *Tocixologic Pathology.* 35(4): 495-516.

Elstrodt, F., Hollestelle, A., Nagel, J.H.A., Gorin, M., Wasielewski, M., Van den Ouweland, A., Merajver, S.D., Ethier, S.P., Schutte, M. (2006) *BRCA1* mutation analysis of 41 human breast cancer cell lines reveals three new deleterious mutants. *Cancer Research.* 66(1):41-45.

Felice, D.L., Sun, J., Liu, R.H. (2009) A modified methylene blue assay for accurate cell counting. *Journal of Functional Foods.* 1(1):109-118.

Foulkes, W.D., Smith, I.E., Reis-Filho, J.S. (2010). Triple-negative breast cancer. *New England Journal of Medicine.* 363:1938-1948.

Frasca, F., Pandini, G., Sciacca, L., Pezzino, V., Squatrito, S., *et al.* (2008) The role of insulin receptors and IGF-1 receptors in cancer and other diseases. *Archives of Physiology and Biochemistry.* 114(1):23-37.

Furnari. F.B., Huang, H.J.S., Cavenee, W.K. (1998) The phosphoinositol phosphatase activity of PTEN mediates a serum-sensitive G_1 growth arrest in glioma cells. *Cancer Research.* 58:5002-5008.

Glick, D., Barth, S., Macleod, K.F. (2010) Autophagy: cellular and molecular mechanisms. *Journal of Pathology.* 221(1):3-12

Gonzalez, C.A., Riboli, E. (2010) Diet and cancer prevention: Contributions from the European Prospective Investigation into Cancer and Nutrition (EPIC) study. *European Journal of Cancer.* 46: 2555-2562.

Gottlieb, R.A., Andres, A.M., Sin, J., Taylor, D.P. (2015) Untangling autophagy measurements: all fluxed up. *Circulation Research.* 116(3):504-514.

Govender, Y. The role of short-term starvation in sensitising breast cancer to chemotherapy. Unpublished MSc thesis, 2013. University of Stellenbosch. (Available at http://scholar.sun.ac.za/handle/10019.1/80007)

Hanjani, N.A., Vafa, M. (2018) Protein restriction, epigenetic diet, intermittent fasting as new approaches for preventing age-associated diseases. *International Journal of Preventive Medicine.* 9:58-77.

Harvey, R.F., Poyry, T.A.A., Stoneley, M., Willis, A.E. (2019) Signalling from mTOR to eIF2α mediates cell migration in response to the chemotherapeutic doxorubicin. *Science Signalling.* 12:1-12.

Hemmings, B.A., Restuccia, D.F. (2012) PI3K-PKB/Akt pathway. *Cold Spring Harbour Perspectives in Biology.* 1(4):9-12.

Hou, J., Jeon, B., Yun, Y., Cui, C., Kim., S. (2019) Ginsenoside Rh2 ameliorates doxorubicin-induced senescence bystander effect in breast carcinoma cell MDA-MB-231 and normal epithelial cell MCF-10A. *International Journal of Molecular Sciences.*20(5):1-15.

Ibiyeye, K.M., Nordin, N., Ajat, M., Zuki, A.B.Z. (2019) Ultrastructural changes and antitumour effects of doxorubicin/thymoquinone-loaded $CaCO_3$ nanoparticles on breast cancer cell line. *Frontiers in Oncology.* 9:1-14.

Inao, T., Iida, Y., Moritani, T., Okimoto, T., Tanino, R., Kotani, H., Harada, M. (2018) Bcl-2 inhibition sensitises triple-negative human breast cancer cells to doxorubicin. *Oncotarget.* 9(39):25545-25556.

Inao, T., Kotani, H., Iida, Y., Kartika, I.D., Okimoto, T., Tanino, R., Shiba, E., Harada, M. (2019) Different sensitivities of senescent breast cancer cells to immune cell-mediated cytotoxicity. *Cancer Science*. 110(9):2690-2699.

James, S.J., Muskhelishvili, L. (1994) Rates of apoptosis and proliferation vary with caloric intake and may influence incidence of spontaneous hepatoma in C57BL/6 x C3H F1 mice. *Cancer Research.* 54:5508-5510.

Jiang, F., Zhou, J., Zhang, D., Liu, M., Chen, Y. (2018) Artesunate induces apoptosis and autophagy in HCT116 colon cancer cells, and autophagy inhibition enhances the artesunate-induced apoptosis. *International Journal of Molecular Medicine.* 42:1295-1304.

Jung, H.J., Kang, J., Choi, S., Son, Y.K., Lee, K.R., Seong, J.K., Kim, S.Y., Oh, S.H. (2017) Pharbitis Nil (PN) induces apoptosis and autophagy in lung cancer cells and autophagy inhibition enhances PN-induced apoptosis. *Journal of Ethnopharmacology.* 208:253-263.

Kabeya, Y., Mizushima, N., Ueno, T., Yamamoto, A., Kirisako, T., Noda, T., Kominami, E., Ohsumi, Y., Yoshimori, T. (2000) LC3, a mammalian homologue of yeast Apg8p, is localised in autophagosome membranes after processing. *The EMBO Journal*. 19(21):5720-5728.

Kato, Y., Ozawa, S., Miyamoto, C., Maehata, Y., Suzuki, A., Maeda, T., Baba, Y. (2013) Acidic extracellular microenvironment and cancer. *Cancer Cell International.* 13:89-95.

Kounakis, K., Chaniotakis, M., Markaki, M., Tavernarakis, N. (2019) Emerging roles of lipophagy in health and disease. *Frontiers in Cell and Developmental Biology.* 7:185-190.

Kroemer, G., Levine, B. (2008) Autophagic cell death: the story of a misnomer. *Nature Reviews Molecular Cell Biology.* 9:1004-1010.

Kuhajda, F.P. (2008) AMP-activated protein kinase and human cancer: cancer metabolism revisited. *International Journal of Obesity.* 32:36-41.

Kulkoyluoglu-Cotul, E., Arca, A., Madak-Erdogan, Z. (2019) Crosstalk between estrogen signalling and breast cancer metabolism. *Trends in Endocrinology & Metabolism.* 30(1):25-38.

Lanza-Jacoby, S., Yan, G., Radice, G., LePhong, C., Baliff, J., *et al.* (2013) Calorie restriction delays the progression of lesions to pancreatic cancer in the LSL-KrasG12D; Pdx-1/Cre mouse model of pancreatic cancer. *Experimental Biology and Medicine.* 238:787-797.

Lazova, R., Camp, R.L., Klump, V., Siddiqui, S.F., Amaravadi, R.K., Pawelek, J.M. (2011) Punctuate LC3B expression is a common feature of solid tumours and associated with proliferation, metastasis, and poor outcome. *Human Cancer Biology.* 18(2):370-379.

Lee, C., Raffaghello, L., Brandhorst, S., Safdie, F.M., Bianchi, G., *et al.* (2012) Fasting cycles retard growth of tumours and sensitise a range of cancer cell types to chemotherapy. *Science Translational Medicine.* 4:124-132.

Lee, C., Safdie, F.M., Raffaghello, L., Wei, M., Madia, F., *et al.* (2010) Reduced levels of IGF-1 mediate differential protection of normal and cancer cells in response to fasting and improve chemotherapeutic index. *Cancer Research.* 70(4):1564-1572.

Leisching, G., Loos, B., Botha, M., Engelbrecht, A.M. (2015) A nontoxic concentration of cisplatin induces autophagy in cervical cancer: selective cancer cell death with autophagy inhibition as an adjuvant treatment. *International Journal of Gynaecological Cancer.* 25(3):380-388.

Longo, V.D., Fontana, L. (2009) Calorie restriction and cancer prevention: metabolic and molecular mechanisms. *Trends in Pharmacological Science*. 31(2):89-98.

Mahan, L.K., Escott-Stump, S., Raymond, J.L. (2012) *Krause's Food and the Nutrition Care Process:* 13th edition. Missouri: Elsevier.

Martin, B.T., Kleiber, K., Wixler, V., Raab, M., Zimmer, B., Kaufmann, M., Strebhardt, K. (2007) FHL2 regulates cell cycle-dependent and doxorubicin-induced p21Cip1/Waf1 expression in breast cancer cells. *Cell Cycle.* 6(14):1779-1788.

Masso-Welch, P., Berlingeri, S.G., King-Lyons, N.D., Mandell, L., Hu, J., Greene, C.J., Federowicz, M., Cao, P., Connell, T.D., Heakal, Y. (2019) LT-IIc, a bacterial type II heat-labile enterotoxin, induces specific lethality in triple negative breast cancer cells by modulation of autophagy and induction of apoptosis and necroptosis. *International Journal of Molecular Sciences.* 20(85):1-20.

McClendon A.K., Osheroff, N. (2007) DNA Topoisomerase II, genotoxicity and cancer. *Mutation Research.* 623(2):83-97.

Melmed S., Polonsky KS., Larsen PR., Kronenberg HM. (2016) *Williams Textbook of Endocrinology.* 13th ed. Philadelphia: Elsevier Saunders.

Milanese, C., Mastroberardino, P.G. (2020) A perspective on DNA damage-induced potentiation of the pentose phosphate shunt and reductive stress in chemoresistance. *Molecular and Cellular Oncology.* 7(3):1-4.

Milczarek, M. (2020) The premature senescence in breast cancer treatment strategy. *Cancers.* 12(1815):1-24.

Minotti, G., Menna, P., Salvatorelli, E., Cairo, G., Gianni, L. (2004) Anthracyclines: molecular advances and pharmacologic developments in antitumor activity and cardiotoxicity. *Pharmacological Reviews*. 56:185-229.

Mizushima, N., Komatsu, M. (2011) Autophagy: renovation of cells and tissues. *Cell.* 147:728-741

Moore, T., Beltran, L., Carbajal, S., Hursting, S.D., DiGiovanni, J. (2012) Energy balance modulates mouse skin tumour promotion through altered IGF-1R and EGFR crosstalk. *Cancer Prevention Research.* 5:1236-1246.

Muranen, T., Iwanicki, M.P., Curry, N.L., Hwang, J., DuBois, C.D., Coloff, J.L., Hitchcock, D.S., Clish, C.B., Brugge, J.S., Kalaany, N.Y. (2017). Starved epithelial cells take up extracellular matrix for survival. *Nature Communications.* 8:13989.

Newell, M., Brun, M., Field, C.J. (2019) Treatment with DHA modifies the response of MDA-MB-231 breast cancer cells and tumours from *nu/nu* mice to doxorubicin through apoptosis and cell cycle arrest. *The Journal of Nutrition.* 149(1):46-56.

O'Flanagan, C.H., Smith, L.A., McDonell, S.B., Hursting, S.D. (2017) When less may be more: calorie restriction and response to cancer therapy. *BioMed Central Medicine.* 13:106-115.

Park, J., Kim, K.P., Ko, J., Park, K. (2016) PI3K/Akt/mTOR activation by suppression of ELK3 mediates chemosensitivity of MDA-MB-231 cells to doxorubicin by inhibiting autophagy. *Biochemical and Biophysical Research Communications.* 477:277-282.

Pilco-Ferreto, N., Calaf, G.M. (2016) Influence of doxorubicin on apoptosis and oxidative stress in breast cancer cell lines. *International Journal of Oncology.* 49(2):753-762.

Poff, A.M., Ari, C., Arnold, P., Seyfried, T.N., D'Agostino, D.P. (2014) Ketone supplementation decreases tumour cell viability and prolongs survival of mice with metastatic cancer. *International Journal of Cancer.* 135:1711-1720.

Qu, X., Yu, J., Bhagat, G., Furuya, N., Hibshoosh, H., Troxel, A., Rosen, J., Eskelinen, E., Mizushima, N., Ohsumi, Y., Cattoretti, G., Levine, B. (2003) Promotion of tumorigenesis by heterozygous disruption of the *beclin 1* autophagy gene. *Journal of Clinical Investigation*. 112(12):1809-1820.

Raffaghello, L., Safdie, F., Bianchi, G., Dorff, T., Fontana, L., *et al.* (2010) Fasting and differential chemotherapy protection in patients. *Cell Cycle*. 9(22):4474-4476.

Rampal, G., Khanna, N., Thind, T.S., Arora, S., Vig, A.P. (2012) Role of isothiocyanates as anticancer agents and their contributing molecular and cellular mechanisms. *Medicinal Chemistry and Drug Discovery.* 3(2):79-93.

Rupniewska, E., Roy, R., Mauri, F.A., Liu, X., Kaliszczak, M., Bellezza, G., Cagini, L., Barbareschi, M., Ferrero, S., Tommasi, A.M., Aboagye, E., Secki, M.J., Pardo, O.E. (2018) Targeting autophagy sensitises lung cancer cells to Src family kinase inhibitors. *Oncotarget.* 9(44):27 346-27 362.

Safdie, F.M., Brandhorst, S., Wei, M., Wang, W., Lee, C., Hwang, S., Conti, P.S., Chen, T.C., Longo, V.D. (2012) Fasting enhances the response of glioma to chemo- and radiotherapy. *Public Library of Science One.* 7(9): 1-9.

Safdie, F.M., Dorff, T., Quinn, D., Fontana, L., Wei, M. (2009) Fasting and cancer treatment in humans: a case series report. *Aging.* 1(12):1-20.

Savitskaya, M.A., Onishchenko, G.E. (2015) Mechanisms of Apoptosis. *Biochemistry (Moscow).* 80(11):1393-1405.

Schafer, K.A. (1998) The cell cycle: a review. *Veterinary Pathology.* 35:461-478.

Seyfried, T.N., Sanderson, T.M., El-Abbadi, M.M., McGowan, R., Mukherjee, P. (2003) Role of glucose and ketone bodies in the metabolic control of experimental brain cancer. *British Journal of Cancer.* 89:1375-1382.

Sherwood, L. (2010) *Human Physiology: From Cells to Systems:* 7th edition. Brooks: Cengage Learning.

Singh, R., Cuervo, A.M. (2012) Lipophagy: connecting autophagy and lipid metabolism. *International Journal of Cell Biology.* doi:10.1155/2012/282041.

Stewart, J.W., Koehler, K., Jackson, W., Hawley, J., Wang, W., *et al*. (2005) Prevention of mouse skin tumour promotion by dietary energy restriction requires an intact adrenal gland and glucocorticoid supplementation restores inhibition. *Carcinogenesis.* 26:1077-1084.

Stipanuk, M., Caudill, M. (2013) *Biochemical, Physiological and Molecular Aspects of Human Nutrition:* 3rd edition. Philadelphia: Elsevier.

Sun, M., Zhang, N., Wang, X., Cai, C., Cun, J., Li, Y., Lv, S., Yang, Q. (2014) Nitidine chloride induces apoptosis, cell cycle arrest, and synergistic cytotoxicity with doxorubicin in breast cancer cells. *Tumour Biology.* 35:10201-10212.

Terzi, M.Y., Izmirli, M., Gogebakan, B. (2016) The cell fate: senescence or quiescence. *Molecular Biology Reports.* 43:1213-1220.

The American Type Culture Collection, 2018. *MCF-12A (ATCC CRL-10782) Culture Method.* The American Type Culture Collection, viewed 3 February 2019, <https://www.atcc.org/Products/All/CRL-10782.aspx#culturemethod>

The American Type Culture Collection, 2018. *BT-549 (ATCC HTB-122) Culture Method.* The American Type Culture Collection, viewed 3 February 2019. <https://www.atcc.org/products/all/HTB-122.aspx#culturemethod>

The American Type Culture Collection, 2018. *MDA-MB-231 (ATCC HTB-26) Culture Method.* The American Type Culture Collection, viewed 3 February 2019. <https://www.atcc.org/products/all/HTB-26.aspx#culturemethod>

Thomas, M., Davis, T., Nell, T., Sishi, B., Engelbrecht, A. (2020) Amino acid starvation sensitises resistant breast cancer to doxorubicin-induced cell death. *Frontiers in Cell and Developmental Biology.* 8:565915.

Torbett, N.E., Luna, A., Knight, Z.A., Houk, A., Moasser, M., Weiss, W., Shokat, K.M. Stokoe, D. (2008) A chemical screen in diverse breast cancer cell lines reveals genetic enhancers and suppressors of sensitivity to PI3K isotype-selective inhibition. *Biochemical Journal.* 415(1):97-110.

Van den Berghe, T., Grootjans, S., Goossens, V., Dondelinger, Y., Krysko, D.V., Takahashi, N., Vandenabeele, P. (2013) Determination of apoptotic and necrotic cell death *in vitro* and *in vivo*. *Methods.* 61:117-129.

Waks, A.G., Winer, E.P. (2019) Breast cancer treatment: a review. *Journal of the American Medical Association.* 321(3):288-300.

World Health Organisation. (2018) *Cancer: Key Facts* [Online] Available at: https://www.who.int/en/news-room/fact-sheets/detail/cancer (Accessed 26 February 2019)

Yakisich, J.S., Venkatadri, R., Azad, N., Iyer, A.K.V. (2016) Chemoresistance of lung and breast cancer cells growing under prolonged periods of serum starvation. *Journal of Cellular Physiology.* 232:2033-2043.

Yi, Y.W., Kang, H.J., Kim, H.J., Hwang, J.S., Wang, A., Bae, I. (2013) Inhibition of constitutively activated phosphoinositide 3-kinase/Akt pathway enhances antitumour activity of chemotherapeutic agents in breast cancer susceptibility gene 1-defective breast cancer cells. *Molecular Carcinogenesis.* 52(9):667-675.

Yao, D., Wang, P., Zhang, J., Fu, L., Ouyang, L., Wang, J. (2016) Deconvoluting the relationship between autophagy and metastasis for potential cancer therapy. *Apoptosis*. 21: 683-698.

Yao, G. (2014) Modelling mammalian cellular quiescence. *Interface Focus.* 4(3):1-10.

Yuan, T.L., Cantley, L.C. (2008) PI3K pathway alterations in cancer: variations on a theme. *Oncogene.* 27:5497-5510.

Zhang, J., Gao, X., Schmit, F., Adelmant, G., Eck, M.J., Marto, J.A., Zhao, J.J., Roberts, T.M. (2017) CRKL mediates p110β-dependent PI3K signalling in PTEN-deficient cancer cells. *Cell Reports.* 20:549-557.

Zhu, H., Liu, L., Deng, H., Li, Z., Sheng, J., He, X., Tian, D., Li, P. (2019) Astrocyte elevated gene 1 (AEG-1) promotes anoikis resistance and metastasis by inducing autophagy in hepatocellular carcinoma. *Journal of Cellular Physiology.* 235:5084-5095.

Zhu, W., Qu, H., Xu, K., Jia, B., Li, H., Du, Y., Liu, G., Wei, H., Zhao, H. (2017) Differences in the starvation-induced autophagy response in MDA-MB-231 and MCF-7 breast cancer cells. *Animal Cells and Systems.* 21(3):190-198.

Zhu, X., Li, W., Ma, J., Shao, N., Zhang, Y., Li, R, Wu, W., Lin, Y., Wang, S. (2015) Knockdown of heme oxygenase-1 promotes apoptosis and autophagy and enhances the cytotoxicity of doxorubicin in breast cancer cells. *Oncology Letters.* 10:2974-2980.

Appendices

Appendix A: Reagents

Phosphate buffered saline (PBS):

- 16g NaCl
- 0.4g KCl
- 2.882g Na_2HPO_4
- 0.481g KH_2PO_4

1. Dissolve reagents in 1.8L dH_2O.
2. Adjust pH to 7.4 and fill up to 2L with dH_2O.
3. Store at room temperature.

Modified RIPA buffer:

- 790mg Tris-base
- 900mg NaCl
- 10ml 10% NP-40
- 10ml 10% Na-deoxycholate
- 5ml 100mM EDTA
- 5ml 100mM EGTA
- 1ml 10% SDS

1. Add Tris-base and NaCl to 50ml dH_2O and stir until dissolved.
2. Adjust pH to 7.4.
3. Add NP-40 and Na-deoxycholate and stir until dissolved.
4. Add EDTA, EGTA and SDS and stir until dissolved.
5. Adjust to final volume of 100ml with dH_2O.
6. Aliquot and store at 4°C.

Appendix B: Protocols

Protocol 1: Western blotting

Cell harvesting using the cell scraper

1. Prepare reagents by placing PBS, RIPA Stock Buffer and eppies on ice.
2. Prepare RIPA Buffer by adding the following reagents per 1 ml of RIPA:
    - 42 µL Protease Inhibitors Cocktail
    - 5 µL PMSF (Add just before use, half-life of 30min)
    - 5 µL Na_3VO_4
    - 5 µL NaF
3. Retrieve cells.
4. Remove media from cells with Pasteur pipette.
5. Wash twice with ice-cold PBS using a Pasteur pipette
6. Add 80 µL RIPA Buffer per well in 6-well plate or 150 µL per T_{25} flask.
7. Incubate on ice for 2-5 minutes.
8. Using a cell scraper, scrape the cells loose and collect in corner of flask. Remember to clean the scraper with ethanol between different groups.
9. Collect the suspension from the flask/plate and transfer to a pre-cooled eppie.
10. Sonicate this for 5 seconds @ 5 amplitude.
11. Incubate in the fridge, on ice, until the foam has settled. (Alternatively, eppies can also be stored at this point in the -80°C freezer).
12. Centrifuge for 2 minutes @16.3g and 4°C.
13. Collect the supernatant in new pre-cooled eppie.
14. Store eppies at -80°C, or perform a Bradford assay to determine the volume needed for 50 µg of protein.
15. Prepare the samples and store them as ready-made sample (protein + sample buffer).

Bradford Protocol

1. If samples are frozen, thaw the protein samples on ice.
2. Thaw a 1 mg/ml BSA stock solution.

3. Prepare a BSA working solution (200 µg/ml) by diluting 100 µl BSA with 400 µl dH_2O (50 µL BSA + 450 µL dH_20 if using 2 mg/ml BSA stock). Vortex to mix.

4. Prepare Bradford standards as follow (in duplicate):

Volumes of components used to establish Bradford standards.

µg Protein	**200 µg/ml BSA**	**dH_2O**	**Bradford Reagent**
0 (Blank)	0 µl	100 µl	900 µl
2	10 µl	90 µl	900 µl
4	20 µl	80 µl	900 µl
8	40 µl	60 µl	900 µl
12	60 µl	40 µl	900 µl
16	80 µl	20 µl	900 µl
20	100 µl	0 µl	900 µl

5. Vortex the protein samples.
6. For each Bradford sample, add 5 µl of protein sample to 95 µl dH_20 and 900 µl Bradford reagent. Prepare each sample in duplicate.
7. Vortex the Bradford samples and standards.
8. Zero the spectrophotometer with a blank and set the absorbance @ 595 nm.
9. Read the absorbencies of each sample.
10. Draw a standard curve using an Excel graph and plot the values of the sample to determine the concentration of protein in each sample.

Stain-free SDS-Page Fast Cast Gel Protocol

Using Bio-Rad® TGX Stain-Free™ FastCast™ Acrylamide Kit, 12%.

1. Get clean pairs of spacer plates and short plates, BioRad casting frames (green), casting stands and the rubber gaskets that go in the bottom of the stand.
2. Place gaskets in the grooves at the base of the casting stands.
3. Clean the plates thoroughly with ethanol and place them in the casting frames with the short plate facing the front. Secure using the clip on the casting stand.

4. Get 3 small beakers and label them for H_2O, resolving gel (bottom) and stacking gel (top).
5. Make up the required resolving gel according to the recipe given by Bio-Rad® to make 4 gels.

Volumes of components used for self-cast resolving gel.

Resolving Gel	
Gel constituent	**4% Gel**
Resolver A	12 mL
Resolver B	12 mL
TEMED	12 µL
10% APS	120 µL

1. Add all the constituents to the beaker, swirling gently to mix.
2. Using a Pasteur pipette, quickly pour the gel mixture between the two plates up to the green line seen at back of the plate from the gasket. Avoid air bubbles by pouring in from the one corner.
3. Allow gel to set (30 to 60 minutes). Prepare 1:10 dilutions of running buffer, TBS-T and transfer buffer.
4. Prepare the stacking gel according to the recipe given by Bio-Rad® to make 4 gels.

Volumes of components used for self-cast stacking gel.

Stacking Gel	
Gel constituent	**4% Gel**
Stacker A	4 mL
Stacker B	4 mL
TEMED	8 µL
10% APS	40 µL

1. Add all the constituents with gentle swirling to mix
2. Using a plastic Pasteur pipette, quickly pour the gel mixture between the two plates up to the top of the front plate.

3. Insert the appropriate comb gently, pushing down and avoiding bubble formation.
4. Allow to set for 1 hour.
5. Retrieve the standard protein marker from the freezer and allow to equilibrate to room temperature.

Western Blot Running Protocol

Day 1

1. Prepare BioRad Fast Cast Stain-Free gels or Self Cast according to instructions.
2. Thaw protein samples on ice, which are prepared in a 2:1 ratio of protein sample to Laemli's buffer.
3. Punch a hole in the lid of each eppie, mix by vortexing briefly and boil for 5 minutes at 95°C.
4. Spin samples down with quick pulse.
5. Assemble the gasket
    - Assemble the gels onto the gasket with the comb facing inside
    - Fill the gasket with running buffer. Check for leaks.
    - Carefully remove the combs and rinse out wells with P200 pipet (set to approx. 100 µL) and a yellow tip.
6. Load the ladder (4 µL BLUeye).
7. Load the samples.
8. Place the gasket into the tank and fill with running buffer. Re-fill gasket if necessary.
9. Attach the lid and plug into power pack.
10. Run at 100 V for approximately 10 minutes (until sample has entered gel).
11. Increase to 150 V and run until blue dye front reaches the bottom of the gel (approximately 1 hour).
12. When finished, activate **immediately**
    - Activate stain-free properties of gel on ChemiDoc (gel activation protocol, 2.5 minutes).

Western Blot Transfer Protocol

Day 1

1. Prepare for transfer:
    a. Soak two pieces of blotting paper in transfer buffer for 2 minutes.
    b. Activate a piece of PVDF membrane in 100% methanol for 10-15 seconds and then soak in transfer buffer for 2 minutes.
    c. Size 7 cm x 8.4 cm – blotting paper and membrane should be same size, preferably gel also
2. Assemble the transfer sandwich on the cassette base (anode) by placing one piece of wet extra thick or 3 pieces of thick filter paper on the bottom, then the membrane, the gel, and finally, the remainder of the wet filter paper on top. Use the blot roller to remove air from between the assembled layers.
3. Once the stacks are positioned in the cassette base, place the cassette lid on the base. The lid is reversible, but ensure that the electrical contacts fit closely into the slots in the base. Press the lid down firmly and turn the dial clockwise to engage the lid pins into the locking slots.
4. Load a second cassette if desired.
5. Slide the cassette (with the dial facing up) into the bay until it makes contact with the magnetic interlock and you hear a click. Cassettes can be inserted into the bays in any order, with or without power to the system.
6. Select the LIST button from the Home menu and the **STANDARD SD** transfer protocol from the Bio-Rad pre-programmed protocols or the user-defined protocol of choice.
7. To initiate the run, press the navigation button that corresponds to A:RUN for the cassette in the upper bay or B:RUN for the cassette in the lower bay.
8. After transfer, disassemble the stack.
    - Blotting paper can be re-used.
    - Gel can be visualised to determine transfer efficiency if desired.
9. Label membrane and rinse in 100% methanol.
    - Labelling – only use soft pencil and not markers or pens.
    - Place membrane only on ethanol cleaned surface.

10. Air-dry membrane
    - Becomes white
    - Hold in fumehood for quicker drying
11. Re-hydrate membrane in 100% methanol
    - Until translucent, 10-15 seconds

Western Blot Antibody Protocol

Day 1

1. Wash membrane in TBS-T for 5 minutes.
2. Image transfer on membrane on Chemidoc
    - Stain-free blot setting
    - If using for normalisation, make sure image is clean and not over-exposed.
3. Block membrane in 5% milk (prepared in TBS-T) for 1 hour with gentle shaking
    - Or 5% BSA (prepared in TBS-T) for when probing for phosphorylated proteins.
4. Wash membrane 3 x for 5 minutes in TBS-T.
5. Incubate membrane on primary antibody overnight at 4°C.
    a. Prepared in 50 ml centrifuge tube.
    b. Dilute antibody in TBS-T to desired concentration, normally 1:1000.
    c. Attach to rotators in walk-in fridge.
        - Make sure tube/s are straight and rotor is balanced.

Day 2

6. Retrieve membranes
    - Stored primary antibody in fridge/freezer
7. Wash membrane 3 x 5 minutes in TBS-T.
8. Incubate membrane on secondary antibody for 1 hour at room temperature.
    a. Prepared in 50 ml centrifuge tube.
    b. Dilute antibody in TBS-T to desired concentration, normally 1:10 000.
    c. Place on roller in Western blot room.

9. Wash membrane 3 x 5 minutes in TBS-T.
10. Develop:
    a. Prepare minimum amount of ECL needed in eppie in a 1:1 ratio.
    b. Place membrane on Chemidoc and check position.
    c. Add ECL to the desired area and roll to ensure even spread. Roll away excess ECL.

Expose using desired settings.

Protocol 2: Immunocytochemistry

GFP-LC3 transfection:

1. Seed a T25 flask and culture until a confluence of 60-70% is attained.
2. Set aside two 500 µl eppies.
3. In the first, add 200 µl media, 15 µl P3000 and 3 µl GFP-LC3 plasmid.
4. In the second, add 200 µl media and 11,25 µl Lipofectamine.
5. Add the contents of the first eppie to the second, pipetting up and down to mix the reagents thoroughly. Incubate for 15 minutes at room temperature.
6. Remove the media from the T25 flask and add 3 ml of fresh media.
7. Add the transfection reagents to the T25 flask, and, once closed, move the flask in a figure-eight motion to ensure even distribution of reagents.
8. Incubate for 24-48 hours at 37°C, and refresh with complete media when transfection is complete.

Selection of GFP-LC3 cells:

1. Seed a T25 flask with cells transfected with GFP-LC3. Culture until approximately 60-70% confluent.
2. Aliquot 4 ml of PenStrep-free media into a 15 ml Falcon tube and add 40 µl of G418 (50 mg/ml). This yields a final concentration of 0,5 mg/ml.
3. Remove the media from the T25 and replace with PenStrep-free media containing G418.
4. Incubate for 24-48 hours at 37°C, and refresh with complete media after selection is complete.

The addition of LysoTracker Red:

For an 8-well chamber slide (volume of 200 µl/well):

1. Add 1 µl of LysoTracker Red (1 mM) to 100µl of media and vortex to get a working solution of 10 µM.
2. Add 2,5 µl of working solution to each well with a total volume of 200 µl.

Cover with foil and incubate at 37°C for 60 minutes prior to imaging.

Protocol 3: Cell cycle analysis

1. Seed and culture cells in either 6-well plates or T25 flasks so that a minimum of one million cells will be attained at the end of the treatment period.
2. Label each treatment group and treat accordingly until cells are ready to be harvested.
3. Remove media and wash all treatment groups once with warm PBS.
4. Trypsinise cells and transfer the cells from each group to separate labelled tubes. Pool triplicate wells (if using a 6-well plate) from each treatment group to form one sample per group.
5. Rinse wells with PBS and add to corresponding tubes so that any remaining cells may be collected and pooled with their respective groups.
6. Take a 20 µl sample from each group and count using a haemocytometer to obtain the total number of cells per group.
7. Centrifuge tubes at 1750 rpm for 4 minutes.
8. Resuspend in PBS and centrifuge again at 1750 rpm for 4 minutes.
9. Fix cells by resuspending the pellet in ice-cold 70% ethanol while vortexing to avoid clump formation.
10. Incubate cells in ethanol on ice for 1 hour.
11. Centrifuge at 3000 rpm for 5 minutes.
12. Carefully wash twice with PBS, avoiding cell loss.
13. Resuspend each pellet in 50 µl RNase A (100 µg/ml) and 400 µl PI (50 µg/ml).
14. Wrap tubes in foil to protect from direct light, and incubate at room temperature for 30 minutes.
15. Analyse samples using a BD FACS Melody cell sorter.

Protocol 4: Cell viability assay using WST1

1. Seed and culture cells in a 48-well plate.
2. Label each group and treat accordingly.
3. When cells are ready to be analysed, add 10 µl of WST1 reagent to each well containing 200 µl of media each. (Do not remove media before adding WST1).
4. Cover the full plate with foil to protect from light and incubate for 60-120 minutes at 37°C.
5. Uncover the plate, remove the lid, and measure the absorbance at 450 nm on Microtiter Plate Reader.
6. Analyse values by obtaining the mean for each treatment group, and express each group's value as a percentage of the control.

Protocol 5: Live cell count with trypan blue

1. Seed and culture cells in either 6-well plates or T25 flasks.
2. Label each treatment group and treat accordingly until cells are ready to be harvested.
3. Pre-label a 15 ml tube for each experimental group.
4. Remove media and wash all treatment groups once with warm PBS.
5. Trypsinise cells and transfer the cells from each group to its respective labelled tube. Pool triplicate wells (if using a 6-well plate) from each treatment group to form one sample per group.
6. Rinse wells with PBS and add to the corresponding tubes so that any remaining cells may be collected and pooled with their respective groups.
7. Centrifuge tubes at 1750 rpm for 4 minutes.
8. Remove supernatant, resuspend in 3 ml PBS and centrifuge again at 1750 rpm for 4 minutes.
9. While centrifugation commences, prepare a 500 µl solution of 0.1% trypan blue from 125 µl trypan blue 0.4% and 375 µl PBS.
10. Remove supernatant and resuspend each pellet in 1000 µl of warm PBS.
11. Transfer 100 µl of this cell suspension to a pre-labelled Eppendorf tube, and add 100 µl of 0.1% trypan blue solution, mixing as you resuspend.
12. Load 10 µl of this suspension onto each of three grids on Neubauer counting chambers.
13. Take images to count the number live (unstained) cells.

Protocol 6: Flow cytometry with propidium iodide staining

1. Seed and culture cells in either 6-well plates or T25 flasks so that a minimum of one million cells will be attained at the end of the treatment period.
2. Label each treatment group and treat accordingly until cells are ready to be harvested.
3. Remove media and wash all treatment groups once with warm PBS.
4. Trypsinise cells and transfer the cells from each group to a separate labelled tube. Pool triplicate wells (if using a 6-well plate) from each treatment group to form one sample per group.
5. Rinse wells with PBS and add to corresponding tubes so that any remaining cells may be collected and pooled with their respective groups.
6. Take a 20 µl sample from each group and count using a haemocytometer to obtain the total number of cells per group.
7. Centrifuge tubes at 1750 rpm for 4 minutes.
8. Remove supernatant, resuspend in PBS and centrifuge again at 1750 rpm for 4 minutes.
9. Resuspend each pellet in the appropriate volume of PBS to yield a final concentration of 10^6 cells per ml.
10. Add 400 µl PI (50 µg/ml).
11. Wrap tubes in foil to protect from direct light. Remove from foil only to analyse samples using a BD FACS Melody cell sorter.